

Politechnika Lubelska
Wydział Budownictwa i Architektury

BUDOWNICTWO
I ARCHITEKTURA

Vol. 20(2) 2021

Politechnika Lubelska
Lublin, 2021

Politechnika Lubelska
Wydział Budownictwa i Architektury

**BUDOWNICTWO
I ARCHITEKTURA**



Vol. 20(2) 2021

Politechnika Lubelska
Lublin, 2021

Rada Naukowa/Scientific Council

Tomasz Bajda (AGH Kraków)
Ivan Baláz (University of Economics in Bratislava)
Mykola Bevez (National University Lviv Polytechnic)
Eduard-Marius Craciun, Ovidius (University of Constanta)
Grażyna Dąbrowska-Milewska (Politechnika Białostocka)
Wiesława Głodkowska (Politechnika Koszalińska)
Adam Goliger (The Council for Scientific and Industrial Research - CSIR)
Zbyněk Keršner (Brno University of Technology)
Halit Cenani Mertol (Atılım University)
Carlos M. Mozos (University of Castilla - La Mancha)
Adam Nadolny (Politechnika Poznańska)
Sandro Parrinello (Pavia University)
Stanislav Pospíšil (Institute of Theoretical and Applied Mechanics)
Wojciech Radomski (Politechnika Łódzka i Politechnika Warszawska)
Elżbieta Radziszewska-Zielina (Politechnika Krakowska)
Petro Rychkov (National University of Water Management and Nature Resources Use)
Shamsher Bahadur Singh (Birla Institute of Technology and Science)
Anna Sobotka (AGH Kraków)
Bogusław Szmygin, Lublin University of Technology, Poland
Thomas Thiis (Norwegian University of Life Sciences)
Viktor Tur (Technical University of Brest)
Tim K.T. Tse (The Hong Kong University of Science and Technology)

Kolegium Redakcyjne/Editorial Board

Redaktor naczelny/Editor-in-Chief: **Wojciech Franus**
Zastępca redaktora naczelnego/Deputy Editor: **Tomasz Lipecki**
Zastępca redaktora naczelnego/Deputy Editor: **Lukasz Borowski**
Sekretariat/Secretary: **Dagna Przesmycka**

Redaktor Numeru/Issue Editor: **Krzysztof Śledziwski**

Adres redakcji/Address:

Politechnika Lubelska, Wydział Budownictwa i Architektury
ul. Nadbystrzycka 40, 20-618 Lublin, e-mail: wb.bia@pollub.pl

Strona czasopisma/Journal website:

<https://ph.pollub.pl/index.php/bia/>

Indeksacja/Indexed in:

Arianta, BASE, BazTech, CEEOL, Dimensions, DOAJ, EBSCO, ERIH Plus, Google Scholar, Index Copernicus, Infona, PBN/POL-Index, Publons, Sherpa Romeo, TIB, WorldWideScience

Publikacja wydana za zgodą Rektora Politechniki Lubelskiej.
Published with the consent of the Rector of Lublin University of Technology.

Finansowana w ramach środków Ministra Nauki i Szkolnictwa Wyższego.
Financing by the Polish Ministry of Science and Higher Education.

© Copyright by Politechnika Lubelska 2021

ISSN 1899-0665

Realizacja/Published by: Biblioteka Politechniki Lubelskiej
Ośrodek ds. Wydawnictw i Biblioteki Cyfrowej
ul. Nadbystrzycka 36A, 20-618 Lublin, email: wydawca@pollub.pl


SPIS TREŚCI
CONTENTS

Dorota Michałowska-Maziejuk, Barbara Goszczyńska <i>Assessment of the early-age compressive strength of concrete</i>	5
Szymon Węgliński <i>Capillary water absorption in mixtures of cohesive soils stabilized with cement and hydrophobic agent</i>	15
Aneta Biała <i>The influence of internal installation solutions in single-family housing on the “EP” factor in light of the new requirements of WT 2021</i>	29
Maciej Tomasz Solarczyk <i>Influence of effective width of flange on calculation and reinforcement dimensioning of beam of reinforced concrete frame</i>	41
Sylwia Anna Borowska, Marta Kosior-Kazberuk <i>Application of fracture energy for the assessment of frost degradation of high-strength concretes</i>	57
Magdalena Grudzińska <i>The influence of sunspaces on the heating demand in living spaces – comparison of calculation methods according to ISO 13790</i>	69
Anna Prokop, Piotr Nazarko, Leonard Ziemiański <i>Digitalization of historic buildings using modern technologies and tools</i>	83
Ewa Jarecka-Bidzińska <i>Hybrid methodology of multi-sensory research of public space in urban planning</i>	95

Assessment of the early-age compressive strength of concrete

Dorota Michalowska-Maziejuk¹, Barbara Goszczyńska²

¹ Department of Concrete Structures and Geotechnics; Faculty of Civil Engineering and Architecture; Kielce University of Technology; 7 Tysiąclecia Państwa Polskiego Av., 25-314 Kielce, Poland; d.michalowska@tu.kielce.pl  0000-0002-8076-6836

² Department of Concrete Structures and Geotechnics; Faculty of Civil Engineering and Architecture; Kielce University of Technology; 7 Tysiąclecia Państwa Polskiego Av., 25-314 Kielce, Poland; b.goszczyńska@tu.kielce.pl  0000-0003-2363-9141

Funding: This study was financed by the scientific and research work carried out as part of the statutory activity for years 2016 – 2018: “Analysis of the load-carrying capacity of reinforced concrete beams reinforced with CFRP composite materials, glued into the concrete cover” no. 02.0.06.00/2.01.01.01.0007; MNSP.BKWB.16.001.

Abstract: This paper analyses the results of concrete compressive strength tests on cubic samples with different w/c ratios during the early stage of hardening (at 7, 14, and 28 days). Statistical and strength parameters were assessed and the quality of the concrete was estimated. The *expected concrete grade*, C25/30, was confirmed against the formulation provided by the prefabrication plant. Then, the amount of individual constituents was adjusted to obtain the *target grade of concrete*, i.e., C20/25. The concrete grade was estimated based on concrete strength parameters measured at three time points and compared with the expected 28-day strength values determined as per Eurocode 2 and with the concrete grade defined by these values. The paper also provides an overview of the most widely used methods of testing concrete compressive strength.

Keywords: concrete, testing machine, concrete compressive strength, destructive method, water-cement ratio

Introduction

An important factor in the safety and use of structures in the rapidly developing construction industry is the assessment and control of quality and durability of materials used in buildings and engineering structures. When a structure is safe while being constructed and during its design service life, the requirements relating to its load-carrying capacity, stability, or use have been met [1]. One of the conditions of ensuring durability of a structure is to produce structural members of materials that maintain the strength and physical characteristics and general performance throughout the service period regardless of any changes in the

purpose of a building, its reconstruction, expansion or external environmental influences [2]. Compromising the quality of materials raises maintenance costs and generates additional costs even before commissioning due to, for example, the necessity to strengthen structural and non-structural elements for improved load carrying capacity resulting from design and workmanship errors. Inadequate quality of materials in main components of a structure or its non-structural elements may be the cause of damage, faults, or, in worst cases, disasters.

Long term investigation of the causes of building accidents and disasters conducted by the Institute of Building Technology showed that in addition to random factors, such as strong winds, gas explosion, fire, or landslide, human errors in the design and construction of structures are critical. Poor quality of building materials adds to these factors greatly [3]-[5]. The most common errors occur during the material manufacturing process, or due to improper storage, transport and unloading, assembly, or finishing works.

According to Art. 62 of the Polish Construction Law [6], when renovating and modernising building structures, as well as during their service life, condition inspections must be performed periodically, and the conclusions and recommendations must be implemented.

It is also reasonable to control the materials used during the construction of buildings, especially when it comes to assessing their strength parameters and quality of workmanship. In case of concrete, the assessment of early-age strength parameters may be necessary:

- to make a decision about the removal of the supporting framework,
- to load structural members before initially planned date,
- to strengthen structural element in the event of insufficient load capacity due to errors, for example design errors,
- to confirm the compressive strength of concrete in case of design or construction errors,
- to resolve the doubts about the compliance of concrete strength with that determined on standardised test specimens.

Assessment of strength parameters and quality of building products used during and after the construction of a building is thus one of the fundamental issues in the diagnosis of building structures.

2. Characterization of concrete strength assessment methods

Concrete strength is one of the basic parameters defined in diagnostics of reinforced concrete structures. Diagnostic tests can be conducted in situ or in properly prepared laboratories. Generally, tests fall into three groups: non-destructive, semi-destructive, and destructive tests [7]. A detailed division of non- and semi-destructive tests used in concrete structure diagnosis, together with an original taxonomy of physical, chemical, and biological methods is discussed in [8].

Non-destructive testing (NDT) does not alter, damage or destroy the structure of the material tested. The most frequently used NDT techniques include ultrasonic and sclerometric methods. The ultrasonic test uses acoustic wave propagation velocity in the hardened concrete mix for predicting the strength of concrete. Measurement accuracy is related to the pulse frequency; the higher the frequency, the more accurate reading is obtained. The pulse generated by a transmitter placed on the surface of the test specimen travels through concrete along path S with a known length. It is then transformed into an electrical signal by the receiver. The time T of the wave pulse travel is measured. Knowing the path that the signal travelled, it is

possible to calculate the velocity V of the wave propagation ($V=S/T$). The indirect estimation of concrete strength R is determined from the hypothetical R - V curve [9].

The second method of non-destructive testing is the sclerometric method, also known as the hardness test. Hardness is the resistance of the tested material to deformation caused by concentrated forces. It is most often measured with sclerometers, the so-called Schmidt hammers (Fig. 1) with different impact energies for specific applications.



Fig. 1. Digital Schmidt hammer [10] (photograph by Dorota Michałowska-Maziejuk)

Hardness measurement involves pressing the plunger rod against the concrete surface until the spring-loaded mass releases and causes an impact. The degree of the rebound, measured against the calibration curves, is the rebound number L which defines the compressive strength of concrete. The method is simple, the measurement can be repeated multiple times and the result is recorded automatically using the hammer as in Fig. 1. The weak point of the rebound hammer test is that it tests the subsurface layer of concrete subject to carbonation (the formation of calcium carbonate $\text{Ca}(\text{OH})_2$). The ultrasonic method in contrast allows estimating the properties of concrete in its internal structure

Semi-destructive methods (SDM) comprise another group of tests. They are partially destructive in that they destroy elements of concrete surface to a limited extent. The most common SDMs are:

- the ‘pull-out’ method – it is based on pulling the blocks or anchors from hardened concrete, while measuring the force needed for them to be pulled out. This method

- is often used to determine the concrete strength gain over time, during the early phase of construction.
- the ‘lock-out’ method – is a variant of the pull-out method and is based on the measuring the force needed to pull out the steel anchors placed in the structure before concreting it.
 - the ‘pull-off’ method – is based on measuring the force required to pull off a steel disc [11] glued to the surface of the tested element, which was earlier specially prepared and cut along its circumference. This technique is used when insulation or strengthening is to be added by drilling grooves in the concrete cover and filling them with the composite material or by gluing the composite on the concrete surface [12].



Fig. 2. A device used in the pull-off method (photograph by Dorota Michałowska-Maziejuk)

Destructive tests involve extracting witness samples from the existing structure and destroying them for strength characterisation. The axial compression test is applied for estimating the compressive strength of concrete. This method is based on the measurement of force needed to destroy the axially compressed sample, with the use of the strength testing machine in the research laboratory. Witness samples are extracted by coring or cast in separate moulds during the manufacture of concrete components. The cores used in the testing should be extracted from the areas which will not weaken the structure, that is, away from joints, edges, and main reinforcement.

This article presents the test results obtained during axial compression and failure of concrete specimens. Analysis of the results allowed the evaluation of concrete grade and early-age quality.

3. Testing programme

The tests were carried out on cubic specimens with a side equal to $b = 100$ mm in the strength-testing machine at three concrete ages ($t_1 = 7$ days, $t_2 = 14$ days, $t_3 = 28$ days). An additional variable factor was the water-cement ratio obtained by changing the amount of cement at a constant amount of water used (Table 1). The test specimens were made of basalt aggregate based concrete grade C20/25. The concrete mix was poured into metal moulds and subjected to vibrations on a vibrating table [13]. The specimens were divided into four series, in which the water-cement ratio was the variable factor. The series designated as “0” was produced in order to verify the recipe for the C25/30 road and bridge concrete provided by the prefabrication plant. Series 1÷3 were made using the provided formulation, which was further modified to obtain concrete C20/25. For this purpose, the water-cement ratio was changed by 0.02 starting from $w/c = 0.48$. The change in cement amount also caused a change in the number of admixtures used in the original formulation. Obtaining the expected grade of concrete was verified on the basis of the mean value of cylindrical compressive strength of concrete, which for concrete grade C20/25 is in interval $a \in <28 \div 33$) according to [1]. The concrete mix formulation for four series is presented in Table 1.

Table 1. The composition of the concrete mix is given in kg per 1m^3 batch

Ingredients	Series 0 (S0)	Series 1 (S1)	Series 2 (S2)	Series 3 (S3)
Basalt aggregate 8/16		731		
Basalt aggregate 2/8		581		
Sand 0/2		691		
Water		150		
Cement CEM I 42,5R	360	310	300	290
ADVA Flow 440	1.98	1.55	1.50	1.45
Darex AEA W	0.36	0.31	0.30	0.20
w/c	0.42	0.48	0.50	0.52

The compression-testing machine, consisting of a hydraulic unit, a load frame and control and measurement electronics can generate a compressive force of 6000 kN. Readings are generated from the liquid pressure sensor. The tester measures and records the required test parameters, as well as performs statistical calculations and plots the relationships between the studied quantities [14].

After demoulding, loose debris was removed and the specimens were placed between the pressure plates of the press. Each time, the upper pressure plate was aligned centrally with the surface of the specimen owing to the ball joint connection with the load frame [15]. The specimens were continuously loaded until failure with a force perpendicular to the direction of concreting at 0.5 MPa/s. After that, the samples were inspected visually and the typical failure pattern was confirmed [16]. The view of a typical failed concrete specimen is shown in Fig. 3, and Fig. 4.



Fig. 3. Concrete specimen after compression test (photograph by Dorota Michałowska-Maziejuk)

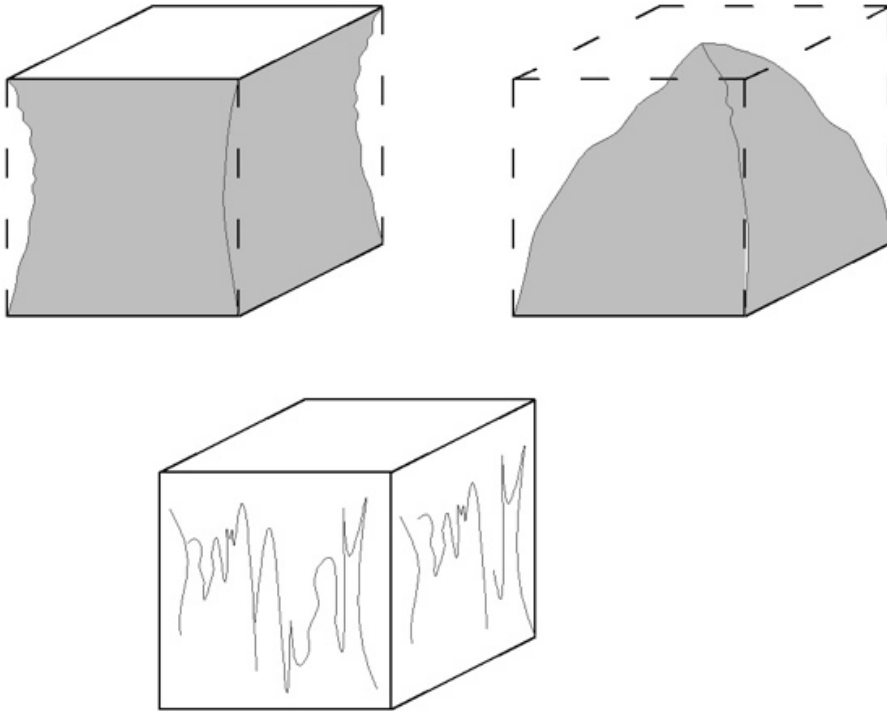


Fig. 4. Correctly damaged concrete specimen (illustration by Dorota Michałowska – Maziejuk)

The measurement of destructive forces of the test specimen series at three concrete ages with different water-cement ratios is summarized in Table 2

Table 2. Results of measurements of destructive forces

Destructive force [kN]											
7 days				14 days				28 days			
S0	S1	S2	S3	S0	S1	S2	S3	S0	S1	S2	S3
390.0	289.5	289.0	248.6	428.6	336.8	349.7	287.6	429.8	364.5	367.3	310.8
324.9	303.1	305.9	240.5	411.7	341.7	347.2	278.8	426.3	361.8	359.9	318.9
365.6	310.7	305.8	242.2	424.5	334.9	334.2	286.2	421.7	374.9	366.5	317.2
368.9	313.6	295.2	249.6	374.4	364.8	342.7	291.4	397.3	364.6	379.4	315.6

4. Estimation of concrete grade and evaluation of statistical and strength parameters

The first value needed for concrete grade estimation, compressive strength f_{ci} for each specimen series, was determined from equation (1) and expressed in MPa:

$$f_{ci} = \frac{F_i}{A_i} \quad (1)$$

where: F_i – maximum load on the i -th specimen at failure, A_i – the area of the compression section of i -th specimen.

The mean value of the concrete compressive strength f_{cm} was calculated from equation (2):

$$f_{cm} = \frac{1}{n} \sum_{i=1}^n f_{ci} \quad (2)$$

where: n – the number of results, f_{ci} – the individual result of concrete compressive strength for i -th specimen.

The measurements of strength values at three concrete ages for w/c ratios 0.42, 0.48, 0.50, 0.52 are shown in Table 3.

Table 3. Compressive strength of the concrete specimens at 7, 14 and 28 days

Compressive strength f_c [MPa]											
7 days				14 days				28 days			
S0	S1	S2	S3	S0	S1	S2	S3	S0	S1	S2	S3
39.00	28.95	28.90	24.86	42.86	33.68	34.97	28.76	42.98	36.45	36.73	31.07
32.49	30.31	30.59	24.05	41.17	34.17	34.72	27.88	42.63	36.18	35.99	31.90
36.56	31.07	30.58	24.22	42.45	33.49	33.42	28.62	42.17	37.49	36.65	31.72
36.89	31.36	29.52	24.96	37.44	36.48	34.27	29.14	39.73	36.46	37.94	31.56
Mean compressive strength f_{cm}^{cubic} cubic specimens [MPa]											
36.2	30.4	29.9	23.5	41.0	34.5	34.3	28.6	41.9	36.6	36.8	31.6
Mean compressive strength f_{cm}^{cyl} recalculated for cylindrical specimens [MPa]											
29.0	24.3	23.9	19.6	33.0	27.6	27.5	22.9	33.5	29.3	29.5	25.2

When estimating the grade of the obtained concrete, the mean value of concrete cylinder compressive strength f_{cm}^{cyl} was calculated in accordance with the rules [1] (Tab. 3). In the case of series S0, S1, and S2 with w/c ratios of 0.42, 0.48, and 0.50 respectively, more than 80% of the strength to be achieved at 28 days was obtained at the first seven days (S0 – 86%, S1 – 83%, and S2 – 81%). For the series of three cubic specimens (w/c=0.52), 77% of the concrete strength was

obtained after 7 days. At 14 days in each of the above cases, over 90% of the concrete strength to be achieved in each series at 28 days was obtained (starting from S0: 98%, 94%, 93%, 91% respectively). Percentage differences between the series are a result of different cement contents for the amount of mixing water used, which has a chemical effect in the concrete, causing hydrolysis and hydration of cement phases [17]. The smaller the cement content in relation to the constant amount of water, the lower the strength of the cement mix obtained at an age of 7, 14, and 28 days. The results of testing the S0 specimens made of concrete mix according to the composition provided by the prefabrication plant for concrete grade C25/30 confirmed achieving this grade already at an age of 14 days without changing it on the 28th day. The results of subsequent series of concrete specimens with a lower cement content relative to the constant amount of water showed that grade C20/25 was obtained at 28 days for series 1 and 2 (w/c ratio 0.48 and 0.50, respectively). For series 3, the results indicated concrete grade C16/20, which was lower than the target grade C20/25. The obtained results for series 3 specimens, together with the estimated concrete grade are shown in Table 4.

Table 4. Concrete grade obtained in the compression test

Series 1			Series 2			Series 3		
7 days	14 days	28 days	7 days	14 days	28 days	7 days	14 days	28 days
C12/15	C16/20	C20/25	C12/15	C16/20	C20/25	C8/10	C12/15	C16/20

During statistical assessment of the homogeneity of concrete, first the value of variance S^2 was estimated, according to formula (3), and then the value of standard deviation S was calculated from formula (4):

$$S^2 = \frac{1}{n-1} \sum_{i=1}^n (f_{ci} - f_{cm})^2 \quad (3)$$

$$S = \sqrt{\frac{1}{n-1} \sum_{i=1}^n (f_{ci} - f_{cm})^2} \quad (4)$$

where: n, f_{ci} – as in formula (2), f_{cm} – mean compressive strength of concrete.

When determining the quality of concrete production, formula (5) was used, which is the relative standard deviation, called the coefficient of variation:

$$v = \frac{S}{f_{cm}} 100\% \quad (5)$$

where: S – standard deviation, f_{cm} – mean compressive strength of concrete.

The values of statistical parameters are compiled in Tables 5 and 6.

Table 5. Statistical evaluation of the results for series 0

	7 days	14 days	28 days
s^2	7.4	6.1	2.1
s	2.7	2.5	1.5
v	7.50%	6.00%	3.50%
v_{sr}	5.70%		

Table 6. Statistical evaluation of the results for series 1÷3

	Series 1			Series 2			Series 3		
	7 days	14 days	28 days	7 days	14 days	28 days	7 days	14 days	28 days
s^2	1.2	1.9	0.3	0.7	0.5	0.7	0.2	0.3	0.1
s	1.1	1.4	0.6	0.8	0.7	0.8	0.5	0.5	0.4
v	3.50%	4.00%	1.60%	2.80%	2.00%	2.20%	1.90%	1.80%	1.10%
v_{sr}	3.03%			2.33%			1.60%		

While determining the coefficient of variation of the test cubes results, it was found that quality of the obtained concrete mix was very good as confirmed by the relative mean standard deviation v_{sr} of no more than 7% [9].

In order to estimate at $t_1 = 7$ days, $t_2 = 14$ days the mean strength of concrete that could be achieved at 28 days, the provisions of [1] were used, formula (6):

$$f_{cm}(t) = \beta_{cc}(t) f_{cm} \quad (6)$$

where: $\beta_{cc}(t)$ – coefficient which depends on the age of the concrete t , expressed with formula (7), f_{cm} – mean compressive strength obtained at 28 days.

$$\beta_{cc}(t) = \exp \left[s \left(1 - \sqrt{\frac{28}{t}} \right) \right] \quad (7)$$

where: s – coefficient depending on the type of cement, t – the age of concrete expressed in days.

By transforming formula (6), the compressive strength f_{cm} of the concrete was calculated for two concrete ages, assuming the coefficient s equal to 0.20. The concrete grade estimated and possible to be achieved after 28 days, calculated at $t_1=7$ days and $t_2=14$ days for the components of the verified composition is C25/30, and for series 1 and 2 series, this will be grade 20/25. For the series 3 specimens it is grade C16/20. All of the estimated grades were equivalent to the concrete strength classes obtained in destructive testing. This confirms that current standard provisions are safe and correct. The concrete grade obtained during destructive tests and estimated on the basis of formula (6) agrees with the assumed grade C20/25 for series 1 and 2, and C25/30 for series 0. In series 3, the concrete grade was lower than assumed. The results of the estimated concrete grades at 28 days are shown in Table 7.

Table 7. Estimation from formula (6). Concrete grade after 28 days

t [days]	Series 0		Series 1		Series 2		Series 3	
	7 days	14 days	7 days	14 days	7 days	14 days	7 days	14 days
$\beta_{cc}(t)$	0.82	0.92	0.82	0.92	0.82	0.92	0.82	0.92
$f_{cm}(28)$	35.41	35.62	29.73	29.95	29.21	29.85	23.96	24.85
Concrete grade	C25/30	C25/30	C20/25	C20/25	C20/25	C20/25	C12/15	C16/20

5. Summary

The compressive strength of cube specimens was evaluated with the destructive method in a strength testing machine used in structural diagnostics. Concrete strength can be evaluated at the early age of the concrete (during construction) as well as later, when in service, during its reconstruction, extension, or while strengthening structural members.

The grade of the concrete manufactured in accordance with the composition provided by the prefabrication plant was the same as that designed. After the modification of the mix composition by weight, the grade in series 1 and 2 of the concrete specimens tested was consistent with grade C20/25, which was also confirmed through the procedure set forth in [1]. Concrete homogeneity in each case was very good. It can therefore be concluded that the provisions of the EC2 standard are formulated in the way that guarantees the correctness of the assessment of concrete strength of the constructed elements of a given structure, which ensures its safety and durability.


The strength and quality of concrete are undoubtedly two of the essential parameters checked in the diagnosis of concrete structures, as they determine the durability of both newly constructed and already existing structures. Failure to ensure proper strength and quality of concrete may lead to failures and construction disasters.

References

- [1] *PN-EN 1992-1-1:2008: Eurokod 2. Projektowanie konstrukcji z betonu. Część 1-1: Reguły ogólne, reguły dla budynków.*
- [2] *PN-EN 1990:2004: Eurokod. Podstawy projektowania konstrukcji.*
- [3] Runkiewicz L., „Ocena trwałości i niezawodności elementów żelbetowych za pomocą metod nieniszczących”, *Materiały budowlane*, 12/2005, no. 400.
- [4] Runkiewicz L., „Zagrożenia, awarie i katastrofy konstrukcji budowlanych”, in *Seminarium „Wybrane problemy wzmocnień i zabezpieczeń konstrukcji żelbetowych”*, Warszawa ITB, 18 January 2019r.
- [5] Runkiewicz L., „O błędach technicznych podczas remontów i modernizacji obiektów budowlanych”, *Inżynieria i Budownictwo*, no. 6/2013.
- [6] *Ustawa z dnia 7 lipca 1994r., Prawo budowlane*, Warszawa, Dz.U. z 2019r. poz. 2170.
- [7] Nagrodzka-Godycka K., *Badanie właściwości betonu i żelbetu w warunkach laboratoryjnych*. Arkady, Warszawa 1999.
- [8] Hoła, J., Bień, J., Sadowski, Ł., & Schabowicz, K., “Non-destructive and semi-destructive diagnostics of concrete structures in assessment of their durability”, *Bulletin of the Polish Academy of Sciences. Technical Sciences*, 63(1), 2015, pp. 87-96.
- [9] Drobiec Ł., Jasiński R., Piekarczyk A., *Diagnostyka konstrukcji żelbetowych. Metodologia, badania polowe, badania laboratoryjne betonu i stali*. PWN, Warszawa 2010.
- [10] Michałowska-Maziejuk D., Raczekiewicz W., „Zastosowanie metody niszczącej i nieniszczącej do oceny wytrzymałości betonu”, in *Różne aspekty jakości materiałów i procesów stosowanych w budownictwie*, Wydawnictwo PŚk, Kielce 2015, T. 70.
- [11] *PN-EN 1542:2000: Pomiar przyczepności przez odrywanie.*
- [12] Łągoda M., *Zalecenia dotyczące wzmocniania konstrukcji mostowych przez przyklejanie zbrojenia zewnętrznego*. IBDIM, Warszawa 2002.
- [13] *PN-EN 12390-2:2001: Badania betonu. Część 2: Wykonywanie i pielęgnacja próbek do badań wytrzymałościowych.*
- [14] Michałowska-Maziejuk D., Teodorczyk M., „The use of a concrete testing machine as teaching equipment in engineering education”, *Aparatura Badawcza i Dydaktyczna*, vol. 23, 2/2018, s. 55-61.
- [15] *PN-EN 12390-4:2001: Badania betonu. Część 4: Wytrzymałość na ściskanie. Wymagania dla maszyn wytrzymałościowych.*
- [16] *PN-EN 12390-3:2002: Badania betonu. Część 3: Wytrzymałość na ściskanie próbek do badania.*
- [17] Piasta J., Piasta W.G., *Beton zwykły. Dobór kruszyw, projektowanie betonu, trwałość betonu, odporność chemiczna i termiczna*. Arkady, Warszawa 1994.

Capillary water absorption in mixtures of cohesive soils stabilized with cement and hydrophobic agent

Szymon Węgliński

*Faculty of Civil and Transport Engineering; Institute of Civil Engineering;
Poznań University of Technology; 5 Piotrowo St., 60-965 Poznań, Poland;
szymon.wegliński@put.poznan.pl  0000-0002-0830-8152*

Abstract: The paper presents the results of research on capillary water absorption of mixtures from cohesive soils – loamy sand and sandy loam – stabilized with cement and the addition of a hydrophobizing agent. The research showed that the appropriate addition of diamidoamine lactate allows to limit the penetration of water inside the stabilized samples, which increases their frost resistance. The mixtures with the additive showed lower capillary water absorption compared to the mixtures stabilized with cement only, especially in the first few hours after soaking with water.

Keywords: stabilization of cohesive soils; a hydrophobizing agent; diamidoamine lactate; frost resistance, capillary absorption

1. Introduction

Due to the problem of weak ground that appears in large numbers in road construction, special attention should be paid to its proper preparation. There are many ways to strengthen the ground (including soil replacement or indirect foundation), which, despite their high efficiency in improving mechanical parameters, generate significant costs. The author believes that in the implementation of construction works, local raw materials and waste materials should be used in the first place. In road construction, such a material, due to low strength parameters (e.g. angles of internal friction or compressibility modules), as well as susceptibility to increased plasticity under the influence of water and volume changes resulting from frost damage, are cohesive soils, which cannot be present in the roadbed.

When water changes from liquid to solid (ice), it increases in volume by approx. 9%. The increase in volume, when water freezes, is not the main cause of blows – it is the formation of ice lenses in the ground. The lenses grow as a result of rising water from damp places or from aquiferous soil (capillary rise phenomenon). The situation occurs when the soil contains a large amount of clay particles and a dusty fraction [1].

A commonly used solution for soil improvement is soil stabilization with hydraulic binders. The most effective method is to stabilize non-cohesive soils with cement. Due to the need to reduce costs during the implementation of investments, it seems beneficial to improve local land, even potentially considered useless.

In the case of cohesive soils, where drainage of water into the depth – due to fine grain-ing and low permeability – is impossible, increasing ice crystals cause uplift of the soil layer. The height of the debris depends on the amount of ice that forms in the ground. The amount of ice depends on the initial soil moisture content, frost exposure time, temperature gradient, grain size, water permeability, thermal conductivity and chemical composition [1], [2]. It is, therefore, important to limit the possibility of water absorption from the surroundings into the cohesive soil layers.

Summarizing the analysis of the literature on the stabilization of cohesive soils [3] – [6], it should be stated that the addition of only cement to the soil as the sole hydraulic binder does not guarantee the compressive strength required by the standard [7]. Moreover, only in a few cases the expected level of frost resistance of the layers was achieved. For binders other than cement, the obtained results are generally worse. The maximum, standard amount of the additive (not more than 10% [7]) does not allow obtaining repeatable results confirming the required compressive strength and frost resistance of the stabilized layer.

Hydrophobizing additives can be used to limit water penetration inside cement-stabilized layers. The researchers started to look for some alternative and high performance materials that are industrially manufactured like crystallising materials, moisture blockers, cementitious coatings and silicate materials [8]. Water-soluble organic silica compounds, i.e. siloxanes, can be used as hydrophobizing agents in the amount of 1%–2% in relation to cement mass [9]. Silane and Siloxane impregnants were one of the first effective hydrophobic treatments to be used for enhancing concrete's impermeability of water and resistance to chemical attacks. Silicate resins is a hydrophobic material that forms a coating in the pores of the concrete and works on repelling water [10]. In addition, more popular are materials extracted from natural resources like natural oils, fatty acids and animal bloods [8]. Sodium acetate, fluoropolymer and silicone resin were an environmentally friendly alternative materials, especially efficient when were applied to wet surfaces [11]. Al-Kheetan et al. suggest that the efficacy of all impregnants determined in relation to moisture content within the concrete is important, which directly ensure the optimal dosage of protective materials, and thus the expected level of protection they could provide [12].

In view of the requirements for the subsoil below the road pavement structure – protection against scaling – the author of the publication proposed the use of an additive to the hydraulic binder in the form of a surfactant – diamidoamine lactate, which was produced from natural raw materials [13]. The publications [14], [15] confirmed the improvement of compressive strength and frost resistance of cohesive soils stabilized with cement with the addition of the above-mentioned hydrophobizing agent. This publication deals with the subject of the susceptibility of cohesive soils stabilized with cement and a hydrophobizing agent to capillary absorption of water from the environment, which results in the formation of heaps destroying surfaces.

2. Materials

The stabilization was carried out on two cohesive soils: loamy sand (Pg) and sandy loam (Gp), which results in the formation of layers that destroy the surface. Both examined cohesive

soils have the same origin, they are the result of the erosion and accumulation of the North Polish continental glacier, the Leszno phase. The main difference is the clay content which determines the soil type – less than 2% for loamy sand and more than 2% for sandy loam. The grain size distribution is shown in Fig 1, and the basic properties are shown in Table 1. The obtained sand indexes confirm their heaping character (according to [16], [17]).

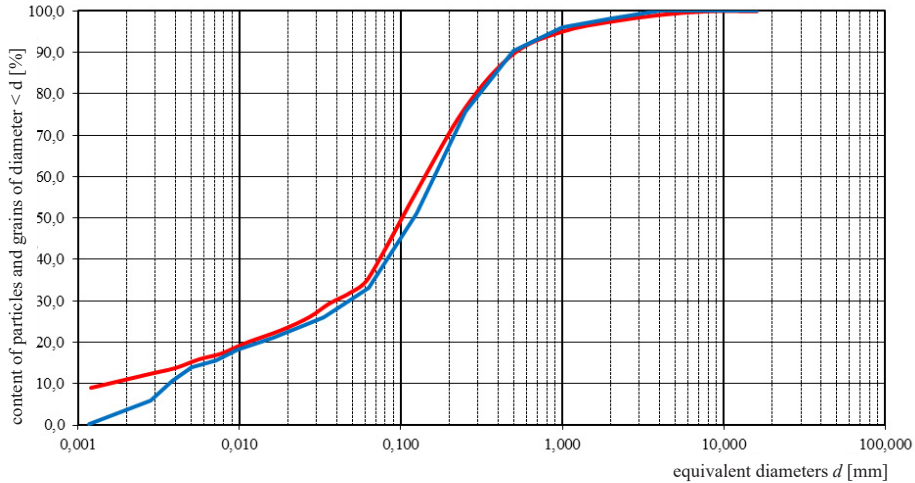


Fig. 1. The particle size distribution curves of the tested soils – red Gp, blue Pg

Table 1. Properties of the investigated soils

	Values		Values
Loamy sand:		Sandy loam:	
clay fraction content [%]	3.4	clay fraction content [%]	11.0
yield point [%]	14.6	yield point [%]	12.0
liquidity limit [%]	21.5	liquidity limit [%]	25.7
plasticity index [%]	6.9	plasticity index [%]	13.7
sand indicator [-]	17	sand indicator [-]	8
optimal humidity [%]	10.0	optimal humidity [%]	10.7
maximum bulk density [g/cm ³]	2.00	maximum bulk density [g/cm ³]	2.01
soil pH	7.13	soil pH	7.95

Common cement CEM II B-S 32.5 R, meeting the requirements of the standard [18], was used as a hydraulic binder for the tests. Cement was chosen because of the popularity of its practical application on construction sites, as it is often used in road construction as a stabilizing binder. The setting time of the cement was 121 minutes, and its average compressive strength, determined after 28 days of hardening, was 47.5 ± 0.6 MPa. The hydrophobizing additive was made with the use of waste fats – used vegetable and animal oils. The process of obtaining diamidoamine lactate is shown in Fig 2.

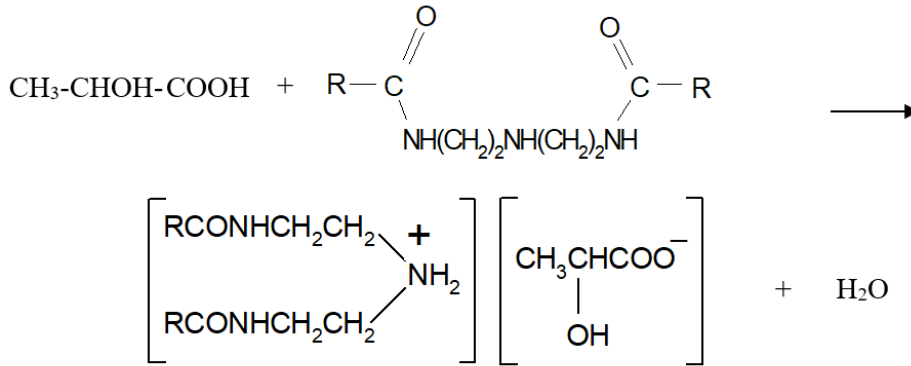


Fig. 2. Scheme of the reaction for the preparation of diamidoamine lactate. *Source:* [13]

The cement addition ranged from 5% to 9% with respect to the dry mass of the soil. Due to the exploratory – pilot nature of the research (diamidoamine lactate was used for the first time as an additive for soil hydrophobization), the amount of lactate was added alternatively, ranging from 3% to 9% in relation to dry weight. From among the prepared mixtures for capillary water absorption tests, the ones that achieved the highest frost resistance indexes in individual groups were selected (see Table 2 [19]).

Table 2. The values of compressive strength and frost resistance indexes of the tested mixtures. *Source:* [19]

	Mark	Compressive strength [MPa] after the period			frost resistance [-]
		7 days	28 days	28 days (after 14 frozen cycles)	Indicator
loamy sand mixtures	7%C	2.14	2.79	1.45	0.52
	7%M-7%C	2.24	3.62	1.27	0.35
	9%M-7%C	2.23	3.69	1.03	0.28
	9%C	3.15	4.06	2.21	0.54
	3%M-9%C	2.56	4.65	3.52	0.76
	5%M-9%C	2.07	3.25	2.45	0.75
sandy loam mixtures	7%C	2.01	2.37	0.15	0.06
	3%M-7%C	1.72	2.95	1.60	0.54
	5%M-7%C	1.16	1.94	0.66	0.34
	7%M-7%C	1.42	2.75	0.55	0.20
	9%C	2.37	4.59	0.46	0.10
	3%M-9%C	1.87	3.15	1.91	0.61
	5%M-9%C	2.23	3.15	1.00	0.32
	7%M-9%C	2.31	3.62	1.55	0.43

3. Capillary water absorption studies

Polish standards for soil stabilized with cement [7], [20], [21] do not require or define capillary water absorption studies. The methodology of determining capillarity is commonly used in the case of testing masonry elements [22], [23]. The test algorithm was taken from the PN-EN 772-11:2011 standard [24]. The following materials and research devices were used for the measurements:

- ventilated dryer with the possibility of maintaining the temperature in the range of $105 \pm 5^\circ\text{C}$,
- vessels (steel sheets) with a depth greater than 20 mm,
- stopwatch,
- potable water,
- laboratory balance with an accuracy of 0.1 g.

After drying to constant weight and cooling to room temperature, the samples were immersed in the vessels to a depth of 5 ± 1 mm. The immersion depth was kept constant during the tests.

Water absorption measurement periods were assumed, counted from the moment of immersion of the samples in water: 10 min (600 s), 30 min (1 800 s), 60 min (3 600 s), 3 h (10 800 s), 8 h (28 800 s), 24 h (86 400 s), 48 h (1 72 800 s), 72 h (259 200 s), 96 h (345 600 s), 120 h (432 000 s).

Before each mass measurement (after the specified saturation time), the sample was dried with a chamois leather.

The coefficient of water absorption due to the rising capillary was calculated in accordance with the standard [24], according to the Eq. 1:

$$C_{ws} = \frac{m_{so,s} - m_{dry,s}}{A_s \sqrt{t_s}} \quad (1)$$

where: $m_{dry,s}$ is a sample weight after drying [g], $m_{so,s}$ is a mass of the soaked sample at time t [g], A_s is sample surface immersed in water [m^2], t_s is saturation time [s], C_{ws} is water absorption coefficient [$\text{g}/(\text{m}^2\text{s}^{0.5})$].

14 soil mixtures stabilized with cement, 6 mixtures made of clay sand and 8 mixtures of sandy loam were tested. Each test series consisted of 3 samples for which the mean capillary absorption as a function of the element of the immersion time was calculated and the mean water absorption after selected measurement periods was determined.

4. Research results and their analysis

4.1. Macroscopic evaluation during research

The samples, dried at the temperature of $105\text{-}110^\circ\text{C}$, were immersed at 5 ± 1 mm in water and subjected to water capillary rising tests. Along with the increasing time of soaking in water, changes in the saturation level of the samples were visible (see Figs 3-6).



Fig. 3. Capillarity test – view 3 hours after immersion – Pg mixtures



Fig. 4. Capillarity test – view 24 hours after immersion – Pg mixtures



Fig. 5. Capillarity test – view after 3 hours from immersion – Gp mixtures



Fig. 6. Capillarity test – view 24 hours after immersion – Gp mixtures

Mixtures in which, in addition to cement, diamidoamine lactate was added, compared to the reference (cement) mixes absorbed water much slower. In the case of mixtures made of loamy sand, water penetrated much faster along the entire height of the sample. Sandy loam mixtures – due to their higher cohesiveness than loamy sand – which are also characterized by lower water permeability, absorbed water much slower. Moreover, samples into which water had penetrated to its full height showed drying and peeling of the edge of the upper surface

4.2. Loamy sand mixtures

The course of changes in the mass of the samples related to their surface area in contact with water as a function of the square root of time is illustrated in Figs 7 and 8.

Water absorption caused by capillary rise depending on the amount of binder used after selected measurement periods is shown in Figs 9 and 10.

The capillary rise of water increases, as well as the values of the amount of water absorbed (see Figs 9 and 10) presented in Figs 7 and 8, allow to conclude that the addition of diamidoamine lactate limits the possibility of capillary rising of water in soils stabilized with cement, especially in the initial absorption period (up to 8 hours). Later in the test, when the sample is saturated with water, the amount of water pulled up is comparable for all mixtures. The addition of lactate in an amount of less than 60% of the binder quantity reduces the amount of water absorbed in the initial period by almost three times. In the case of significant addition of a hydrophobizing agent (more than the hydraulic binder), lactate increased the absorption. The above may be caused by too high affinity for water (lactate is a 10% solution of the active substance in water). Referring to the frost resistance results, it should be noted that the mixtures characterized by lower capillarity obtained higher frost resistance.

4.3. Sandy loam mixtures

The course of the sample mass change in relation to their surface area in contact with water as a function of the square root of time is illustrated in Figs 11 and 12.

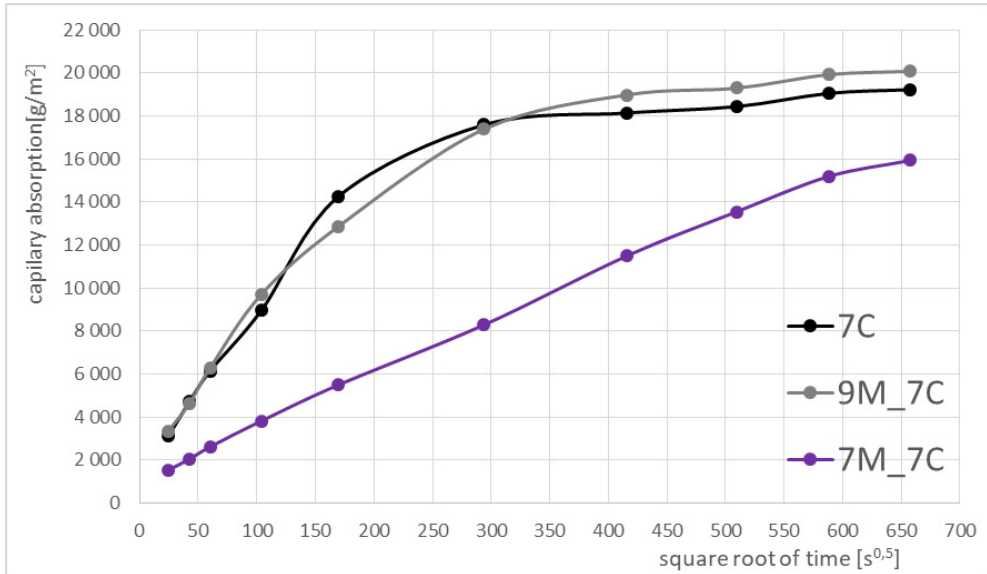


Fig. 7. Graph of capillary absorption of Pg mixtures with 7% binder content and optional addition of diamidoamine lactate

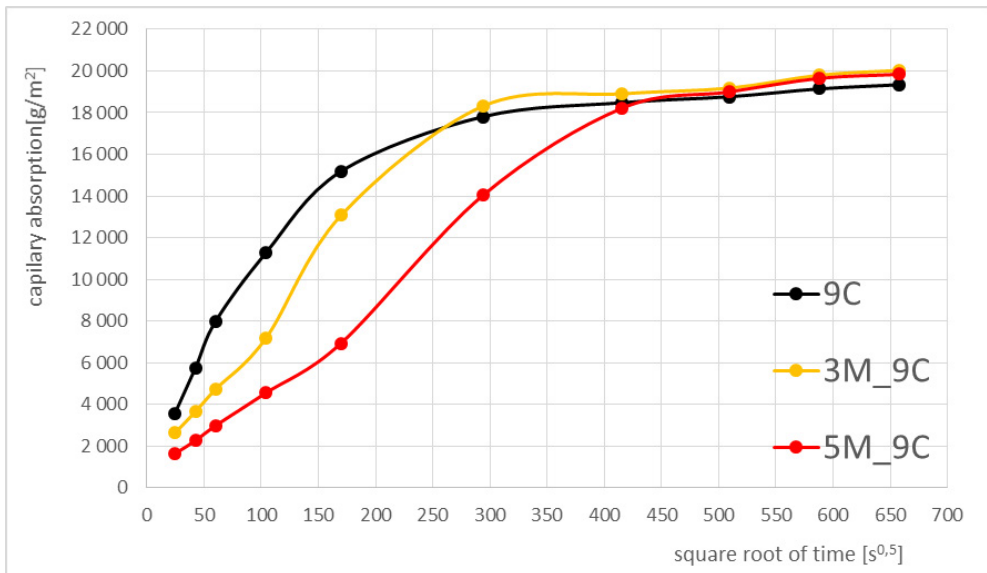


Fig. 8. Graph of capillary absorption of Pg mixtures with 9% binder content and optional addition of diamidoamine lactate

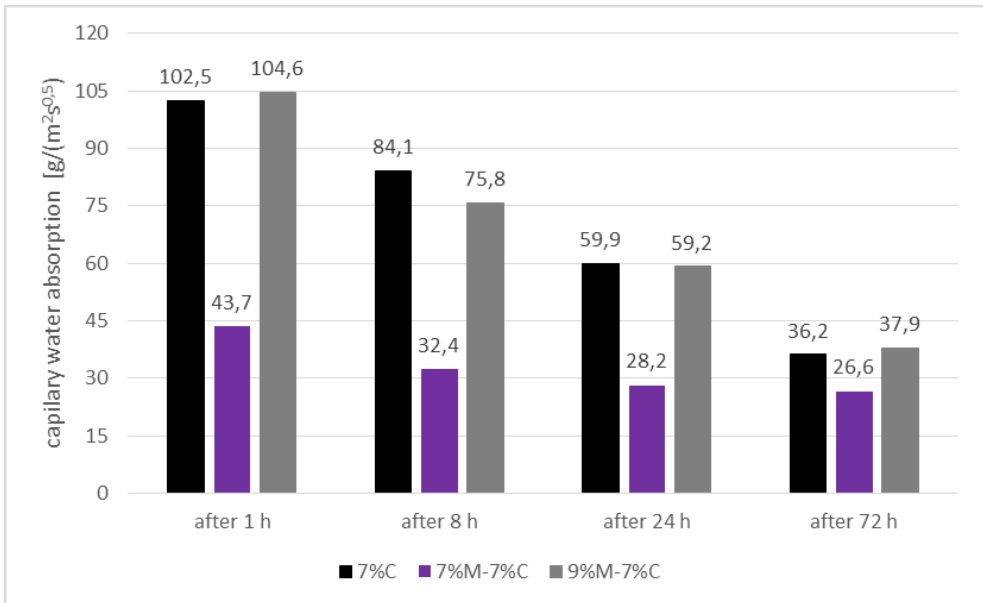


Fig. 9. Capillary water absorption values of Pg mixtures with 7% binder addition for selected measurement periods

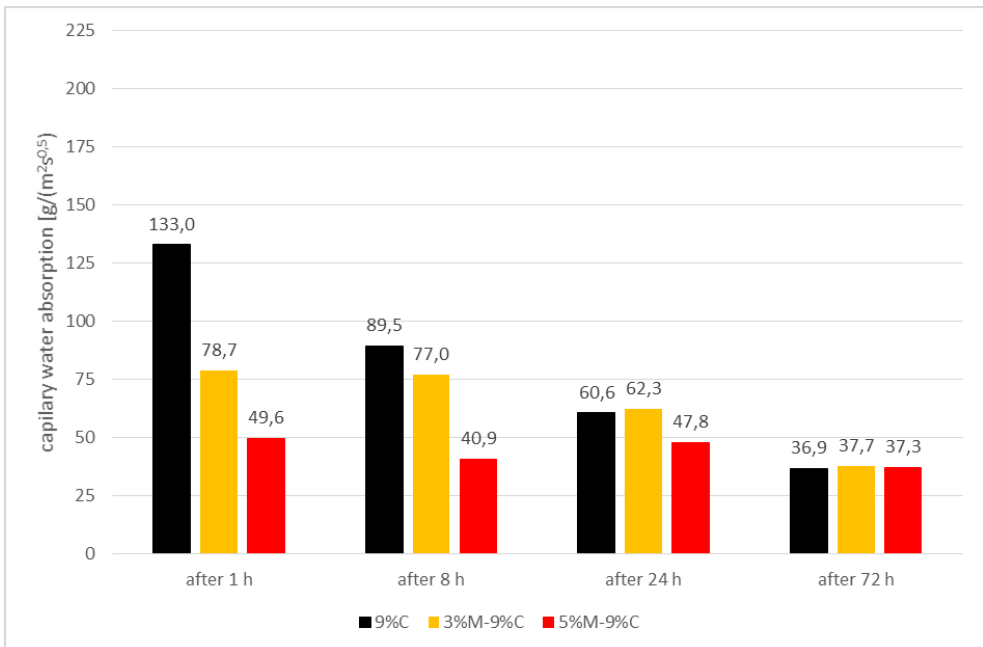


Fig. 10. Capillary water absorption values of Pg mixtures with 9% binder addition for selected measurement periods

Water absorption of sandy loam mixtures caused by capillary rise depending on the amount of binder used after selected measurement periods is shown in Figs 13 and 14

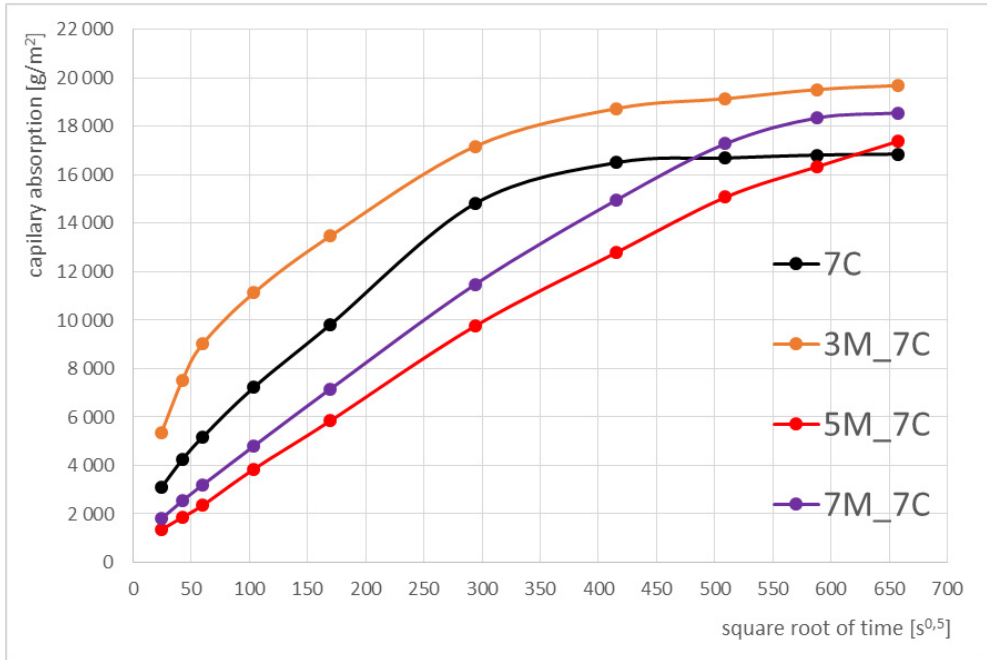


Fig. 11. Graph of capillary absorption of Gp mixtures with 7% binder content and optional addition of diamidoamine lactate

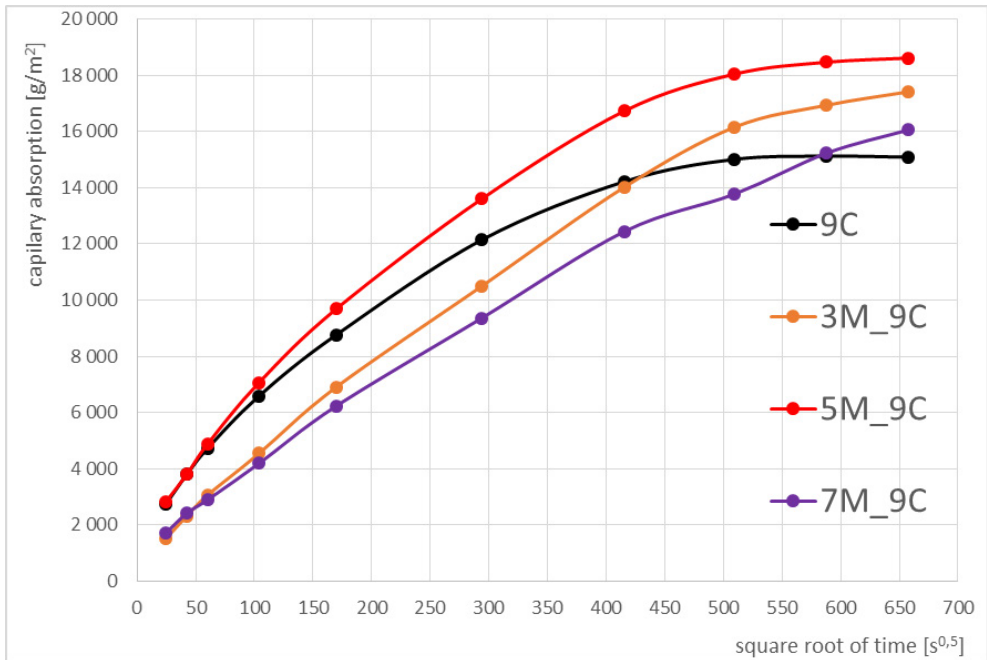


Fig. 12. Graph of capillary absorption of Gp mixtures with 9% binder content and optional addition of diamidoamine lactate

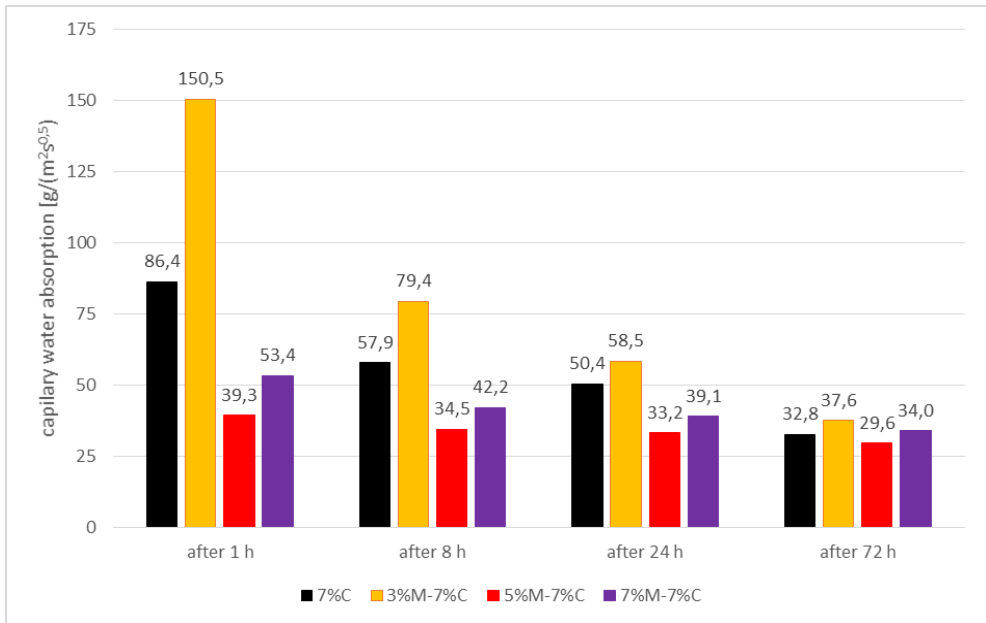


Fig. 13. Capillary water absorption values of Gp mixtures with 7% binder addition for selected measurement periods

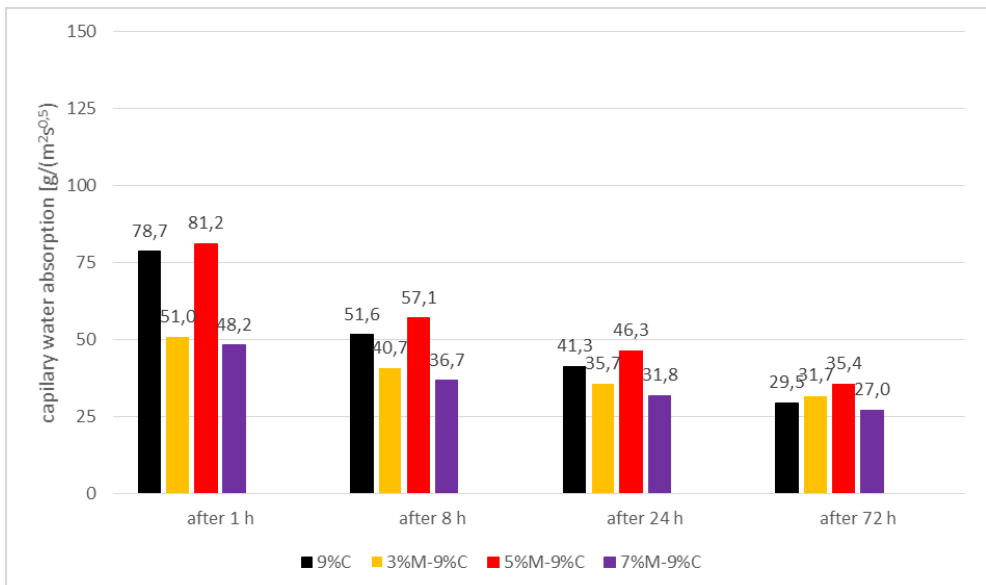


Fig. 14. Capillary water absorption values of Gp mixtures with 9% binder addition for selected measurement periods

When analyzing the illustrated increases in capillary rise of water and the amount of water absorbed, it should be noted that in the case of mixtures with 7% cement addition only 5% and 7% addition of diamidoamine lactate allowed to obtain a lower capillarity of the tested

samples. In the case of mixtures with 9% cement content, the addition of a hydrophobizing agent in the amount of 3% and 7% allowed to reduce capillary absorption. Compared to loamy sand mixtures, it cannot be clearly determined what amount of additive is optimal to limit capillary water absorption of loam clay mixtures.

5. Conclusions

In road construction, an important aspect of proper substrate preparation is ensuring its frost resistance. Due to the molecular structure and low water permeability, cohesive soils should not be present in the frost zone. By using soil stabilization with hydraulic binders, we can increase their bearing capacity and improve frost resistance. The recommended, standard amounts of hydraulic binder do not allow for high frost resistance parameters for cohesive soils. Improvement in the frost resistance indices was found in the case of the addition of diamidoamine lactate as a hydrophobizing agent. In order to evaluate the effect of the hydrophobizing additive, studies of capillary water absorption of the mixtures stabilized in this way were undertaken. Due to the lack of typical methods of assessing capillary water absorption by soil mixtures stabilized with a binder, the author of the publication proposed a methodology taken from the study of masonry elements.

For loamy sand, the reduction of water penetration was observed with the addition of a hydrophobizing agent in an amount not exceeding 5% of the dry soil mass. The mixtures were characterized by lower water absorption, especially in the first hours after soaking with water, which means that the stabilized mixture will absorb water slower from the environment immediately after execution. For mixtures made of sandy loam, which is a more cohesive soil with a higher content of clay particles, which have an impact on low water permeability, it was observed that water penetrates slower inside the samples. The addition of a hydrophobizing agent reduces capillary water absorption, but the exact relationship between the amount of additive and the possibility of reducing water capillary rise cannot be determined. Unlike loamy sand mixes, higher amounts of hydrophobizing agent additive reduce water ingress inside the mix.


References

- [1] Wiłun Z., *Zarys geotechniki*, Warszawa: WKiŁ, 2013
- [2] Rafalski L., Wilczek J., Kraszewski C., „Ochrona przeciwmrozowa nawierzchni drogowych na przykładzie wybranych krajów”, *Drogownictwo*, no. 2, (2014), pp. 39-45.
- [3] Cyske W. and Kluska I., „Porównanie właściwości wybranych środków do stabilizacji gruntów na budowie autostrady A1”, *Drogi i mosty*, vol. 6, no. 1, (2007), pp. 5-17.
- [4] Glinicka M., „Właściwości geotechniczne gruntów spoistych z terenu Białegostoku wzmocnianych cementem lub wapnem”, *Drogi i mosty*, vol. 5, np. 4, (2006) pp. 23-39.
- [5] Kamiński B., „Bezpieczna dla środowiska stabilizacja cementem portlandzkim leśnych gruntów drobnoziarnistych”, *Zarządzanie Ochroną Przyrody w Lasach*, vol. 2, (2008), pp. 272-278.
- [6] Porszke A., „Analiza właściwości gruntów stabilizowanych spoiwem Silment CQ-25 w różnych warunkach pielęgnacji próbek-artykuł dyskusyjny”, *Drogownictwo*, no. 9-10, (2006), pp 318-320.
- [7] *PN-S-96012:1997 “Roads – Subbase and subgrade of cement stabilised soils”*
- [8] Al-Kheetan M.J., Rahman M.M., Chamberlain D.A., “Moisture evaluation of concrete pavement treated with hydrophobic surface impregnants”, *International Journal of Pavement Engineering*, vol. 21, no. 14, (2020), pp. 1746-1754. <https://doi.org/10.1080/10298436.2019.1567917>

- [9] Suchorab Z., Barnat-Hunek D., Franus M., Lagod G.: "Mechanical and Physical Properties of Hydrophobized Lightweight Aggregate Concrete with Sewage Sludge", *Materials*, vol. 317, no. 9, (2016), pp 1-18. <https://doi.org/10.3390/ma9050317>
- [10] Dai J.G., Akira Y., Wittmann F.H., Yokota H., Zhang P., "Water repellent surface impregnation for extension of service life of reinforced concrete structures in marine environments: the role of cracks", *Cement and Concrete Composites*, vol. 32, no. 2, (2010), pp. 101–109. <https://doi.org/10.1016/j.cemconcomp.2009.11.001>
- [11] Al-Kheetan M.J., Al-Tarawneh M.A., Ghaffar S.H., Chougan M., Jweihan Y.S., Rahman M.M., "Resistance of hydrophobic concrete with different moisture contents to advanced freeze–thaw cycles", *Structural Concrete*, vol. 22, no. S1, (2021) pp. 1-12. <https://doi.org/10.1002/suco.202000214>
- [12] Al-Kheetan M.J., Rahman M.M., Balakrishna M.N., Chamberlain D.A., "Performance enhancement of self-compacting concrete in saline environment by hydrophobic surface protection", *Canadian Journal of Civil Engineering*, vol. 46, no. 8, (2019), pp. 677-686. <https://doi.org/10.1139/cjce-2018-0546>
- [13] Babiak M., Kosno J., Węgliński S., Jaszkievicz, A., "Research on the influence of a hydrophobizing agent based on amidoamines on frost resistance and durability of cohesive soils", *Przemysł chemiczny*, vol. 95, no. 11, (2016) pp. 2376-2379. <https://doi.org/10.15199/62.2016.11.48>
- [14] Babiak M., Kosno J., Węgliński, S., „Ekologiczny środek do stabilizacji gruntów spoistych zwiększający ich wytrzymałość i mrozoodporność”, *Materiały budowlane*, no. 2, (2017), pp. 24-26. <https://doi.org/10.15199/33.2017.02.06>
- [15] Błaszczyński T., Babiak M., Kosno J., Węgliński S., "Freeze-thaw Resistance and Increased Strength of Cohesive Soils Modified with a Cationic Surfactant", *Procedia Engineering*, vol. 172, (2017), pp. 111-118. <https://doi.org/10.1016/j.proeng.2017.02.032>
- [16] *Katalog typowych konstrukcji nawierzchni podatnych i półsztywnych*, Generalna Dyrekcja Dróg Krajowych i Autostrad, Warszawa: 2014
- [17] *PN-S-02205: 1998 "Roads – Earthwork – Specifications and testing"*
- [18] *PN-EN 197-1: 2012 "Cement – Part 1: Composition, specifications and conformity criteria for common cements"*
- [19] Węgliński S., "The effect of hydraulic road binders and cement with diamidoamine lactate additive on the compressive strength and freeze-thaw resistance of cohesive soils", *Cement, Lime, Concrete*, vol. 25, no. 6, (2020), pp. 432-443. <https://doi.org/10.32047/cwb.2020.25.6.1>
- [20] *PN-EN 14227-10:2006 "Hydraulically bound mixtures – Specifications – Part 10: Soil treated by cement"*
- [21] *PN-EN 14227-15: 2015-12 "Hydraulically bound mixtures – Specifications – Part 15: Hydraulically stabilized soils"*
- [22] Garbalińska H., Głowacka A., „Symulacyjne badania dotyczące rozprzestrzeniania się zawilgocenia kapilarnego w ścianach z bloczków silikatowych”, *Polska Energetyka Słoneczna*, vol. 43, no. 1-4, (2015), pp. 55-58.
- [23] Garbalińska H., Cederholm A., „Współczynnik sorpcji betonu komórkowego badany na próbkach suszonych i niesuszonych”, *Czasopismo Inżynierii Lądowej, Środowiska i Architektury*, vol. 61, no. 3/II, (2014), pp. 163-172.
- [24] *PN-EN 772-11:2011 "Methods of test for masonry units – Part 11: Determination of water absorption of aggregate concrete, autoclaved aerated concrete, manufactured stone and natural stone masonry units due to capillary action and the initial rate of water absorption of clay masonry units"*

The influence of internal installation solutions in single-family housing on the “EP” factor in light of the new requirements of WT 2021

Aneta Biała

*Division of Engineering in Architecture; Institute of Architecture and Spatial Planning;
Faculty of Architecture; Poznań University of Technology;
2 Jacka Rychlewskiego St., 61-131 Poznań, Poland;
aneta.biala@put.poznan.pl  0000-0002-8967-046X*

Abstract: The first part of the article presents the upcoming changes in the regulations regarding energy consumption by single-family housing. Current and forthcoming requirements in 2021 for building insulation and maximum *EP* primary energy demand factor were indicated. The second part of the paper presents the results of research aimed at determining what type of heat source for heating purposes and the type of ventilation will be able to meet the latest requirements. The analysis was based on the determination and comparison of the *EP* factor in the considered single-family building for selected heating variants assuming two different types of ventilation: gravitational and mechanical supply-exhaust with a heat recovery system. Based on the results obtained, an attempt was made to determine the tendency of changes in the design of single-family buildings in terms of choosing the type of heating and ventilation.

Keywords: energy consumption, building energy efficiency, energy performance

1. Introduction

Due to more and more intensive development of the building industry, more and more attention is focused on its energy efficiency, i.e., above all, on reducing its energy consumption. The instrument in this assessment is the energy characteristics, including the annual rate of demand for non-renewable primary energy (*EP*), taking into account losses arising at the stage of energy production and transmission [1].

From 2021 on, designers will have to face new requirements for buildings known as WT 2021. They will have a significant impact on many architectural, construction and installation solutions, especially those related to the choice of heating system. Currently, most of the energy used for heating and domestic hot water (DHW) is supplied from non-renewable sources, which have a significant negative impact on the environment and increase the operating costs of the systems [2]. In order to reduce the building’s primary energy demand, in addition to reducing

the heat transfer coefficient U [$W/(m^2K)$] of the building envelope, renewable energy sources such as heat pumps, photovoltaic cells or standard systems are increasingly being used, but with higher efficiency than traditional ones, such as condensing gas boilers [3].

The article attempts to assess the extent to which changes will have to be made to the architecture of single-family housing. It focuses on examining what installation solutions, including the energy source and type of ventilation, will be able to meet the new WT 2021 requirements for maximum primary energy demand (EP). The energy performance-based indicator of the annual design primary energy demand of the building for heating, ventilation and domestic hot water preparation was used for the analysis.

2. Overview of regulations

The continuous economic development of many countries results in a constantly increasing demand for energy, of which over 40% is consumed by the construction sector [2], [4]. The main sources of fuel are non-renewable resources, including hard coal, oil and natural gas. Fossil fuels are the main source of carbon dioxide emissions and pose a real threat to the natural environment, therefore a number of measures have been taken throughout the European Union to reduce the demand and consumption of primary energy, mainly by promoting renewable energy sources [2], [5].

The first document on improving energy efficiency and energy labelling in the field of construction was Directive 2002/91/EC of the European Parliament and Council of 16 December 2002 on energy performance [6]. It resulted in the introduction in all EU member states of the obligation to carry out energy certificates for newly built, modernized or sold facilities. This was primarily aimed at improving the comfort of use and operation of facilities. Currently, from 1 January 2013, Directive 2010/31/EU of the European Parliament and Council (EU) of 19 May 2010 on the energy performance of buildings ($EPBD$) is in force [7]. The implementation of the regulations of the $EPBD$ directive in Poland was carried out through the Act on Energy Characteristics [8] as well as through the amendment of the Regulation of the Minister of Infrastructure on technical conditions to be met by buildings and their location of 5 July 2013 [9]. Its amendment assumed the introduction of restrictions gradually, in three stages. The first stage was implemented from January 2014, the second from January 2017 and the last one will be effective from the end of December 2020. The changes of selected limit values of the heat transfer coefficient and the maximum EP coefficient for heating, ventilation and domestic hot water preparation for single-family buildings are presented in Table 1.

Table 1. Heat transfer coefficients of building partitions [9]

	Before 2014	From 2014	From 2017	From 2021
Value of the heat transfer coefficient of building partitions U [W/m^2K]				
External walls	0.30	0.25	0.23	0.20
Flat ceilings, roofs	0.30	0.20	0.18	0.15
Floor on the ground	1/1.5	0.30	0.30	0.30
Partial maximum values of $EPH+W$ ratio for heating, ventilation and hot water preparation [$kWh/(m^2 - year)$].				
Single-family building	-	120	95	70

The first significant change in the amendment of the technical conditions was the tightening of the requirements for the heat transfer coefficient for building partitions U [$\text{W}/\text{m}^2\text{K}$]. Before 2014, all external partitions, including walls and roofs, had to have a maximum U -value of $0.30 \text{ W}/\text{m}^2\text{K}$, while the floor on the ground was marked with a minimum resistance R of $1.5 \text{ m}^2\text{K}/\text{W}$. Gradually, these indices were reduced to be $0.20 \text{ W}/\text{m}^2\text{K}$ for external walls, $0.15 \text{ W}/\text{m}^2\text{K}$ for ceilings/roofs and $0.30 \text{ W}/\text{m}^2\text{K}$ for floors on the ground at the end of December 2020. As a result of the introduced changes, it will be necessary to use better quality materials, with better thermal insulation properties and increased thickness of the insulation layer.

Another significant change was the introduction from 2014 of a new indicator – annual calculated primary energy demand for a building for heating, ventilation and domestic hot water preparation – EP [$\text{kWh}/\text{m}^2\text{-year}$] and its limit value depending on the type of building. Based on the parameters of the external environment, building architecture and the adopted building and installation solutions, the amount of energy required to cover the demand for heating and ventilation ($Q_{\text{P,H}}$), domestic hot water preparation ($Q_{\text{P,W}}$), air conditioning, cooling ($Q_{\text{P,C}}$) and lighting of the building ($Q_{\text{P,L}}$) is determined according to the formula below. (1) [8]

$$Q_{\text{P}} = Q_{\text{P,H}} + Q_{\text{P,W}} + Q_{\text{P,C}} + Q_{\text{P,L}} \text{ [kWh]} \quad (1)$$

In the case of single-family housing, the first two components are taken into account, namely: energy for heating and ventilation as well as for domestic hot water preparation $Q_{\text{P,H+W}}$. According to WT 2021, all newly designed single-family buildings should have the maximum value of $EP_{\text{H+W}}$ demand reduced to $70 \text{ kWh}/(\text{m}^2\text{-year})$. In comparison with the restrictions introduced in 2014, this value is lower by over 40%. In order to meet the new criteria, it will probably be necessary to move away from traditional heat sources and increase the share of renewable energy sources, as well as to use more and more efficient ventilation devices [10].

Single-family construction is characterized by the least restrictive requirements for energy performance and, consequently, great freedom in choosing the heat source. According to the statistics of the Central Statistical Office (GUS), in 2018 the most popular heat sources in the residential construction industry were solid fuels (45.4%) and network heat (40.4%), followed by natural gas (13.9%), electricity (5.3%), liquid fuels (0.5%) and renewable energy sources (0.13%) [11]. However, less than 10% of them were equipped with ventilation devices with heat recovery.

In connection with the approaching change in the energy efficiency requirements for buildings, it is necessary to analyze the factors that make it possible to meet them. The article focuses on analyzing how the new requirements of the maximum value of the EP coefficient will affect the possibility of using specific solutions of internal installations, including heat sources for heating, ventilation and DHW as well as the type of ventilation.

3. Research method – thermal model of the building

In order to carry out the analysis, a simplified design of a single-family building was adopted as a calculation model, which is presented in Fig. 1. The building was designed on a $10 \times 10 \text{ m}$ rectangular projection, with two overground storeys with a flat roof covered with tar paper, made in traditional brick technology from Porotherm 25 $P+W$ hollow blocks. The cubic capacity of the building is 600 m^3 and the usable area is 140 m^2 . The location of the

building in relation to the sides of the world was adopted according to the principle of entrance from the north and larger glazing from the south.

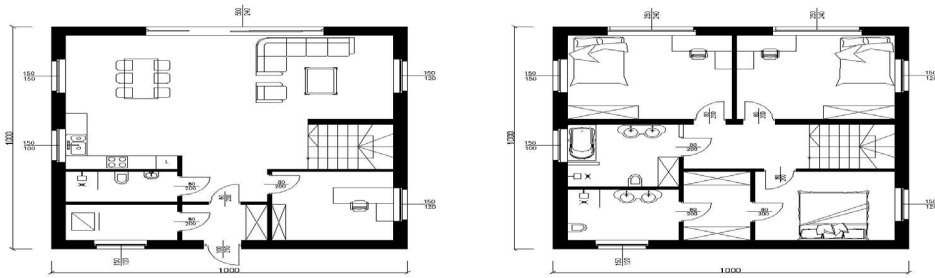


Fig. 1. Simplified plan of the building source: own study

For the purposes of calculations, the maximum values of heat transfer coefficients of individual building partitions have been assumed in accordance with the guidelines of technical conditions, which will be in force from 2021, while thermal bridges have been omitted due to their low impact on the final EP value. The windows were assumed to be 3-chamber windows with high tightness class. The building is located in the city surrounded by other buildings of similar height. Detailed data are presented in Table 2.

Table 2. Heat transfer coefficients of analyzed building partitions [8]

Type of partition	Heat transfer coefficient U [W/m ² K]
External wall	0.20
Floor on the ground	0.30
Roof	0.15
External window	0.9
Front door	1.3

The aim of this article is to present the possibility of the analyzed building to meet the maximum primary energy consumption coefficient depending on the heat source used for heating, ventilation and hot water. Therefore, the most popular variants of heat sources such as: hard coal, natural gas, electricity, heating oil, biomass boilers, heat from a CHP plant* and a heat pump were adopted for the analysis. Each variant has been calculated in two versions, the first one assumes gravitational ventilation of the object, while the second one assumes mechanical supply and exhaust ventilation with heat recovery of 80%. In addition, each variant was calculated on the assumption that 50% of energy will be drawn from photovoltaic panels. Detailed characteristics of the proposed variants are presented in Table 3.

Table 3. General characteristic of considered variants

Variant	Type of fuel	Characteristics	Type of ventilation
I.A	Natural gas 100%	$w_{i, \text{gas}} = 1.1 \eta_{\text{tot, gas}} = 0.84$	Gravitational
I.B			Mechanical
I.C	Natural gas 50%	$w_{i, \text{gas}} = 1.1 \eta_{\text{tot, gas}} = 0.84$	Gravitational
I.D	Solar energy 50%	$w_{i, \text{solar}} = 0 \eta_{\text{tot, solar}} = 0.89$	Mechanical
II.A	Heating oil 100%	$w_{i, \text{oil}} = 1.1 \eta_{\text{tot, oil}} = 0.84$	Gravitational
II.B			Mechanical
II.C	Fuel oil 50%	$w_{i, \text{oil}} = 1.1 \eta_{\text{tot, oil}} = 0.84$	Gravitational
II.D	Solar energy 50%	$w_{i, \text{solar}} = 0 \eta_{\text{tot, solar}} = 0.89$	Mechanical
III.A	Hard coal 100%	$w_{i, \text{coal}} = 1.1 \eta_{\text{tot, coal}} = 0.84$	Gravitational
III.B			Mechanical
III.C	Hard coal 50%	$w_{i, \text{coal}} = 1.1 \eta_{\text{tot, coal}} = 0.84$	Gravitational
III.D	Solar energy 50%	$w_{i, \text{solar}} = 0 \eta_{\text{tot, solar}} = 0.89$	Mechanical
IV.A	Biomass (wood, pellet) 100%	$w_{i, \text{biomass}} = 0.2 \eta_{\text{tot, biomass}} = 0.62$	Gravitational
IV.B			Mechanical
IV.C	Biomass (wood, pellet) 50%	$w_{i, \text{biomass}} = 0.2 \eta_{\text{tot, biomass}} = 0.62$	Gravitational
IV.D	Solar energy 50%	$w_{i, \text{solar}} = 0 \eta_{\text{tot, solar}} = 0.89$	Mechanical
V.A	Electricity 100%	$w_{i, \text{electric}} = 3 \eta_{\text{tot, electric}} = 0.87$	Gravitational
V.B			Mechanical
V.C	Electricity 50%	$w_{i, \text{electric}} = 3 \eta_{\text{tot, electric}} = 0.87$	Gravitational
V.D	Solar energy 50%	$w_{i, \text{solar}} = 0 \eta_{\text{tot, solar}} = 0.89$	Mechanical
VI.A	Heat pump 100%	$w_{i, \text{pump}} = 0 \eta_{\text{tot, pump}} = 0.87$	Gravitational
VI.B			Mechanical
VI.C	Heat pump 50%	$w_{i, \text{pump}} = 0 \eta_{\text{tot, pump}} = 0.87$	Gravitational
VI.D	Solar energy 50%	$w_{i, \text{solar}} = 0 \eta_{\text{tot, solar}} = 0.89$	Mechanical
VII.A	District heat 100%	$w_{i, \text{unit}} = 0.8 \eta_{\text{tot, unit}} = 0.87$	Gravitational
VII.B			Mechanical
VII.C	District heat 50%	$w_{i, \text{unit}} = 0.8 \eta_{\text{tot, unit}} = 0.87$	Gravitational
VII.D	Solar energy 50%	$w_{i, \text{solar}} = 0 \eta_{\text{tot, solar}} = 0.89$	Mechanical

w_i – coefficient of input of non-renewable primary energy for the generation and delivery of the final energy carrier to the building,
 η_{tot} – average total seasonal efficiency of the system

The research assumed the following unchanging climatic, location and operating data for the variants:

- climate classification: II,
- location: Poznań,
- outside air temperature: -18°C ,
- building shading: a building in the city surrounded by buildings of similar height,
- indoor temperature: 20°C ,
- ventilation air stream: $200 \text{ m}^3/\text{h}$ – calculated with a simplified method based on [9],
- coefficient of solar radiation permeability through glazing $g=0.75$,
- unit daily water consumption: $\text{VCW} = 1.4 \text{ dm}^3/\text{m}^2 \text{ day}$,
- type of receiver: underfloor water heating with central and local regulation with a two-joint or proportional regulator P .

For the purpose of the analysis, it was assumed that the demand for domestic hot water of 5735.06 kWh/year is provided by the same source as the heating. Depending on the energy source, the corresponding type of heat source was selected as shown in Table 4.

Table 4. Summary of the heat source depending on the type of energy

Energy source	Type of heat source
Natural gas	Low-temperature gas condensing boilers (55/45°C) with nominal output up to 50 kW
Heating oil	Indoor oil furnaces
Hard coal	Coal boilers manufactured after 2000.
Biomass (wood, pellet)	Biomass boilers (wood: billets, briquettes, pellets, chips)
Electricity	Electrothermal heaters
Heat pump	Glycol/water heat pumps (55/45°C), compression-type, electro-powered
District heat	Compact district heating unit with casing with nominal output up to 100 kW

4. Research results

For the examined object the analysis of the primary energy demand (*EP* index) was carried out, depending on individual variants I-VII. The value of the *EP* index below 70 kWh/(m²-year) was assumed as the criterion. It was determined by means of a simplified method of calculating the heat demand of the building, using the Regulation of the Minister of Infrastructure and Development on the methodology of determining the energy performance of a building or part of a building and energy performance certificates [8].

The following graphs show the calculated primary energy demand calculated in 2 stages.

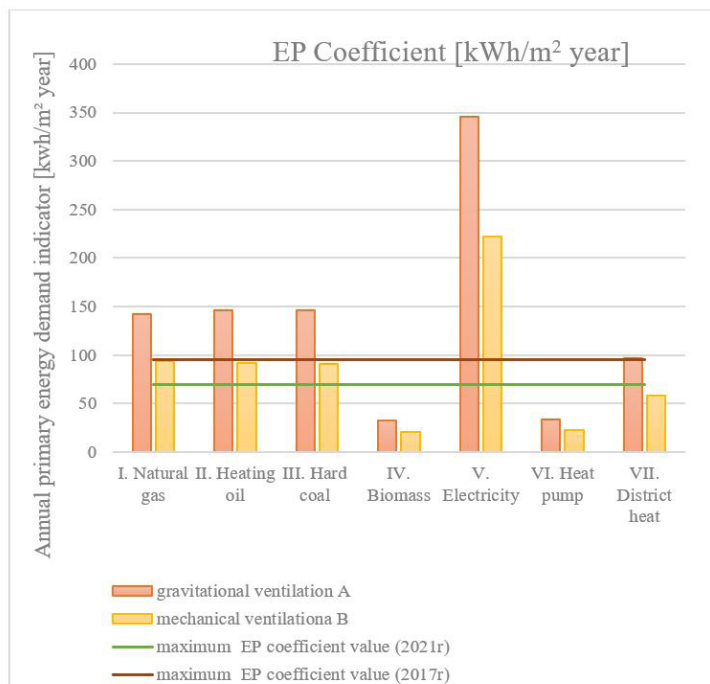


Fig. 2. Primary Energy coefficient (*EP*) for different types of source of heat

The first part of the study focused on the comparison of *EP* index for variants I-VII. A, I-VII. B, i.e. in which the heat demand is provided in 100% by one source. The data are presented in Fig. 2. Each fuel type was calculated with the assumption of natural ventilation – A and mechanical ventilation with heat recovery – B. The green line in the graph indicates the limit value of the *EP* index (70 kWh/m² year) required from 2021, while the red line indicates the current limit value (95 kWh/m² year). Analyzing the above graph it can be seen that in the case of fossil and liquid fuels (variants I-III), with the regulations in force, only the variant with mechanical ventilation ensures that the maximum *EP* indicator is met at the borderline, while from 2021 no variant from I-III, regardless of the type of ventilation, will meet the requirements. Mains heat meets current and past requirements only if mechanical ventilation is used. Renewable energy sources, including biomass boilers and heat pumps – variants IV and VI – are characterized by more than three times lower *EP* index than required, while the highest electricity – variant V.A V.A- 346 kWh/m² year V.B – 222 kWh/m² year

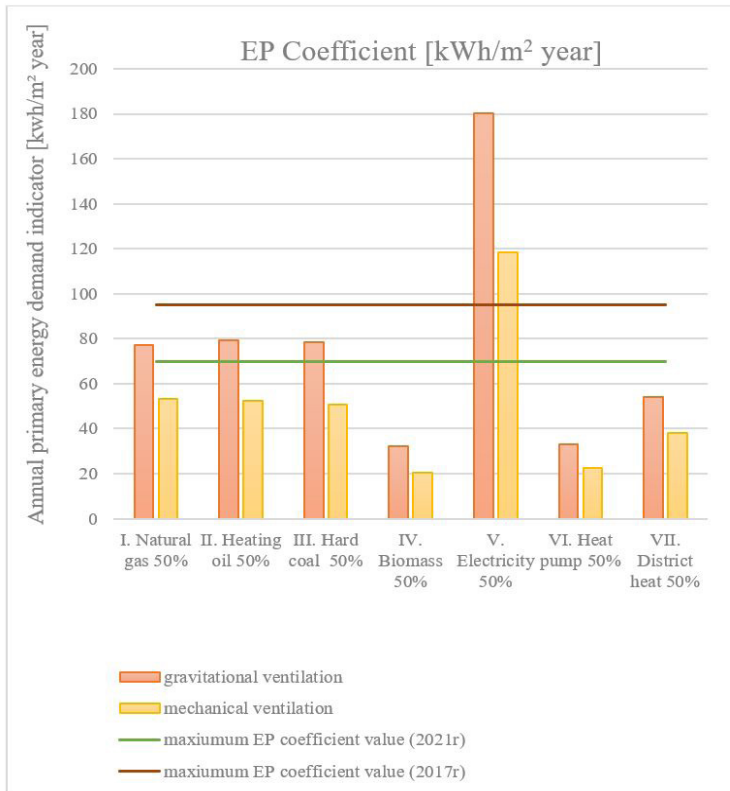


Fig. 3. Primary energy coefficient (EP) for different types of source of heat supported by photovoltaic panels

In the next stage of the research, an analysis was carried out concerning the influence of the assembly of photovoltaic panels on the EP indicator for the object under study. For each variant it was assumed that 50% of the demand is covered by solar energy. The results are shown in Fig. 3. The differences between variants A – B and C – D are significant. Only electricity, despite being supported by a 50% renewable energy source, still deviates significantly from the results of other sources and exceeds the maximum indicators. The use of mechanical ventilation (variant D) in all other cases is sufficient for the EP indicator to meet the new standards. For popular fossil (I.D, III.D) and liquid (II.D) fuels, EP is around 50 kWh/m² year, while for variants with gravity ventilation – I.C, IIC, and IIIC still exceeds them and is around 80 kWh/m² year. For renewable energy sources (IV and VI) the use of photovoltaic panels has a slight impact on the EP ratio.

In the last stage of the study, an attempt was made to determine what conditions would have to be met in order for the variants I.C.II.C.III.C, V.C and V.D to be applied from 2021. The use of both natural gas, coal and fuel oil with gravity ventilation will only be possible with an additional photovoltaic installation that will provide more than 60% of the energy demand. To be able to design a building based solely on electricity, the solar installation would have to provide more than 83% of the energy demand for gravity ventilation and 71% for mechanical ventilation. A graphical overview is presented in Figure 4

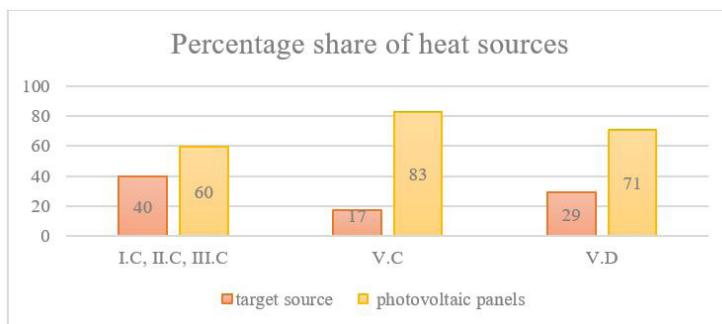


Fig. 4. Demand of primary energy (*EP*) for different types of source of heat

According to the analyses, the type of ventilation used in the facility has a large impact on the *EP* indicator. In a building with mechanical ventilation it is about 35% lower than in the case of gravity ventilation. As can be seen from Figure 2 in the light of the current WT 2017 regulations for variants I-III, the key to meeting the requirements turned out to be the choice of mechanical ventilation with heat recovery. For example, for variants III.A, i.e. using a coal-fired boiler together with gravity ventilation, the *EP* ratio was about 145 kWh/m² a year, while for variant III.B it was already within 90 kWh/m² year. The lower the value of *EP* ratio as in the case of variants with renewable energy sources (IV.A – 32 kWh/m² year, IV.B – 20 kWh/m² year) the less important the type of ventilation.

The presented differences are mainly due to the fact that in the case of gravitational ventilation, heat losses for air exchange in the facility constitute 40% of total losses. The use of mechanical ventilation with heat recovery significantly reduces them to 14%. The list of heat losses for the analyzed object is presented in Table 5 and Figure 5.

Tab. 5. Comparison of heat losses in a building depending on the type of ventilation

	Gravitational ventilation	Mechanical ventilation [recovery 80%]
Heat loss by penetration	13742.38 (60%)	13742.38 (86%)
Heat loss for ventilation	9188.62 (40%)	2192.34 (14%)
Total heat loss	22931 (100%)	15934.72 (100%)

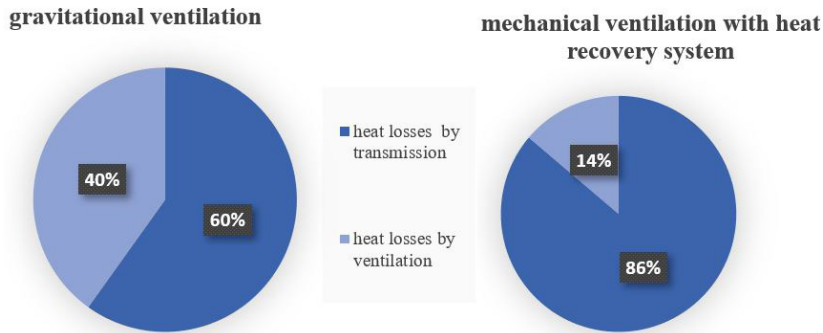


Fig. 5. The percentage share of heat loss in a building depending on the type of ventilation

5. Summary and conclusions

It is a current priority in all Member States of the European Union to introduce measures to reduce energy consumption mainly from fossil fuels and promote the use of renewable energy sources in the construction sector. More and more stringent regulations in this area will result in limiting the use of non-renewable energy sources. Currently, with respect to single-family construction, which is the subject of analysis, predominantly solid fuels are used for heating purposes, including coal and wood, and increasingly often gaseous fuel. Since 2021, after tightening the guidelines for maximum energy consumption coefficient *EP* and heat conduction ratios, it will be more and more difficult to choose an appropriate way of heating a facility that will meet them.

Consequently, the article analyzes how selected installation solutions, including the selection of the heat source and ventilation system of the object, affect the value of the building's *EP* ratio assuming the construction of building partitions characterized by the maximum permissible *U*-values. This analysis shows that traditional boilers, even with high efficiency, will not be able to meet the restrictive standards. In order to obtain the *EP* ratio below the required value, a significant share of renewable energy in the total energy balance will be required.

A detailed analysis shows the directions of development of single-family housing in installation issues and leads to the following conclusions:

The use of traditional heating systems fired exclusively with hard coal, fuel oil or natural gas will be hardly possible from 2021.

Mechanical ventilation with heat recovery reduces the total heat loss for the building by about 30%, which significantly reduces the *EP* ratio.

New restrictions will result in a significant increase in design as the main heat source for biomass boilers, heat pumps or mixed production with photovoltaic panels.


A heating system based only on renewable energy sources will not force the use of mechanical ventilation in single-family facilities.

References

- [1] Wilk-Słomka B., „Rozwiązania architektoniczno-budowlano-instalacyjne a efektywność energetyczna budynku jednorodzinnego”, *Fizyka budowli w teorii i praktyce*, vol. VI, no 2 – 2011, pp. 91-96.
- [2] Krawczyk D. and Sojko-Gil A., „Wpływ termomodernizacji obiektów na wartość wskaźników EP i EK na przykładzie budynku przedszkola”, *Civil and Environmental Engineering / Budownictwo i Inżynieria Środowiska*, 1 (2010), Oficyna Wydawnicza Politechniki Białostockiej pp. 199-204.
- [3] Lis A. „Energochłonność budynków edukacyjnych i ich izolacyjność cieplna w świetle aktualnych wymagań”, *Budownictwo o zoptymalizowanym potencjale energetycznym*, 1(15) 2015, pp. 101-108.
- [4] Siuta-Olcha A., Cholewa T. and Guz Ł. „Analiza porównawcza potrzeb energetycznych jednorodzinnych budynków mieszkalnych o różnym standardzie wykonania”, *Proceedings of ECOpole*, vol. 5, No. 1 2011, pp. 287-292.
- [5] Leiteda Cunha José S. R. and Aguiar L. B. “Phase change materials and energy efficiency of buildings: A review of knowledge”, *Journal of Energy Storage*, Volume 27, February 2020. <https://doi.org/10.1016/j.est.2019.101083>
- [6] *Directive 2002/91/EU of the European Parliament and Council of 16 December 2002 on the energy performance of buildings*, Official Journal of the European Union L 1/65 of 4.1.2003.
- [7] *Directive 2010/31/EU of the European Parliament and Council of 19 May 2010 on the energy performance of buildings*, Official Journal of the European Union L 153/13 of 18.6.2010.
- [8] *Regulation of the Minister of Infrastructure and Development of 27 February 2015 on the methodology for determining the energy performance of a building or part of a building and energy performance certificates*, Warsaw, Journal of Laws, 2015, item. 376.
- [9] *Ordinance of the Minister of Infrastructure of 12 April 2002 on technical conditions to be met by buildings and their location*, Warsaw, Journal of Laws 2002, No. 75, item 690, as amended.
- [10] Mojowska W. and Gładyszewska-Fiedoruk K., „Analiza strat ciepła domu jednorodzinnego wykonanego w dwóch technologiach”, *Civil and Environmental Engineering / Budownictwo i Inżynieria Środowiska*, 1 (2010), Oficyna Wydawnicza Politechniki Białostockiej, pp. 229-233.
- [11] CSO, “Energy consumption in households in 2018”, statistical analyses, Warsaw 2019. Available: https://stat.gov.pl/files/gfx/portalinformacyjny/en/defaultaktualnosci/3304/2/5/1/energy_consumption_in_households_in_2018.pdf [Accessed: 13 May 2020]
- [12] Veolia Energia Poznań S.A., „Struktura paliw”. Available: <https://energiadlapoznania.pl/wazne-informacje-i-dokumenty/dane-techniczne/> [Accessed: 13 May 2020]

Influence of effective width of flange on calculation and reinforcement dimensioning of beam of reinforced concrete frame

Maciej Tomasz Solarczyk

*Department of Concrete Structures; Faculty of Civil and Environmental Engineering;
Gdańsk University of Technology; 11/12 Narutowicza St., 80-233 Gdańsk, Poland;
maciej.solarczyk@pg.edu.pl  0000-0001-6070-0736*

Abstract: The paper analyses the influence of modelling the cross-section of a beam in two-storey reinforced concrete frame of industrial warehouse with dimensions: 18.0 m × 32.0 m using bar elements on the results of bending moments, the value of elastic deflection and the dimensioning of reinforcement due to bending. Six options were considered: a beam as a rectangular section and five T-beam variants with different definitions of effective flange width. The differences in obtained results were commented on. Conclusions useful for the designing of reinforced concrete structures were presented. The procedure for determining the effective flange width in the context of PN-EN 1992-1-1:2008 and PN-B 03264:2002 standards with a commentary on the use of effective flange width in calculations and construction of reinforcement in reinforced concrete structures were described. Brief description of determining the reinforcement due to bending according to the simplified method given in PN-EN 1992-1-1:2008 was presented. In addition, the standard formula for determining the minimum cross sectional area of reinforcement (9.1N) in PN-EN 1992-1-1:2008 with a proposal for its strict determination for the T-beam with the flange in tension was analysed.

Keywords: reinforced concrete structures; effective width of flange, minimum cross sectional area of reinforcement, PN-EN 1992-1-1:2008, PN-B 03264:2002

1. Introduction

Nowadays, designers of engineering structures have a wide range of programs for determination of internal forces and reinforcement dimensioning in reinforced concrete structures [1], [2]. The use of spatial calculation models of objects is becoming increasingly popular. By creating a single design file, the designer has a full spectrum of internal forces values. However, it also has its disadvantages – due to the multitude of design combinations, the interpretation of results may be difficult [3]. The calculation time of spatial models is substantial. Creating a 3D model requires considerable experience for the designer. It is necessary to accurately

map the location of subsequent elements of the structural system, which was pointed out by Starosolski [4], Kossakowski [5], [6], Godycki-Ćwirko et al. [7], Nagrodzka-Godycka et al. [8] and Wojdak [9] in their publications.

In the case of frame structures, they are most often modelled as plane frame. This approach allows the subsequent parts of the frame to be modelled as beam elements. The most important task in a cast structures is to determine the cross section of beam of the frame between the beam and floor slab.

The paper analyses the effect of the beam cross section of a reinforced concrete frame on the results of internal forces, elastic deflection values and reinforcement dimensioning. Six models with different definition of effective width of the flange have been analysed. An in-depth numerical analysis of the effective flange width (spatial model) is presented in [10].

In addition, the paper presents a procedure for determining the minimum cross-sectional area of the longitudinal tension reinforcement according to the recommendations of standard [11] for a T-section with the flange in tension. The issue of minimum reinforcement due to cracking was raised by Knauff [12], [13], [14] and [15] in his publications.

2. Effective width of flange in standard terms

The effective width of flange, in addition to its use in the definition of the construction model, is necessary to determine the dimensioning of the reinforcement due to bending. Section 3.2.3 of [16] states that: *The appropriate flange width calculated for considered span and the position of the section should always be used to check the ultimate resistance of the beam sections.*

Moreover, the effective width is necessary for determining the minimum cross-sectional area of longitudinal tension reinforcement according to the formula (9.1N) in [11]. It depends on the size b_t – mean width of the tension zone. Its determination may cause some complications in case of the flange in tension.

According to the recommendations of standard [11], section 9.2.1.2 (2), the effective width is additionally used to determine the width at which the tension reinforcement is to be spread at intermediate supports of continuous beams (Fig. 1.): *At intermediate supports of continuous beams, the total area of tension reinforcement A_s of a flanged cross-section should be spread over the effective width of flange. Part of it may be concentrated over the web width.*

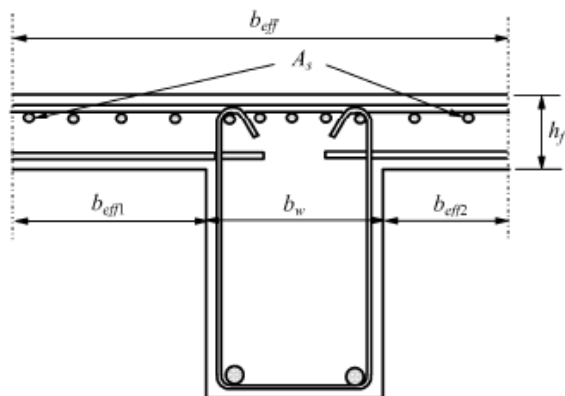


Fig. 1. Placing of tension reinforcement in flanged cross-section; source: Figure 9.1 in [11]

The effective flange width must be determined to define the longitudinal shear stress at the junction between one side of a flange and the web in the shear between web and flanges procedure according to clause 6.2.4 in [11].

The effective flange overhang can be determined from formula (5.7a) in [11]:

$$b_{eff,i} = \min \begin{cases} 0,2 \cdot b_i + 0,1 \cdot l_0 \\ 0,2 \cdot l_0 \\ b_i \end{cases} \quad (1)$$

The effective flange width can be determined from formula (5.7) in [11]:

$$b_{eff} = \min \begin{cases} \sum b_{eff,i} + b_w \\ b \end{cases} \quad (2)$$

The designations given in formulas (1) and (2) are defined in Fig. 2 and Fig. 3.

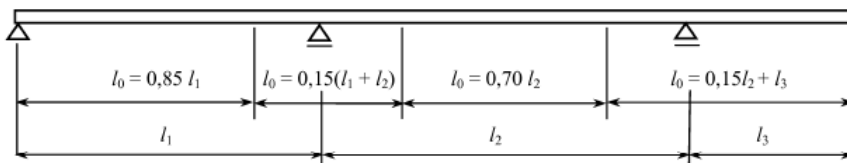


Fig. 2. Definition of l_0 for calculation of effective flange width; source: Figure 5.2 in [11]

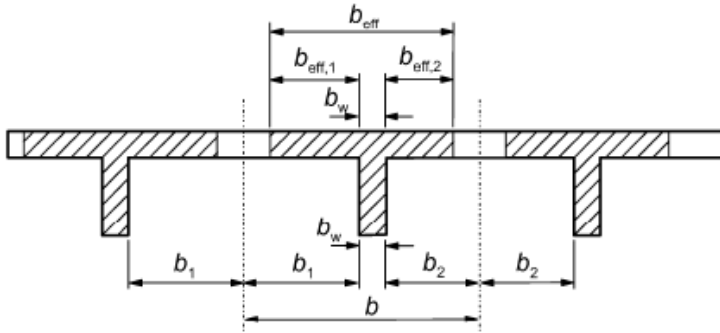


Fig. 3. Effective flange width parameters; source: Figure 5.3 in [11]

Standard [17], in addition to the recommendations given in [11], introduces an additional restriction on the width of the flange when checking the ultimate limit state (ULS). It is to be assumed that for a double-sided overhang $b_{\text{eff}1}$ or $b_{\text{eff}2} \leq 6h_f$ (according to formula (19a) in [17]), and for a single-sided overhang $b_{\text{eff}1} \leq 4h_f$ (according to formula (19b) in [17]). The publication [18] treats the consequences of the choice of design standards [11] or [17] for material consumption on the example of a flat ceiling.

3. Parameters of the analyzed reinforced concrete plane frame

The paper analyses the influence of modelling the beam of a reinforced concrete plane frame using bar elements on the results of internal forces – bending moments and elastic deflection values. The calculations were performed in Autodesk Robot Structural Analysis (ARSA) version 2015 [1]. The object of the analysis is two-storey frame in building with dimensions (width \times length): 18.0 m \times 32.0 m forming part of construction of an industrial warehouse. A single beam has a span $L = 9.0$ m. Subsequent frames are set at a distance of $B = 4.0$ m. The structure is made of concrete class C25/30. Steel class A-IIIIN, grade B500SP is used to dimensioning the reinforcement. The storey height is $H = 4.0$ m. The supports of the frame beams are reinforced concrete columns with dimensions (width \times height): 30 cm \times 60 cm. The columns are fixed in foundation footings. The total height of the frame beam is $h = 75$ cm. The width of the beam web is $b_w = 30$ cm. The height of the flange which is a one-way floor slab is equal to 15 cm (Fig. 4).

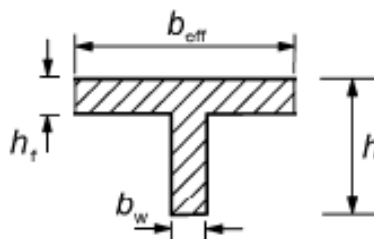


Fig. 4. Description of dimensions of the T-section; source: Figure 5.3 in [11]

A steel truss with a span of 18.0 m was used as a construction of roofing. The following were assumed as the loads: the self-weight of the structure (from the ARSA program excluding the beam – a characteristic load of 19.5 kN/m was transferred on it). Also added the complementary load from the finishing layers located on the floor: 1.5 kN/m² (estimate; characteristic value), which gave the load on the frame of 6 kN/m and an imposed load – according to Table 6.3 in [19], the areas where goods can be accumulated belong to category E1; according to Table 6.4 in [19], the characteristic imposed load on floor for this category is 7.5 kN/m²; which gave the load on the frame of 30 kN/m. The complementary load from the finishing layers of roof is assumed as characteristic value equal 5 kN/m.

Following calculation combinations were assumed (according to point 6.4.3.2 in [20]): ULS1 with imposed load on the left span of frame beam, ULS2 with imposed load on the right span of frame beam and ULS3 with imposed load on both spans simultaneously.

Due to the course of the bending moments in the frame beam (rigid connection of external column to the beam), the distances l_0 between points of zero bending moment have been established by modifying Fig. 5.2 in [11] as shown in Fig. 5.

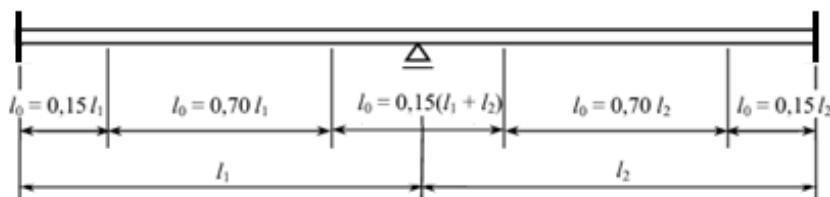


Fig. 5. Definition of l_0 for calculation of effective flange width – adaptation to the task under consideration; source: Figure 5.2 in [11]

The article analyses six different ways of modelling a beam of reinforced concrete plane frame using bar elements:

- variant 1 – frame beam assumed as a rectangular beam with dimensions $b_w \times h$ (Fig. 6),
- variant 2 – frame beam assumed as a T-section with a flange width equal to the spacing of successive frames $B = 4.0$ m,
- variant 3 – frame beam assumed as a T-section with a flange with widths determined by the standard [11] with the definition of different widths for subsequent sections between points of zero bending moment using recommendations [11] (Fig. 8),
- variant 4 – frame beam assumed as a T-section with a flange with widths determined by the standard [11] with definition of different widths for subsequent sections between points of zero bending moment using the bending moment diagram obtained from variant 1 of the calculations,
- variant 5 – frame beam assumed as a T-section with a flange with widths determined by the standard [11] with definition of different widths for subsequent sections between points of zero bending moment using the recommendations [11], but taking into account a gradual change of the effective width of flange along the length of the beam (varying linearly from the support to the middle of the span),

- variant 6 – frame beam assumed as a T-section with a flange along the whole length of an element of width equal to the effective width of flange calculated using the standard [11] in the span section.

The calculations in variant 3 fulfil the recommendations given in section 4.4.3.2 in [17]: *For the calculations, the effective flange width b_{eff} in T-sections – constant over the entire length of the element under consideration where the moment of the same sign occurs – may be taken.*

Variant 6 of the calculations fulfils the recommendation of clause 5.3.2.1 (4) in [11]: *For structural analysis, where a great accuracy is not required, a constant width may be assumed over the whole span. The value applicable to the span section should be adopted, and from Section 9.2.6 in [21]: In the calculation of statically indeterminate system, the cross-section is usually assumed to be constant over the entire length, and in the calculation of beam deflections, the decisive stiffness is determined from the cross-section in the span.*

As shown in Table 1. the most similar values of the distances l_0 to the ones recommended in [11] are obtained for the calculation in the ULS3 combination corresponding to the location of the imposed load on both spans which leads to extreme bending moments at the inner support. These values were used to calculate the effective flange width in variant 4.

Table 1. Comparison of l_0 values for different calculation variants

Calculation variant	External support node 2 and 6 – see Fig. 6	Span between nodes 2 and 4; 4 and 6	Inner support node 4
As recommended in [11], Fig. 5	1.35 m	6.3 m	2.7 m
Variant 1), combination ULS1	1.38 m	6.0 m	4.53 m
Variant 1), combination ULS2	2.08 m	4.01 m	4.54 m
Variant 1), combination ULS3	1.46 m	5.54 m	4.0 m

Table 2 shows a comparison of the effective width of flange b_{eff} calculated for the value l_0 determined according to the recommendations [11] and for the moment diagram in the ULS3 combination in variant 1 of the calculation. The greatest differences occur in the effective width of flange for the inner support – about 25%.

Table 2. Comparison of effective width of flange b_{eff} values in characteristic points of beam of reinforced concrete frame

Calculation variant	External support node 2 and 6 – see Fig. 6	Span between nodes 2 and 4; 4 and 6	Inner support node 4
As recommended in [11], Fig. 5	84 cm	230 cm	138 cm
Variant 1, combination ULS3	88.4 cm	214.8 cm	184 cm

4. Analysis of bending moments and elastic deflection in the frame

Fig. 6 and Fig. 8 show the geometry of the analyzed reinforced concrete frame in variant 1 and 3 of calculations respectively. Fig. 7 and Fig. 9 show bending moment envelope from the combination of ULS1, ULS2 and ULS3 in variant 1 and 3 of calculations respectively.

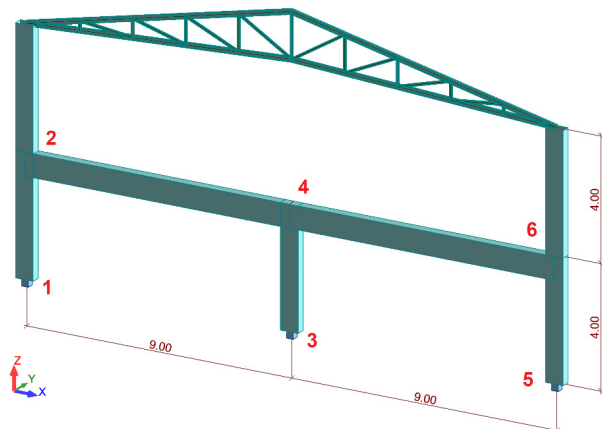


Fig. 6. Geometry of reinforced concrete frame in variant 1 of calculations

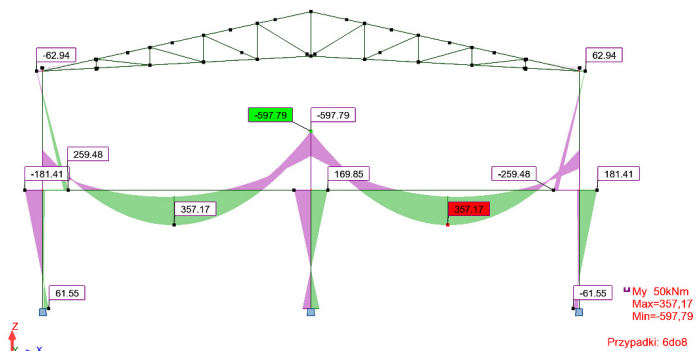


Fig. 7. Envelope of bending moments for calculations in variant 1

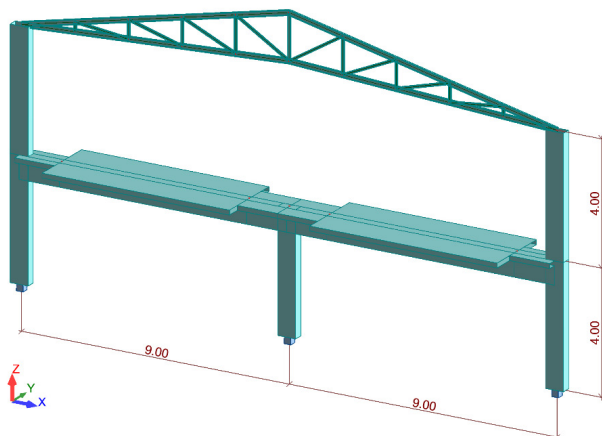


Fig. 8. Geometry of reinforced concrete frame in variant 3 of calculations

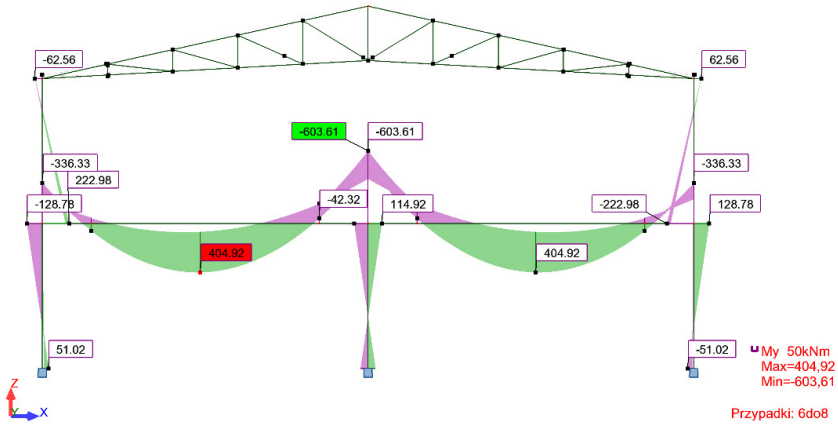


Fig. 9. Envelope of bending moments for calculations in variant 3

Table 3 presents the values of bending moments [kNm] and elastic deflection [cm] read from the calculations results in the ARSA program at characteristic points of the considered reinforced concrete frame, depending on the calculation variant (see also Fig. 7 and Fig. 9).

Table 3. List of bending moments [kNm] and elastic deflection [cm] at characteristic points of considered reinforced concrete frame

Location	Variant 1	Variant 2	Variant 3	Variant 4	Variant 5	Variant 6
External support (node 2 and 6 – see Fig. 6)	407.05	327.99	336.33	339.5	333.28	340.27
Span (between nodes 2 and 4; 4 and 6)	357.17	399.56	405.06	394.94	402.29	393.33
Inner support (node 4)	597.79	632.31	603.61	620.34	614.74	627.28
External column upper node (node 2 and 6)	181.41	121.91	128.78	132.45	127.6	130.47
External column lower node (node 1 and 5)	61.55	47.61	51.02	51.39	49.3	49.76
Inner column upper node (node 4)	169.85	105.85	114.92	120.95	119.56	114.46
Inner column lower node (node 3)	85.72	59.19	63.07	66.18	65.02	62.96
Span – elastic deflection (between nodes 2 and 4; 4 and 6)	0.73	0.37	0.42	0.44	0.44	0.41

Table 4 compares the percentage differences of bending moments and deflections with the calculation in variant 6 (according to the simplified recommendation from section 5.3.2.1 (4) in [11]) – considered to be the effective solution in terms of the amount of work involved in creating the calculation model and generating loads. The positive percentage difference represents an overestimation of the magnitude, while the negative magnitude represents an underestimation.

Table 4. Comparison of bending moment values and elastic deflection in the span in relation to the variant 6 of calculations

Location	Variation 1	Variation 2	Variation 3	Variation 4	Variation 5
External support (node 2 and 6 – see Fig. 6)	19.63%	-3.61%	-1.16%	-0.23%	-2.05%
Span (between nodes 2 and 4; 4 and 6)	-9.19%	1.58%	2.98%	0.41%	2.28%
Inner support (node 4)	-4.70%	0.80%	-3.77%	-1.11%	-2.00%
External column upper node (node 2 and 6)	39.04%	-6.56%	-1.30%	1.52%	-2.20%
External column lower node (node 1 and 5)	23.69%	-4.32%	2.53%	3.28%	-0.92%
Inner column upper node (node 4)	48.39%	-7.52%	0.40%	5.67%	4.46%
Inner column lower node (node 3)	36.15%	-5.99%	0.17%	5.11%	3.27%
Span – elastic deflection (between nodes 2 and 4; 4 and 6)	78.05%	-9.76%	2.44%	7.32%	7.32%

The calculations in Variant 1 – rectangular beam, overwhelmingly exceed the bending moments compared to the calculations in Variant 6. This is particularly true for columns, where the differences can be up to 50%. For the beam, the span moment is lower by about 10% and at the internal support by about 5%. In the case of the external support, the difference is much greater – an overvaluation of about 20%. The magnitude of elastic deflection varies significantly – as much as about 80% of variant 1 revalues the deflection compared to variant 6.

The calculations in Variant 2 for bending moments are similar to the values obtained from calculations in variant 6, especially in the beam where the differences do not exceed 5%. Slightly larger differences occur in the bending moments in the columns, but do not exceed 10%. However, it is worth noting that this modelling of the beam results in an underestimation of the elastic deflection by about 10%.

In variant 3 and variant 4 only in a few places the bending moments in the column are overestimated by more than 5%.

The most accurate calculation model is variant 5, but due to the difficulties in creating model and applying loads – it is not a solution often used in designing of structures. It is worth noting that the calculations in variant 6 in bending moments at each of the characteristic locations of the considered reinforced concrete frame do not exceed 5%, which can be considered as a satisfactory degree of accuracy. Only the elastic deflection of the beam is overestimated by about 7%.

5. Reinforcement dimensioning due to bending using simplified method

In this section, the procedure for dimensioning of reinforcement due to bending using simplified method is presented.

Auxiliary coefficient (according to formula (4.51) in [22], taking into account the recommendations [11]):

$$\mu_{eff} = \frac{M_{Ed}}{b \cdot d^2 \cdot \eta \cdot f_{cd}} \quad (3)$$

where: M_{Ed} – design value of the applied internal bending moment, b – the width of the compression zone, d – effective depth of a cross-section, η – coefficient defining the effective strength (according to formula (3.21) and (3.22) in [11]), f_{cd} – design value of concrete compressive strength (according to formula (3.15) in [11]).

Range of the effective compression zone (formula (4.52) in [22]):

$$\xi_{eff} = 1 - \sqrt{1 - 2 \cdot \mu_{eff}} \quad (4)$$

Limit range of the effective compression zone (according to formula (4.19) in [22], taking into account the recommendations [11]):

$$\xi_{eff,lim} = \lambda \cdot \frac{\varepsilon_{cu3}}{\varepsilon_{cu3} + \frac{f_{yd}}{E_s}} \quad (5)$$

where: λ – coefficient defining the effective height of the compression zone (according to formula (3.19) and (3.20) in [11]), ε_{cu3} – ultimate compressive strain in the concrete for the bilinear stress-strain relation (according to Table 3.1 in [11]), f_{yd} – design yield strength of the reinforcement, E_s – design value of the modulus of elasticity of reinforcing steel (according to Section 3.2.7 (4) in [11]).

The cross-sectional area of the tension reinforcement when $\xi_{eff} \leq \xi_{eff,lim}$ (according to formula (4.52) in [22], taking into account recommendations [11]):

$$A_{s1} = \xi_{eff} \cdot d \cdot b \cdot \frac{\eta \cdot f_{cd}}{f_{yd}} \quad (6)$$

The minimum cross-sectional area of the tension reinforcement is determined by the formula (9.1N) in [11]:

$$A_{s,min} = \max \begin{cases} 0,26 \cdot \frac{f_{ctm}}{f_{yk}} \cdot b_t \cdot d \\ 0,0013 \cdot b_t \cdot d \end{cases} \quad (7)$$

where: f_{ctm} – mean value of axial tensile strength of concrete, f_{yk} – characteristic yield strength of the reinforcement, b_t – mean width of the tension zone; for a T-beam with the flange in compression, only the width of the web is taken into account in calculating the value of b_t .

It should be noted that standard [11] also provides a simplified method to determine the minimum cross-sectional area of the tensile reinforcement. Note 2 to Section 9.2.1.1 in [11] states that: *Alternatively, for secondary elements, where some risk of brittle failure may be accepted, $A_{s,min}$ may be taken as 1,2 times the area required in ULS verification.* However, the standard [11] does not define the term “secondary elements” anywhere, which is a serious problem in the interpretation of this recommendation. The minimum reinforcement should

be used to limit the effects of unexpected change in the stiffness of the element during the transition from phase I (uncracked) to phase II (cracked) [23].

Determining the mean width of the tension zone b_t in the case of a flange in the tension may cause some design complications. The simplification of considering only the web part of the section is on the unsafe side – it underestimates the value of the minimum cross-section area of the tension reinforcement. Formula (9.1N) in [11] is given for the rectangular section. It can be determined by calculating the cracking moment on the basis of theory of phase I and on the basis of theory of phase II.

Cracking moment calculated according to the theory of phase I (right before cracking):

$$M_{cr} = f_{ctm} \cdot W_x \tag{8}$$

where: W_x – section modulus before cracking calculated for the extreme tensile fibers of the element.

Cracking moment calculated according to the theory of phase II (right after cracking):

$$M_{cr} = A_{s1} \cdot f_{yk} \cdot \left(d - \frac{x_{II}}{3} \right) \tag{9}$$

where: x_{II} – height of the compression zone after the cracking (phase II).

By comparing the values obtained from formulas (8) and (9), it can be obtained a formula for determining the minimum cross-sectional area of the tension reinforcement:

$$A_{s,min} = \frac{f_{ctm} \cdot W_x}{f_{yk} \cdot \left(d - \frac{x_{II}}{3} \right)} \tag{10}$$

The value of the minimum cross-sectional area of the tension reinforcement given by formula (10) depends on the material data (mean value of axial tensile strength of concrete and characteristic yield strength of the reinforcement), but also on geometrical values. The height of the compression zone in phase II depends on the cross-sectional area of the tension reinforcement (and so on $A_{s,min}$). Therefore, equation (10) becomes an iterative equation. This is not a significant problem in nowadays numerical calculations.

The procedure of determining the minimum cross-sectional area of the tension reinforcement for the tension of the upper fibres (according to Fig. 4) of the T-section is presented below.

First moment of area in phase I calculated in relation to the upper edge:

$$S_x = b_{eff} h_f \frac{h_f}{2} + b_w h_w \left(h_f + \frac{h_w}{2} \right) + (\alpha_e - 1) A_{s,min} a_1 \tag{11}$$

where: h_w – web height; $h_w = h - h_f$; α_e – the ratio of modulus of elasticity of reinforcing steel to secant modulus of elasticity of concrete: $\alpha_e = E_s/E_{cm}$; if the cracking is expected to appear in the element for loads with duration causing creep, the effective modulus of elasticity ratio can be used: $\alpha_e = E_s/E_{c,eff}$, where the effective modulus of elasticity for concrete can be determined from formula (7.20) in [11]: $E_{c,eff} = E_{cm}/(1 + \varphi(\infty, t_0))$; $\varphi(\infty, t_0)$ – the final value of the creep coefficient, a_1 – the distance from the extreme tension fibre of element to the centre of gravity of the tension reinforcement.

Equivalent cross-section area of the T-beam:

$$A = b_{eff} h_f + b_w h_w + (\alpha_e - 1) A_{s,min} \tag{12}$$

Distance from the extreme tension fibre of element to the neutral axis of the equivalent cross-section:

$$v' = \frac{S_x}{A} \quad (13)$$

Second moment of area of the equivalent cross-section in phase I (uncracked):

$$I_I = \frac{b_{eff} h_f^3}{12} + b_{eff} h_f \left(v' - \frac{h_f}{2} \right)^2 + \frac{b_w h_w^3}{12} + b_w h_w \cdot \left(v' - h_f - \frac{h_w}{2} \right)^2 + (\alpha_e - 1) A_{s,min} (v' - a_1)^2 \quad (14)$$

The section modulus of equivalent cross-section:

$$W_x = \frac{I_I}{v'} \quad (15)$$

The height of the compression zone in phase II (cracked) can be determined from formula (7.1) given in [23]:

$$x_{II} = d \left(\sqrt{(\alpha_e - 1) \rho_l ((\alpha_e - 1) \rho_l + 2)} - (\alpha_e - 1) \rho_l \right) \quad (16)$$

where: ρ_l – reinforcement ratio for longitudinal reinforcement; $\rho_l = A_{s,min}/(b_w \cdot d)$.

If $x_{II} > h_w$ the cross-section is actually T-shaped and the height of the compression zone should be determined by solving a quadric equation:

$$(\alpha_e - 1) A_{s,min} (d - h_w - x) - b_w h_w \left(\frac{h_w}{2} + x \right) - b_{eff} x \frac{x}{2} = 0 \quad (17)$$

where: x – the height of the part of compression zone located only in the flange of T-section.

The height of the compression zone is then:

$$x_{II} = x + h_w \quad (18)$$

By knowing the section modulus determined by formula (15) and the height of the compression zone in phase II – formula (16) or (18), the minimum cross-sectional area of the tension reinforcement can be determined from formula (10).

The following parameters were assumed and calculated: $d = 70$ cm (the same for the dimensioning of the reinforcement in the span and on supports); $f_{cd} = 16.67$ MPa; $f_{ctm} = 2.6$ MPa; $\lambda = 0.8$; $\eta = 1.0$; $\varepsilon_{cu3} = 0.0035$; $f_{yk} = 500$ MPa; $f_{yd} = 434.78$ MPa; $E_s = 200$ GPa; $\xi_{eff,lim} = 0.493$.

The result of the strict minimum cross-sectional area of the tension reinforcement (10) can be compared to that given in standard formula (7). Then the equivalent rectangular cross-section corresponding to the T-section can be determined. The difference in the minimum cross-sectional area of the tension reinforcement determined between formula (10) and (7) can be presented in relation b_t/b_w , which is shown in Table 5.

As shown in Table 5, the minimum cross-sectional area of the tension reinforcement determined from formula (10) differs from that determined from formula (7) on the assumption that $b_t = b_w$ (assuming calculations for a rectangular cross-section – variant 1). In the case of variant 2 of the calculations, the difference is more than five times, for the calculations in variant 3, 4 and 5, depending on the section under consideration, the difference is not more than three times. For variant 6 of the calculations, the difference is slightly greater than three times.

Table 5. Minimum cross sectional area of reinforcement with specified of width b_{eff} and b_t

	Parameter	Variant 1	Variant 2	Variant 3	Variant 4	Variant 5	Variant 6
External support	A_{smin} [cm ²] eq. (10)	2.21	14.58	4.41	4.58	2.21	9.61
	b_{eff} [cm]	-	400.0	84.0	88.4	30.0	230.0
	b_t [cm] eq. (7)	23.4	154.0	46.6	48.4	23.4	101.5
	b_t / b_w	0.78	5.13	1.55	1.61	0.78	3.38
Inner support	A_{smin} [cm ²] eq. (10)	2.21	14.58	6.45	8.08	6.45	9.61
	b_{eff} [cm]	-	400.0	138.0	184.0	138.0	230.0
	b_t [cm] eq. (7)	23.4	154.0	68.2	85.3	68.2	101.5
	b_t / b_w	0.78	5.13	2.27	2.84	2.27	3.38

Tables 6, 7 and 8 shows the reinforcement dimensioning due to bending for: the external support, the span and the inner support respectively. In each cases (except for the reinforcement at the external support in variant 2 of the calculation) the cross-sectional area of the tensile reinforcement determined due to bending in ULS is larger than the minimum cross-sectional area of the tension reinforcement – formula (10). Moreover the assumed cross-sectional area of tensile reinforcement $A_{\text{s1,prov}}$ in the span and on the inner support in each of the calculation variants is equal, which proves that from a practical point of view (reinforcement made directly on the construction site) the calculation variant is of little importance. The difference occurs on the extreme support, however it is shown for the calculations in variant 1 and 2, which may be considered too far-reaching simplification in the construction modelling.

Table 6. Dimensioning of the reinforcement on the external support

Parameter	Variant 1	Variant 2	Variant 3	Variant 4	Variant 5	Variant 6
M_{Ed} [kNm]	407.05	327.99	336.33	339.5	333.28	340.27
b [cm]	30.0	30.0	30.0	30.0	30.0	30.0
μ_{eff} [-] eq. (3)	0.166	0.134	0.137	0.139	0.136	0.139
ξ_{eff} [-] eq. (4)	0.183	0.144	0.148	0.150	0.147	0.150
$\xi_{\text{eff}} \leq \xi_{\text{eff,lim}}$	yes	yes	yes	yes	yes	yes
A_{s1} [cm ²] eq. (6)	14.72	11.61	11.94	12.06	11.82	12.09
A_{smin} [cm ²] eq. (10)	2.21	14.58	4.41	4.58	2.21	9.61
$A_{\text{s1}} \geq A_{\text{smin}}$	yes	no	yes	yes	yes	yes
$A_{\text{s1,prov}}$ [cm ²]	5 ϕ 20 15.71	5 ϕ 20 15.71	4 ϕ 20 12.57	4 ϕ 20 12.57	4 ϕ 20 12.57	4 ϕ 20 12.57

Table 7. Dimensioning of the reinforcement in the span

Parameter	Variation 1	Variation 2	Variation 3	Variation 4	Variation 5	Variation 6
M_{Ed} [kNm]	357.17	399.56	405.06	394.94	402.29	393.33
b [cm]	30.0	400.0	230.0	214.8	230.0	230.0
μ_{eff} [-] eq. (3)	0.146	0.012	0.022	0.023	0.021	0.021
ζ_{eff} [-] eq. (4)	0.158	0.012	0.022	0.023	0.022	0.021
$\zeta_{eff} \leq \zeta_{eff,lim}$	yes	yes	yes	yes	yes	yes
A_{s1} [cm ²] eq. (6)	12.74	13.21	13.46	13.13	13.36	13.06
A_{smin} [cm ²] eq. (10)	2.84	2.84	2.84	2.84	2.84	2.84
$A_{s1} \geq A_{smin}$	yes	yes	yes	yes	yes	yes
$A_{s1,prov}$ [cm ²]	5 ϕ 20 15.71	5 ϕ 20 15.71	5 ϕ 20 15.71	5 ϕ 20 15.71	5 ϕ 20 15.71	5 ϕ 20 15.71

Table 8. Dimensioning of the reinforcement on the inner support

Parameter	Variation 1	Variation 2	Variation 3	Variation 4	Variation 5	Variation 6
M_{Ed} [kNm]	597.79	632.31	603.61	620.34	614.74	627.28
b [cm]	30.0	30.0	30.0	30.0	30.0	30.0
μ_{eff} [-] eq. (3)	0.244	0.258	0.246	0.253	0.251	0.256
ζ_{eff} [-] eq. (4)	0.284	0.304	0.288	0.297	0.294	0.301
$\zeta_{eff} \leq \zeta_{eff,lim}$	yes	yes	yes	yes	yes	yes
A_{s1} [cm ²] eq. (6)	22.90	24.51	23.17	23.94	23.68	24.27
A_{smin} [cm ²] eq. (10)	2.21	14.58	6.45	8.08	6.45	9.61
$A_{s1} \geq A_{smin}$	yes	yes	yes	yes	yes	yes
$A_{s1,prov}$ [cm ²]	8 ϕ 20 25.13	8 ϕ 20 25.13	8 ϕ 20 25.13	8 ϕ 20 25.13	8 ϕ 20 25.13	8 ϕ 20 25.13

6. Summary and conclusions from the calculations

As shown by the comparative analysis of bending moments, the method of defining the flange width of the T-section has no significant impact on the results. Modelling the beam of a frame with variation 3, 4 and 5 may present problems in defining the section along the length of the element, especially for more complex structures. In addition, it generates a considerable amount of work time. Variation 1 of the calculations (rectangular beam) is too approximate. The bending moment and the elastic deflection values differ significantly from those obtained with T-section of the frame beam. Variation 2 underestimates the deflection values, which may disqualify this solution in the design of reinforced concrete structures due to the Serviceability Limit State in later calculations. Variation 6 of the calculations (recommended by [11]) is rational in terms of the values of internal forces, as well as in terms of time of structure definition in computer program. However, it should be emphasized that the effective width should be determined for all cross-sections along the length of the beam due to the calculations of reinforcement at the Ultimate Limit State, shear between web and flanges and spread of reinforcement on the intermediate support of continuous beams.

Furthermore, significant differences in the minimum cross-sectional area of the tension reinforcement should be noted. In each case of T-section beams with a flange in the tension zone, this value should be determined precisely. However, from the engineering point of view, a simplified criterion can be assumed – if the cross-sectional area of the tension reinforcement in element A_{s1} (value from calculations in the Ultimate Limit State) for flange in tension is more than three times larger than the minimum cross-sectional area of the tension reinforcement determined from the standard formula – as for rectangular cross-section (7) – the exact verification of the $A_{s,min}$ can be omitted. However it may be the decisive condition for the section resistance and the minimum cross-sectional area of the tension reinforcement must be determined precisely.


References


- [1] Ambroziak A., Kłosowski P., *Autodesk Robot Structural Analysis Podstawy obliczeń*. Wydawnictwo Politechniki Gdańskiej, Gdańsk, 2013.
- [2] Ambroziak A., Kłosowski P., *Autodesk Robot Structural Analysis Wymiarowanie konstrukcji stalowych i żelbetowych*. Wydawnictwo Politechniki Gdańskiej, Gdańsk, 2016.
- [3] Solarczyk M.T., Ambroziak A., „Simplified method of applying loads to flat slab floor structural models”, in *2nd Baltic Conference for Students and Young Researchers BalCon 2018*, Gdańsk, 2018. <https://doi.org/10.1051/mateconf/201821903002>
- [4] Starosolski W., „Uwagi o obliczaniu belek w trakcie modelowania stropów płytowo-żebrowych”. *Przegląd Budowlany*, No. 9, p. 50-53.
- [5] Kossakowski P., „Inżynierski problem komputerowego modelowania pracy żelbetowej płyty dwuprzęsłowej z uwzględnieniem sprężystej podatności belki”, *Przegląd Budowlany*, No. 10, p. 19-24.
- [6] Kossakowski P., „Uwzględnienie wpływu sprężystej podatności belek w numerycznym modelowaniu stropów żelbetowych”. *Przegląd Budowlany*, No. 11, p. 24-31.
- [7] Godycki – Ćwirko T., Nagrodzka – Godycka K., Piotrkowski P., „Dome over the Gdynia seaport building”. *Archives of Civil Engineering*, issue 60, no. 2, pp. 223-239. <https://doi.org/10.2478/ace-2014-0015>
- [8] Nagrodzka – Godycka K., Godycki – Ćwirko T., Wojdak R., „Reinforced concrete thin wall dome after eighty years of operation in maritime climate environment”, *Structural Concrete*, issue 5, no. 17, pp. 710-717. <https://doi.org/10.1002/suco.201500180>
- [9] Wojdak R., „Żelbetowa konstrukcja wsporcza zadaszzenia stadionu na EURO 2012 w Gdańsku”. *Inżynieria Morska i Geotechnika*, No. 2 (2012), p. 125-134.
- [10] Ciesielczyk K., Szumigała M., Ścigała J., „The numerical analysis of the effective flange width in T-section reinforced concrete beams”, in *Modern Building Materials, Structures and Techniques, MBMST 2016, Procedia Engineering*, volume 172, 2017, pp. 178-185. <https://doi.org/10.1016/j.proeng.2017.02.047>
- [11] PN-EN 1992-1-1:2008. *Eurokod 2: Projektowanie konstrukcji z betonu. Część 1-1: Reguły ogólne i reguły dla budynków*.
- [12] Knauff, M. Grzeszykowski, B. Golubińska, A., „Minimum reinforcement for crack width control in RC tensile elements”, *Archives of Civil Engineering*, issue 65, no. 1, pp. 111-128. <http://doi.org/10.2478/ace-2019-0008>
- [13] Knauff, M. Grzeszykowski, B. Golubińska, A., „Minimum reinforcement for crack width control – design example”. *Inżynieria i Budownictwo*, annual 74, no. 5, 2018, pp. 232-236.
- [14] Knauff, M. Grzeszykowski, B. Golubińska, A., „Minimum reinforcement for crack width control in RC elements subjected to small eccentricity tension”. *Inżynieria i Budownictwo*, annual 74, no. 3, 2018, pp. 134-138.

-
- [15] Knauff, M. Golubińska, A., „Simple method for determining minimum reinforcement area to control cracking”. *Inżynieria i Budownictwo*, annual 69, no. 6, 2013, pp. 330-333.
- [16] Knauff M. et al., *Podstawy projektowania konstrukcji żelbetowych i sprężonych według Eurokodu 2*. Dolnośląskie Wydawnictwo Edukacyjne, Wrocław, 2006.
- [17] PN-B 03264:2002. *Konstrukcje betonowe, żelbetowe i sprężone. Obliczenia statycznie i wymiarowanie*.
- [18] Kargol W., Szaferin J., „The consequences of the choice of design standards for the use of material on the example of glued laminated roof beam”, *Budownictwo i Architektura*, vol. 8, no. 1, pp. 35-45. <https://doi.org/10.35784/bud-arch.2256>
- [19] PN-EN 1991-1-1:2004. *Eurokod 1: Oddziaływania na konstrukcje. Część 1-1: Oddziaływania ogólne Ciężar objętościowy, ciężar właściwy, obciążenia użytkowe w budynkach*.
- [20] PN-EN 1990:2004. „Eurokod 0: Podstawy projektowania konstrukcji.”.
- [21] Knauff M., *Obliczanie konstrukcji żelbetowych według Eurokodu 2*. Wydawnictwo Naukowe PWN, Warszawa, 2012.
- [22] Łapko A., Jensen B. Ch., *Podstawy projektowania i algorytmy obliczeń konstrukcji żelbetowych*. Arkady, Warszawa, 2009.
- [23] Solarczyk M.T., „Szerokość rozwarcia rys w konstrukcjach żelbetowych według PN-EN 1992-1-1:2008 oraz PN-B 03264:2002”, in *Współczesne budownictwo w badaniach młodych naukowców*, Wydawnictwo Politechniki Gdańskiej, Gdańsk, 2017.

Application of fracture energy for the assessment of frost degradation of high-strength concretes

Sylwia Anna Borowska¹, Marta Kosior-Kazberuk²

¹ Department of Building Structures; Faculty of Civil Engineering and Environmental Sciences;
Białystok University of Technology;
45 E Wiejska St., 15-351 Białystok, Poland;
s.borowska@doktoranci.pb.edu.pl  0000-0003-2100-2673

² Department of Building Structures; Faculty of Civil Engineering and Environmental Sciences;
Białystok University of Technology;
45 E Wiejska St., 15-351 Białystok, Poland;
m.kosior@pb.edu.pl  0000-0001-8171-2242

Abstract: Knowledge of fracture mechanics parameters can help for a more accurate assessment of frost degradation of high-strength concrete. High strength concretes, despite the tight structure, are characterized by increased brittleness. Cracks in the concrete structure are places of accumulation of significant stresses. Additional stresses resulting from cyclic freeze/thaw stimulate the material destruction processes. The basic strength parameters of concrete do not take into account structural defects of the material and do not give a complete description of susceptibility to damage caused by, e.g., frost degradation. This study aimed to determine the relationship between frost degradation of high-strength concretes and changes in the value of their fracture energy associated with the initiation of cracking after 150, 250, 350 and 450 freeze/thaw cycles. The research was carried out using $100 \times 100 \times 400$ mm samples, with a pre-initiated 30 mm deep notch. The I load model under a three-point bending test was used, based on the procedure recommended by RILEM. Concrete with a compressive strength of 90 MPa with steel fibres and a mixture of steel and basalt fibers was tested. The obtained results allow for the evaluation of frost degradation using fracture energy G_F and critical crack tip opening displacement $CTOD_c$.

Keywords: fracture energy, frost resistance, high strength concrete, fiber, fiber reinforced concrete

1. Introduction

Internal material defects associated with manufacturing inaccuracies and loss of durability are avoided in standard calculations and the dimensioning of components. Despite the use of safety factors, the analysis results are random. The basic information about the concrete

is assumed on the basis of dimensions, material data and the standardization of its parameter (compressive strength, longitudinal modulus of elasticity, tensile strength). Even minor defects in the initial period of the structure's use, together with the destructive impact of the external environment, lead to the progress of degradation and loss of durability. A more detailed analysis of the effect of material defects on the loss of HSC durability as a result of cyclic freeze/thaw is possible by analyzing changes in the concrete fracture mechanics parameters [1]. Modern material engineering aims to ensure the best possible durability of concrete structures. At the same time, it aims to minimize the cross-sectional dimensions of the structure and comply with the conditions of sustainable development. During the design process, it is the following the rational use of building materials that ensures high insulation of buildings and minor material losses. For this purpose, structural elements are increasingly frequently made of high-strength concretes, characterized by a tighter structure and more favourable mechanical parameters than normal concretes, which allows to reduce the consumption of materials. The use of HSC as a material for vertical structural elements leads to larger usable spaces. High strength concrete facade elements are much thinner and lighter [2].

To ensure the high durability of external concrete structures, their frost resistance should be guaranteed. Cyclical freeze/thaw leads to the accumulation of significant internal stresses and, as a consequence, to degradation of the concrete structure. The degree of damage caused by freeze/thaw depends primarily on the size and distribution of internal pores in the concrete, as well as the presence of discontinuities and defects. The larger and less frequently the pores are spaced, the more frozen water will accumulate in them. It can create more tensile stress when the ice forms and then defrosts concrete components (aggregates, cement, water), which vary in thermal properties [3]. However, if the structure of the material is compact, with no internal defects, then there is less chance of freezing water accumulating in certain areas. By reducing the water-cement ratio and using various additives to increase the strength of the concrete, it is possible to achieve a more airtight HSC structure compared to standard concrete. However, high strength concretes are prone to sudden cracking due to their quasi-brittle behaviour, which in combination with internal damage developing as a result of external factors may lead to a loss of load-bearing capacity of the structure [4]. Changing the material characteristics of high-strength concrete from quasi-brittle to quasi-plastic is possible by adding fibers with high tensile strength (steel, basalt) to the concrete mix [5]. Fibers in reinforced concrete members can also completely or partially replace standard reinforcement with steel rods. This change contributes to a reduction in production costs, material consumption in the bar plant, pollution emissions, and overall construction costs. The right amount of steel fibers added to the concrete matrix, correctly distributed, increases the bending tensile strength [6].

Degradation of high-strength concretes as a result of cyclic freeze/thaw is revealed by the development of discontinuities initially occurring in the concrete element. Due to the complex microstructure of the concrete, the strength properties are not sufficient to describe the behaviour of the material. The highest stress concentration is associated with the tip of the gap, discontinuity, or crack. A coherent model representing the destruction of concrete can be shown by the fracture energy changes. It is the basic parameter of fracture mechanics, describing the susceptibility of a material to crack propagation, as the amount of energy absorbed during the crack formation in the material subjected to degradation. The use of fracture mechanics in the analysis of the structure can lead to avoiding many design errors and a better understanding of the material behaviour. The higher the fracture energy, the material is less susceptible to failure [7].

This work aimed to present the relationship between the degree of frost degradation of high-strength concretes with the addition of steel and mixed steel and basalt fibers and without fibers, described by the durability factor DF [8], and changes in fracture energy values G_F after 150, 250, 350 and 450 freeze/thaw cycles. Based on the load–deflection relationship function, the focus is on the area related to crack initiation and on the cover area. The tests were carried out on the basis of RILEM [9] recommendation under a three-point bending test. Changes in the HSC brittleness parameter due to cyclic freeze/thaw were also determined [10].

2. Experimental program

2.1. Materials and sample preparation

In the study, the specimens with dimensions of 100 mm × 100 mm × 400 mm were used, according to the method of determining the parameters of fracture mechanics recommended by Jenq Y. S. and Shah [10]. The concrete was made of Portland cement CEM I 42.5 R (440.5 kg/m³). Gravel limited to 11 mm and river sand 0-2 mm was applied. The content of the 0/2 mm aggregate fraction in the mixture was 346 kg/m³ (18% by mass), the 2/5 mm fraction – 372 kg/m³ (22% by mass), and the 5/11 mm fraction – 1112 kg/m³ (60% by mass). A superplasticizer was used in the amount of 1.65% of the binder mix. Concrete with compressive strength of 90 MPa was tested. A constant water-binder ratio $w/s=0.31$ was provided. The consistency of fresh concrete by the slump test was determined as S3. Three categories of concrete were prepared: MB1 – high strength concrete without fibers, MB2 – high strength concrete with 0.50% (by volume) steel fibers, and MB3 – high strength concrete with 0.25% (by volume) steel fibers and 0.25% (by volume) basalt fibers. Dramix steel fibers with a length of 50 mm and a diameter of 1 mm and a tensile strength of 900 MPa and a modulus of elasticity of 200 GPa were used. Also, basalt fibers were used with an equal length of 50 mm and diameter of 0.02 mm, tensile strength of 1 680 MPa and modulus of elasticity 89 GPa. Steel fibers had a hooked end with a 3D structure. Mixtures with the addition of fibers had an increased content of superplasticizer to 1.85% to obtain uniform consistency and to prevent the formation of compact fiber forms. After demoulding, the specimens were kept in a water bath at a temperature of 18 +/- 2° C until the start of the test. The concrete curing process lasted 28 days. In each test piece, a 3 mm wide and 30 mm deep primary notch was cut in the middle of the span using a circular saw. The dimensions of the test specimen, as well as the place of load application and support points are shown in Fig. 1. Altogether, eighteen beam specimens from each of the three series (MB1, MB2, MB3) were prepared: 3 test pieces not subjected to cyclic freeze/thaw, 3 test pieces frozen up to 150 cycles, 3 test pieces frozen up to 250 cycles, 3 test pieces frozen up to 350 cycles, 3 test pieces frozen up to 450 cycles, 3 test pieces intended for the initial estimation of the fracture strength. After each 50 freeze/thaw cycles, the changes of modulus of elasticity were checked using a non-destructive method. After another 100 cycles, starting from 150 freeze/thaw cycles, another 3 specimens were set aside for fracture mechanics parameter analysis. When the DF value of all the series of tested concretes fell below 60%, then the fracture mechanics parameters of the concretes were determined after 150, 250, 350 and 450 freeze/thaw cycles respectively

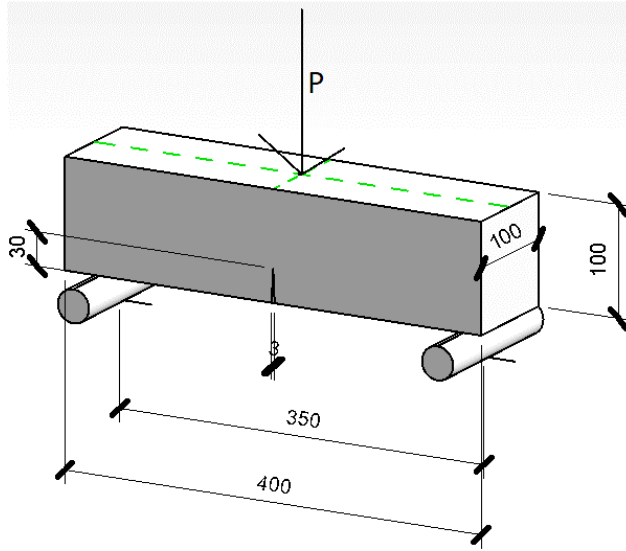


Fig. 1. The geometry of test specimens and the way of load application. *Source:* own research

2.2. Test methodology

Examination to determine fracture energy was carried out using the Zwick/Roell Z250 testing machine, based on RILEM TC 89-FMT [9] recommendations. The force was applied by controlled displacement of the piston to reach its maximum value after 5 minutes. The study was carried out under mode I of concrete fracture (tensile at bending) in a three-point bending test. The value of fracture energy was determined based on the field under the diagram of the relation between the applied load and the deflection at the point of force application ($P - \delta$) and the Eq. 1, proposed in [11].

$$G_F = \frac{\int_0^{\delta} P(\delta) d\delta + mg\delta}{(D - a_0)B} \quad (1)$$

where: $\int_0^{\delta} P(\delta) d\delta$ – field under the force-deflection diagram; m – mass; D – depth (100 mm); B – width (100 mm); a_0 – deep of the initial notch (30 mm).

The fracture energy is a measure of the resistance of the material to brittle failure. The value of fracture energy consists of numerous causes, the most important of which are: surface energy, the energy of formation of new cracks, the energy of plastic deformation, energy related to fracture bridging, the energy of polymorphic transformation, the energy related to crack entanglement [12]. It is assumed that a crack propagates when the stress reaches a value exceeding the tensile strength of the given material at its tip and the further behavior of the material passes into the plastic area, as shown in Fig. 2. The measurement of the relationship $P - \delta$ was carried out until half of the maximum force of the specimen in the plastic state is reached. The evaluation of frost degradation of high-strength concretes was carried out using the ASTM C 666 methodology (Procedure B: rapid freezing in air and thawing in water) [8], which is used to determine the concrete durability index DF , according to the Eq. 2

$$DF = \frac{PN}{300} \cdot 100[\%] \tag{2}$$

where: N – number of freeze/thaw cycles, P – relative value of dynamic modulus of elasticity.

Concrete is considered resistant to cyclic freeze/thaw when the DF index is above 60%. Determination of the HSC resonant frequencies was done with the Resonant Frequency Meter Controls C311-R. The frequency measuring station for 0, 150, 250, 350, and 450 freeze/thaw cycles is shown in Fig.3.

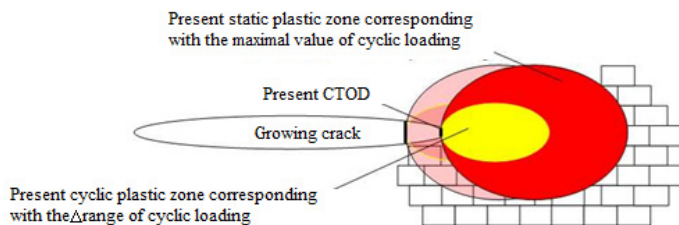


Fig. 2. Plastic zones before fracture *Source:* [13]

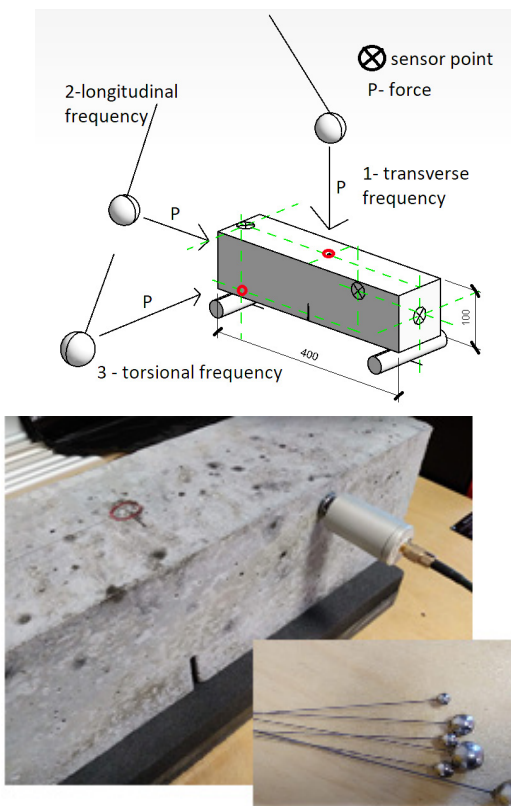


Fig. 3. Determination of the durability index according to ASTM C 666. Test sensor application points and dynamic actions. *Source:* own research

Jenq and Shah [10] suggest measuring an additional diagnostic parameter Q for concrete, which is of great importance for high-strength concretes. This parameter is a measure of concrete brittleness and depends on its modulus of longitudinal elasticity and characteristic fracture mechanics parameters: stress intensity factor K_{IC} and critical crack tip opening displacement $CTOD_c$, according to Eq. 3. It is believed that the higher the value of parameter Q , the lower the concrete brittleness.

$$Q = \left(\frac{E \cdot CTOD_c}{K_{IC}} \right)^2 \quad (3)$$

where: E – modulus of elasticity; $CTOD_c$ – critical crack tip opening displacement; K_{IC} – critical value of stress intensity factor.

The analysis also determined the changes in the critical value of the release of potential energy G_{IC} as a result of cyclic freeze/thaw, according to Eq. 4, respectively in a flat deformation state. This value is directly related to the critical stress-intensity value of primary K_{IC} , Young's E-modulus, and Poisson's factor, assumed for concrete of 0.2.

$$G_{IC} = \frac{(1-\nu^2)K_{IC}^2}{E} \quad (4)$$

where: ν – Poisson's factor; E – Young's module; K_{IC} – the critical value of the stress intensity factor.

3. Results and discussion

The average values of longitudinal modulus of elasticity E , fracture energy G_f , toughness index Q , and durability index DF of concretes after 150, 250, 350, and 450 freeze/thaw cycles are presented in Tab. 1. The loss of frost resistance described both by the DF factor and a significant decrease in fracture energy values for HSC without fibers (MB1) and with steel fibers (MB2) occurred after 450 freeze/thaw cycles. The fracture energy for the MB1 series fell by more than 60% after 450 cycles compared to unfrozen concrete. The value of the durability index after 450 freeze/thaw cycles dropped to 16.12% and according to ASTM C 666 [8], when this index falls below 60%, then the concrete loses its resistance to cyclic freeze/thaw. Concrete with steel fibers (MB2) after 450 freeze/thaw cycles was characterized by almost three times higher fracture energy than concrete without fibers (MB1). However, there is also a 45% decrease in fracture energy compared to non-frozen concrete and a low DF value of 18.70%. The addition of steel fibers to HSC leads to crack bridging when a fracture process develops in the concrete, despite the matrix-fiber boundary stratification. This mechanism contributes to an increase in the fracture energy value while propagating the internal defects in the concrete, which is reflected in the low DF factor. In the case of concretes with mixed fibers (MB3), the loss of durability was observed already after 150 freeze/thaw cycles based on a decrease of DF factor to 6.50%. The presence of steel and basalt fibers with high tensile strength values contributed to the fact that, despite a very low DF value, the fracture energy was higher than that of HSC after 450 freeze/thaw cycles without fibers when the frost resistance loss of this type of concrete was determined. The relatively low resistance of high-strength concretes with mixed steel and basalt fibers (MB3) to cyclic freeze/thaw described by DF was due to a possible lack of adhesion of basalt fibers to the cement matrix. The concrete of the MB3 series has undergone numerous cracks and the aggregate has been separated from the cement matrix. In the case of concretes with steel fibers (MB2) and without fibers (MB1), an increase in the DF factor became apparent between 150 and 250 freeze/thaw cycles. This

is due to an increase in the strength of the concrete during the time before the loss of frost resistance and is shown in the analysis of fracture energy values at the very beginning of the test to 150 freeze/thaw cycle. It can be assumed that the loss of resistance to cyclic freeze/thaw occurs when the energy associated with resisting crack growth decreases. Without added fibers, the change in fracture energy associated with the loss of cyclic freeze/thaw resistance was greater than 60%. For HSC with steel fibers, it was greater than 45% and for mixed fibers, it was 30%.

Table 1. Fracture mechanic parameters, brittleness parameter and durability factor determined on the basis of research. *Source:* own research

Sample	Number of freeze/thaw cycles <i>n</i>	<i>E</i> [GPa]	<i>GF</i> [Nm/m ²]	<i>Q</i> [mm]	<i>DF</i> [%]
MB1 fibreless	0	45.73 (0.90)*	15.01	210.47	100.00
MB1 fibreless	150	45.23 (0.33)*	35.93	189.59	50.04
MB1 fibreless	250	45.80 (0.45)*	20.16	190.45	83.67
MB1 fibreless	350	45.63 (0.53)*	19.89	190.31	70.68
MB1 fibreless	450	8.10 (0.32)*	5.85	190.93	16.12
MB2 with steel fibers	0	44.60 (1.02)*	27.03	190.57	100.00
MB2 with steel fibers	150	43.87 (0.68)*	41.16	189.57	48.53
MB2 with steel fibers	250	42.30 (0.79)*	34.57	190.73	80.03
MB2 with steel fibers	350	43.60 (1.06)*	18.64	191.50	68.40
MB2 with steel fibers	450	9.30 (2.59)*	14.73	190.76	18.70
MB3 with mixed fibers	0	48.27 (2.59)*	35.67	192.00	100.0
MB3 with mixed fibers	150	3.50 (1.07)*	23.57	182.00	6.46

The improvement of frost resistance of HSC described by durability factor *DF* analysis based on ASTM C666A method by adding 0.10% (by volume) polypropylene fibers is presented in [14]. The decrease in *DF* index below 60% HSC with fibers occurred after about 460 freeze/thaw cycles, while without fiber addition, concrete with 80 MPa compressive strength lost its frost resistance after 390 cycles. During the study of frost resistance of high-strength concrete with the addition of 0.5% steel fibers analysed in [15] by weight loss

and decrease in compressive strength after cyclic freeze/thaw, the loss of frost resistance was already noted after 100 freeze/thaw cycles in the case of no air-entraining and freezing in water. In the case of air-entrained concrete mix and freezing in air, no significant decrease in weight and compressive strength was observed after 100 cycles. In the analysis [16] of the high-performance concrete with steel fibers and mineral additives, after a period of 300 freeze/thaw cycles, the relative elastic modulus was 85.7%, indicating that the concrete did not undergo significant frost degradation during the test period. Analyzing the frost resistance of ultra-high-strength concretes with the addition of 1% steel fibers, it was found that after 180 freeze/thaw cycles, with a DF factor of 89%, there was a significant reduction in the weight of the concrete specimens ($>7.14\%$), which was due to the difficulty in proper fiber placement [17].

The parameter Q describing the brittleness of concrete indicates a slight influence of the addition of steel fibers and a mixture of steel and basalt fibers in the amount of 0.5% on the brittleness. In order to observe the change in concrete characteristics from quasi-brittle to quasi-plastic, the fiber addition in the mixture should be greater. Also, cyclic freeze/thaw did not significantly change the Q parameter.

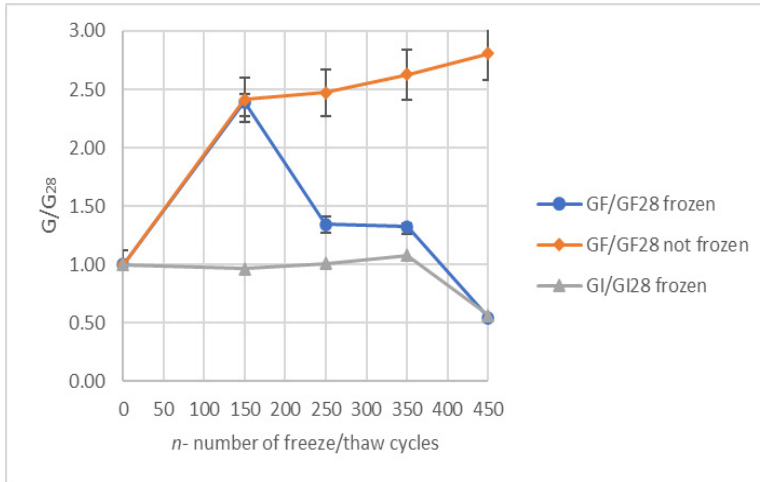


Fig. 4. Changes in fracture energy G_F and critical energy release G_I after n freeze/thaw cycles for MB1 series concretes. A description of the designations is included in the text. *Source*: own research

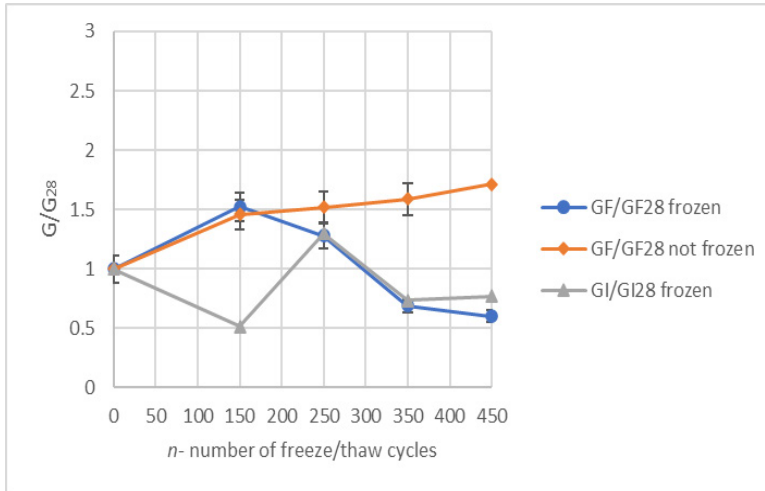


Fig. 5. Changes in fracture energy and critical energy G_F and critical energy release G_I after n freeze/thaw cycles for MB2 series concretes. A description of the designations is provided in the text. *Source:* own research

Figs 4-6 show an analysis of changes in fracture energy values versus the number of freeze/thaw cycles to concretes tested after 28 days of curing and concretes not subjected to freeze/thaw cycles. Changes in the critical release of G_{IC} energy release in flat deformation state after 150, 250, 350, 450 freeze/thaw cycles were also determined. The markings in the diagrams are respectively: G_F/G_{F28} frozen – change of fracture energy of frozen concrete after n freeze/thaw cycles compared to fracture energy after 28 days of curing of unfrozen concrete; G_F/G_{F28} not frozen – change of fracture energy of unfrozen concrete after n freeze/thaw cycles to fracture energy after 28 days of curing of unfrozen concrete; G_I/G_{I28} – change of the rate of fracture energy release of unfrozen concrete after n freeze/thaw cycles to unfrozen concrete after 28 days of curing. Up to 150 freeze/thaw cycles, a homogeneous increase of fracture energy of frozen and unfrozen concretes is visible for both HSC without fibers (MB1), where $G_F/G_{F28}=2.42$ as well as HSC with steel fibers (MB2), where $G_F/G_{F28}=1.51$. Concrete with mixed, steel, and basalt fibers (MB3) has been characterized by decreased fracture energy up to 34% after 150 freeze/thaw cycles since the beginning of the cycle. Concrete of the MB3 series not subjected to cyclic freeze/thaw with an increase in strength over time is characterized by an increase in fracture energy up to 67% after a period equal to 150 freeze/thaw cycles (50 days). The critical rate of energy release of fibreless concrete is constant up to 350 freeze/thaw cycles, followed by a sudden drop. This indicates the hardly predictable characteristics of high-strength concrete material, which changes its properties. In the case of HSC with steel fibers, an alternating increase and decrease in the critical rate of energy release in subsequent freeze/thaw cycles is noticeable, due to the presence of bridging fibre scratches. In the MB3 series, up to 50 freeze/thaw cycles, there is a sharp 89% drop in the energy release rate, followed by a constant value until the end of the test

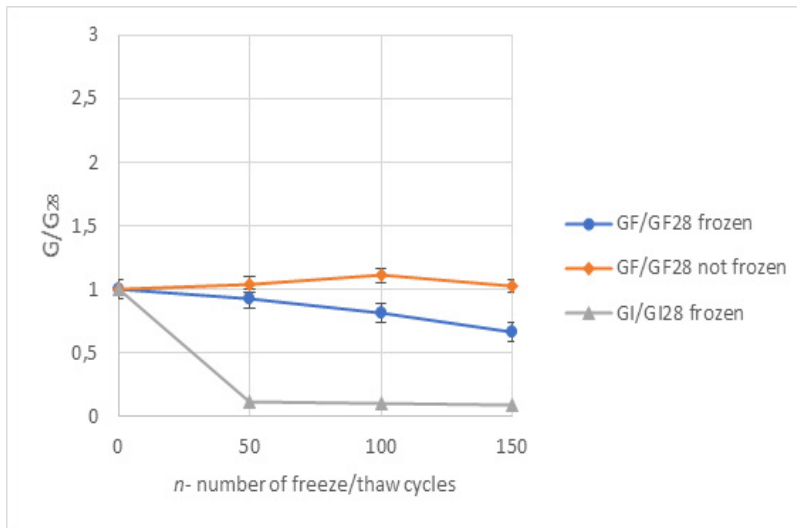


Fig. 6. Changes in fracture energy G_F and critical energy release G_I after n freeze/thaw cycles for MB3 series concretes. A description of the designations is provided in the text. *Source:* own research

4. Conclusions

The frost degradation of high-strength concretes, assessed on the basis of changes in fracture energy values, made it possible to obtain a more accurate description than in the case of classical methods of processes taking place in concrete as a result of cyclic freeze/thaw. Analyses using the parameters of fracture mechanics of concrete structures exposed to the destructive external environment show the progress of propagation of initial discontinuities and internal cracks – the cyclic freeze/thaw of high-strength concrete results in a significant reduction of fracture energy. As frost degradation progresses, the rate of release of the energy required for crack growth is reduced. The addition of 0.5% of steel fibers to high-strength concrete results in a slight improvement in the mechanical characteristics of the degraded material but does not significantly increase its durability under cyclic freeze/thaw conditions. The loss of adhesion of basalt fibers to the cement matrix leads to a reduction in frost resistance of high strength concrete. Cyclic freeze/thaw, as well as the presence of 0.5% of fibers (steel and basalt), did not significantly change the parameter describing concrete brittleness Q . Research should be continued on the fiber content in HSC, which would have a decisive influence on the improvement of fracture mechanics and durability parameters.


References

- [1] Golewski G., Sadowski T., “The parameters of concrete fracture mechanics are determined on the basis of experimental tests according to the I crack model”, *Construction Review*, no. 7–8, (2005), pp. 28–33.
- [2] Smith G.J., Rad F.N., “Economic Advantages of High-Strength Concretes in Columns”, *Concrete International*, vol. 11, no. 4, (1989), pp. 37–43.
- [3] Józwiak – Niedźwiedzka D., “Preventing peeling of concrete surfaces with the use of moistened drug aggregate”, *Roads and Bridges*, no. 2, (2006), pp. 37–54.

- [4] Cheng Y., Zhang Y., Jiao Y., “Quantitative analysis of concrete property under effects of crack, freeze-thaw and carbonation”, *Construction Building Materials*, no. 129, (2016), pp. 106-115. <https://doi.org/10.1016/j.conbuildmat.2016.10.113>
- [5] Song P.S., “Mechanical properties of high – strength steel fiber reinforced concrete”, *Construction and Building Materials*, vol. 18, no. 9, (2004), pp. 669-73.
- [6] Holschemacher K., Mueller T., Ribakov Y., “Effect of steel fibres on mechanical properties of high – strength concrete”, *Materials and design*, no. 31, (2010), pp. 2604-2615. <https://doi.org/10.1016/j.matdes.2009.11.025>
- [7] Kosior- Kazberuk M., “Variations in fracture energy of concrete subjected to cyclic freezing and thawing”, *Civil and Mechanical Engineering*, no.13, (2013), pp. 254-259. <https://doi.org/10.1016/j.acme.2013.01.002>
- [8] ASTM C 666: 2008 *Standard Test Method for Resistance of Concrete to Rapid Freezing and Thawing*.
- [9] Shah S.P., “Size – effect method for determining fracture energy and process zone size of concrete, RILEM TC 89–FMT”, *Materials and Structures*, no. 23, (1990),pp. 461–465.
- [10] Jenq Y.S., Shah S.P., “A two parameter fracture model for concrete”, *Journal of Engineering Mechanics*, no. 111, (1985), pp. 1227–1241.
- [11] Elices M, Guinea G, Planas J., “Measurement of the fracture energy using three-point bend tests: part 3 – influence of cutting the P- δ tail”, *Material Structures*, vol. 25, no. 6, (1992), pp.327–34.
- [12] Neimitz A., *Mechanika pękania*, PWN, Warszawa 1998.
- [13] Lesiuk G., “Application of a New, Energy-Based ΔS^* Crack Driving Force for Fatigue Crack Growth Rate Description”, *Materials*, no. 12, (2019), pp. 1-13. <https://doi.org/10.3390/ma12030518>
- [14] Ma H., Yu H., Li C., Tan Y., Cao W., Da B., “Freeze-thaw damage to high- performance concrete with synthetic fibre and fly ash due to ethylene glycol deicer”, *Construction and Building Materials*, no. 187, (2018), pp. 197-204. <https://doi.org/10.1016/j.conbuildmat.2018.07.189>
- [15] Wawrzeniarczyk J., Molendowska A., Kłak A., “Frost durability of steel fiber self-compacting concrete for pavements”, *The Baltic Journal of Road and Bridge Engineering*, vol. 11, no. 1, (2016), pp. 35-42. <https://doi.org/10.1088/1757-899X/471/3/032023>
- [16] Lee, J.S., “Properties on the Freeze-Thaw Resistance of High Performance Concrete Using Fibers and Mineral Admixtures”, *Materials Science Forum*, vol. 893, (2017), pp. 375-379. <https://doi.org/10.4028/www.scientific.net/MSF.893.375>
- [17] Smarzewski P., Barnat-Hunek D., “Effect of fiber Hybridization on durability Related Properties of Ultra-High Performance Concrete”, *International Journal of Concrete Structures and Materials*, vol. 11, no. 2, (2017), pp. 315-325. <https://doi.org/10.1007/s40069-017-0195-6>

The influence of sunspaces on the heating demand in living spaces – comparison of calculation methods according to ISO 13790

Magdalena Grudzińska

*Department of Construction; Faculty of Civil Engineering and Architecture;
Lublin University of Technology; Nadbystrzycka Street 40, 20-618 Lublin, Poland;
m.grudzinska@pollub.pl  0000-0001-9271-8797*

Funding: This work was supported by the Ministry of Science under grant number FN-9/2021.

Abstract: The calculation method presented in ISO 13790 was developed during the research project PASSYS. It aimed to work out the way of estimating energy demand while taking into account different passive solar systems. The standard includes two calculation methods for sunspaces – a full and simplified method. They differ in terms of basic assumptions and the treatment of solar gains in the sunspace and conditioned rooms. There are some doubts about the interpretation of equations presented in the standard, especially when it comes to modelling the solar radiation distribution within the solar space. The paper presents a discussion on the basic hypotheses applied in full and simplified methods, together with the author's suggestions regarding modifications to the ISO 13790 calculation methods. The modified methods allowed to satisfactorily predict the functioning of the exemplary sunspaces with a smaller area of glazed partitions and higher radiation absorptivity of the casing, that is spaces similar in terms of solar radiation utilisation to traditional living spaces. The phenomena typical for sunspaces with a high degree of glazing, such as the retransmission of reflected radiation, were not sufficiently taken into account in the calculation methods of the standard.

Keywords: passive sunspace systems, heating demand, ISO 13790, dynamic simulations

1. Introduction

The current version of the ISO 13790 [1] standard was accepted by The European Committee for Standardization in 2008, and its Polish version was approved one year later as PN-EN ISO 13790 standard “Energy performance of buildings. Calculation of energy consumption for heating and cooling”. Although the policy regarding technical conditions that the buildings and their location should have [2] does not include the Polish version of the standard, the current methodology for preparing energy performance certificates for buildings [3] is based on it. The calculation method was developed during the PASSYS research

project [4], aiming to work out a way of estimating the energy demand taking into account the influence of passive systems. The ISO 13790 norm was replaced by ISO 52016-1 [5] in 2017, also presenting calculation procedures for sunspaces. However, this method requires information about the direct and diffuse components of solar radiation. It may restrict its use in Poland because climatic data included in publicly available Typical Meteorological Years contain only total solar radiation incident on planes with different slopes.

Quasi-stationary methods of the standard [1] are based on the hypothesis of constant heat flow in building partitions. Calculations are performed by averaging climatic parameters for quite long periods (e.g. one month or the entire heating season). Phenomena related to the dynamic behaviour of the building, such as the accumulation and release of heat, are taken into account indirectly through the introduction of a heat gain utilization factor.

Appendix E of the standard [1] contains two calculation methods for non-conditioned sunspaces – a full and a simplified one, differing in fundamental concepts and the way of taking into account solar gains in the sunspace and the adjacent heated rooms. Equations included in the standard are formulated in a quite generalised way, and the interpretation of calculation methods raises certain doubts, especially in the area of modelling the distribution of solar radiation in the sunspace. These problems were discussed in the subject literature many times [6], [7], however, a comprehensive solution has yet to be found.

This article presents the author's suggestions for modifying both methods, as well as correcting the discrepancies of calculation algorithms. Results obtained with the use of the modified full and simplified methods of the quasi-steady state were compared with the results of more accurate dynamic simulations with an hourly step, which allowed to determine the recommended scope of the use of each method.

2. ISO 13790 methods

Heating demand in a monthly, quasi-stationary method is set out as in Eq. 1:

$$Q_{H,nd} = Q_{H,ht} - \eta_{H,gn} Q_{H,gn} \quad (1)$$

where: $Q_{H,nd}$ – energy demand for heating during the time step [MJ], $Q_{H,ht}$ – total heat transfer, including heat losses through building partitions, and heat losses for heating ventilation air [MJ], $Q_{H,gn}$ – total heat gains, including internal gains and gains from solar radiation [MJ], $\eta_{H,gn}$ – gain utilisation factor, calculated as in Eqs 2 and 3:

$$\eta_{H,gn} = \frac{1 - \gamma_H^{a_H}}{1 - \gamma_H^{a_H+1}} \text{ for } \gamma_H > 0 \text{ and } \gamma_H \neq 1 \quad (2)$$

$$\eta_{H,gn} = \frac{a_H}{a_H + 1} \text{ for } \gamma_H = 1 \quad (3)$$

γ_H – heat gains and losses relation (Eq. 4):

$$\gamma_H = \frac{Q_{H,gn}}{Q_{H,ht}} \quad (4)$$

a_H – dimensionless numerical parameter (Eq. 5),

$$a_H = a_{H,0} + \frac{\tau}{\tau_{H,0}} \quad (5)$$

$a_{H,0}$ – referential numerical parameter set out on the national level, for a monthly method, $a_{H,0} = 1$ [-], $\tau_{H,0}$ – relative time constant, set out on the national level, for a monthly method, $\tau_{H,0} = 15$ hours, τ – time constant of the building zone characterising the internal thermal inertia [hours], (Eq. 6),

$$\tau = \frac{C_m / 3600}{H_{tr} + H_{ve}}, \quad (6)$$

C_m – the internal thermal volume of the zone [J/K], H_{tr} – total coefficient of heat loss through partitions [W/K], H_{ve} – total coefficient of heat loss through ventilation [W/K].

2.1. Heat gains from the sunspace – full method

The method presented in the standard can be used only for the evaluation of non-conditioned sunspaces, i.e. neither heated nor cooled. In the partition wall between the living space and the sunspace, the presence of permanent openings allowing airflow is excluded. If they do exist, the sunspace should be regarded as a part of conditioned space.

Heat losses through the partition wall between the conditioned space and sunspace are determined with the inclusion of temperature reduction factor $b_{tr} < 1$, which means that heat is transmitted into the environment of higher temperature than external conditions. The temperature reduction factor is determined as follows (Eqs 7 and 8):

$$b_{tr} = \frac{\theta_{int,H} - \theta_s}{\theta_{int,H} - \theta_e} = \frac{H_{se}}{H_{is} + H_{se}} \quad (7)$$

$$\theta_s = \frac{\theta_{int,H} H_{is} + \theta_e H_{se}}{H_{is} + H_{se}} \quad (8)$$

where: $\theta_{int,H}$ – set-point temperature for heating in the living space [°C], θ_e – average external temperature in the given calculation step [°C], θ_s – average internal temperature of the sunspace in the given calculation step [°C], H_{is} – coefficient of heat transfer through the partition between the living space and sunspace [W/K], H_{se} – coefficient of heat transfer through sunspace casing to the outside [W/K].

In the calculation of the coefficient b_{tr} (Eq. 7), it is the heat transfer through the partition and the casing of the sunspace that is taken into account, rather than the influence of solar gains on the sunspace temperature θ_i . It is compensated for by including indirect gains from the sunspace Q_{si} in the energy balance of living spaces.

Heat gains in the building's heated zone obtained through a sunspace Q_{ss} [MJ] are treated as a sum of direct Q_{sd} and indirect Q_{si} gains (Eq. 9):

$$Q_{ss} = Q_{sd} + Q_{si} \quad (9)$$

Direct gains reach the conditioned zone through the partition wall between the sunspace and living space. These gains are derived from multiple transmissions (first through the sunspace glazing, and then through windows or doors in the partition wall) or from radiation absorbed on the partitions' surface. Indirect gains are determined by ISO 13790 as (Eq. 10):

$$Q_{sd} = F_{sh,e} (1 - F_{F,e}) g_e \left((1 - F_{F,w}) g_w A_w + \alpha_p A_p \frac{H_{p,tot}}{H_{p,e}} \right) I_p t \quad (10)$$

where: $F_{sh,e}$ – reduction factor taking into account shading of the sunspace by external obstacles (buildings, trees, hills, elements of the same building) [-] (Eq. 11):

$$F_{sh,e} = F_{hor} F_{ov} F_{fin} \quad (11)$$

F_{hor} – reduction factor from horizon [-], F_{ov} – reduction factor from overhangs [-], F_{fin} – reduction factor from pilasters [-], $F_{F,e}$ – frame area fraction in the sunspace outer glazing area [-], $F_{F,w}$ – frame area fraction in the total area of the window in the partition wall [-], g_e – total solar energy transmittance of the sunspace glazing [-], g_w – total solar energy transmittance of window glazing in the partition wall [-], A_w – window area of the partition wall [m²], A_p – opaque area of the partition wall [m²], α_p – absorptivity of the partition wall [-], $H_{p,tot}$ – heat transfer coefficient from the internal environment through the opaque part of the partition wall and the sunspace to the external environment [W/K], $H_{p,e}$ – heat transfer coefficient from the absorbing (external) surface of the partition wall through the sunspace to the external environment [W/K], I_p – solar irradiance of the partition wall in a given calculation step [W/m²], t – duration of the calculation step [Ms].

Indirect gains are released to the air in sunspace volume through convection, coming from the energy absorbed on the surface of the casing. They are treated as gains derived from non-conditioned space with the temperature reduction factor $(1 - b_{tr})$. They are calculated by summing up the gains from each opaque absorption area in the volume of the sunspace and subtracting the gains transmitted by conduction directly through the partition wall, included in Q_{sd} (Eq. 12):

$$Q_{si} = (1 - b_{tr}) F_{sh,e} (1 - F_{F,e}) g_e \sum_j (I_j \alpha_j A_j) - F_{sh,e} (1 - F_{F,e}) g_e \alpha_p A_p \frac{H_{p,tot}}{H_{p,e}} I_p t \quad (12)$$

where (the remaining nomenclature as above): b_{tr} – temperature reduction factor in the given month [-], I_j – solar irradiance on the “ j ” opaque interior surface of the sunspace in a given time step [W/m²], α_j – absorptivity of the “ j ” opaque interior surface of the sunspace [-], A_j – area of the “ j ” opaque interior surface of the sunspace [m²].

2.2. Heat gains from the sunspace – a simplified method

On the national level, the use of the simplified method is allowed, subject to the following modifications:

- in the living space, solar gains from the sunspace are ignored – direct gains “supplied” by opaque and glazed parts of the partition wall or indirect gains from the sunspace casing are not included in the heat balance,
- these gains are included as a substitute, through the use of the temperature reduction factor b_{tr}^* while calculating heat transmission from the heated space to the sunspace; it is assumed then that temperature in the sunspace θ_s^* is the result of not only inflow and outflow of heat through the casing (as in the full method), but also of solar gains in its volume (Eqs 13 and 14):

$$b_{tr}^* = \frac{\theta_{int,H} - \theta_s^*}{\theta_{int,H} - \theta_e} \neq b_{tr} = \frac{H_{se}}{H_{is} + H_{se}} \quad (13)$$

$$\theta_s^* = \frac{\Phi_u + \theta_{int,H} H_{is} + \theta_e H_{se}}{H_{is} + H_{se}} \quad (14)$$

where: Φ_u – average solar gains in sunspace volume in the calculation step [W].

2.3. Proposed modifications of both methods

The abovementioned methods require some kind of commentary because the equations provided in the standard are not entirely consistent. Firstly, in Eqs 10 and 12 the multiplier $F_{sh,e}(1 - F_{F,e})g_e$ is related to the exterior casing of the sunspace. It should be therefore related to the intensity of the radiation incident on the external casing, not with the intensity of the radiation reaching the partition wall I_p or the interior part of the casing I_j . Secondly, the subtraction of the element regarding direct gains by the casing in the Eq. 12 means that these gains are not at all taken into account in the calculations (it is shortened with the analogical element in the Eq. 10). The subtracted element should also be multiplied by $(1 - b_{tr})$, which can be physically interpreted as diminishing the indirect gains from the partition wall by a part conducted directly to the interior of the living space. Such notation was placed in the draft of the standard, which was made available by CEN in 2007 to submit comments before the final version was published [8]. Thirdly, the multiplier “ t ” meaning the duration of the calculation step occurs in Eqs 10 and 12 with the component I_p but is omitted in the component I_j . Moreover, the standard does not precise the way the radiation intensity in the sunspace should be specified.

Taking the above into account, it was proposed that the calculation of gains Q_{sd} and Q_{si} is performed as follows (Eqs 15-19):

$$Q_{sd} = \left((1 - F_{F,w}) g_w A_w + \alpha_p A_p \frac{H_{p,tot}}{H_{p,e}} \right) I_p t \quad (15)$$

where (remaining nomenclature is as above):

$$I_p = f_p \frac{1}{A_w + A_p} \sum_k F_{sh,ek} A_{sol,k} I_{sol,k} \quad (16)$$

f_p – the part of solar radiation that is transmitted into the sunspace, incident on the area of the partition wall [-], k – the number of collecting (glazed) surfaces of the external casing of the sunspace facing the given direction, $F_{sh,ek}$ – shading reduction factor of the collecting surface “ k ” of the sunspace, connected with external obstacles [-], $A_{sol,k}$ – an effective area of the sunspace’s collecting surface “ k ” [m²] (Eq. 17), $I_{sol,k}$ – the intensity of solar radiation on surface “ k ” of the sunspace’s exterior casing [W/m²],

$$A_{sol,k} = (1 - F_{F,ek}) g_{ek} A_{ek} \quad (17)$$

$F_{F,ek}$ – frame area fraction of the sunspace external glazing in the surface “ k ” [-], g_{ek} – total solar energy transmittance of the sunspace glazing on plane “ k ” [-], A_{ek} – the area of external glazing of the sunspace in surface “ k ” [m²].

$$Q_{si} = (1 - b_{tr}) \left(\sum_j (I_j \alpha_j A_j) - \alpha_p A_p \frac{H_{p,tot}}{H_{p,e}} I_p \right) t \quad (18)$$

where (the remaining nomenclature is as above):

$$I_j = f_j \frac{1}{A_j} \sum_k F_{sh,ek} A_{sol,k} I_{sol,k} \quad (19)$$

f_j – the part of solar radiation transmitted into the sunspace, incident on the surface “ j ” of its internal wall [–].

Suggestions for the calculation of coefficients f_p and f_j were presented in part 4.

3. Dynamic simulations

More complex simulation methods are used to carry out computer calculations. The calculation step estimated here is much shorter than in quasi-stationary methods – it can be, for example, one hour or several minutes. This allows to include heat exchange processes that are dependent on temperature change and exposure to solar radiation as discrete dynamic processes [9], [10]. Dynamic simulations can also be used as validation methods for the less accurate procedures (such as quasi-stationary methods) [11], [12].

Postulates concerning the possibility of using the commonly available simulation tools for modelling sunspace systems formulated based on various research works ([13] – [15], among others) were included synthetically in work [16]. The main requirements that the computer programmes should meet to correctly calculate the solar gains in rooms with a high degree of glazing are as follows:

- the capability of defining the actual geometry of the room as well as glazed elements, considering their dimensions, placement in partitions, and orientation in terms of the direction they are facing,
- detailed analysis of solar radiation reaching the walls of the living space, taking into account the division into direct and diffuse components, and also relevantly accurate modelling of radiation incident onto leaning surfaces (e.g. using the models which are taking into account scattered radiation anisotropy),
- description of the radiation transmitted into the living spaces, considering the actual beam path through glazing; the distribution of direct radiation incident on individual internal partitions with the help of weighted proportionality coefficients (taking into account surface area and optic features of the partition, i.e. the ability to absorb and reflect the radiation) or configuration coefficients used for modelling radiative heat exchange is not sufficient,
- the capability of taking into account radiative heat exchange with the sky.

In this work, calculations are performed with the use of BSim simulation program, which meets the above requirements [17]. The algorithms of the program are based on the control volume method, in which building construction elements and air zones are represented by nodal points of specified physical properties, such as density, conduction, and heat capacity. For each of the air zones, there is a balance equation that takes into account the heat flux flowing through the casing, the transmission of solar radiation by transparent elements, heat fluxes generated by installation systems and carried through ventilation, infiltration, or interzonal mixing of air. Processes that are constant in time are modelled via the division into time steps of finite duration, usually lasting up to 1 hour.

The user’s data (e.g. from own measurements) can be inputted into the program as climatic data, or data representing typical meteorological years prepared under the procedures binding in a given country. The essential input parameters include air temperature, the intensity of the direct and diffuse solar radiation, and the relative air humidity. Data regarding the direction and speed of the wind may also be desired, especially if more detailed modelling of the natural exchange of air is being planned. In this research, a Typical Meteorological Year for

Warsaw created under the procedures described in [18], available on the <https://dane.gov.pl> website, was used.

4. The comparison of presented calculation methods

Below there is presented the energy demand obtained for an exemplary living space adjacent to the sunspace, calculated with the help of the proposed modification of algorithms of the full and simplified method. The results were compared with dynamic simulations of the same living space arrangements carried out with assumptions as close as possible to the assumptions of steady-state methods.

The living space has two exterior walls – the wall facing south is adjacent to the sunspace (glazed balcony), and the full, eastern wall is exposed to the external air (Fig. 1). Insulating properties of the partitions are quite high, which corresponds to constructions built after 2014 (Tab. 1). Apart from solar gains in the living space, internal gains on the 3.0 W/m^2 level (according to Appendix G ISO 13790) were assumed. The air exchange in the room equals 0.5 1/h , and the air is supplied from the outside to meet the requirement of the standard [1] of the lack of infiltration between the sunspace and conditioned space.

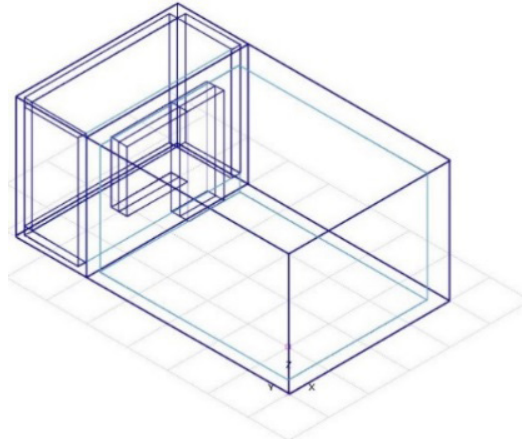


Fig. 1. A diagram of the living space and the sunspace in BSim program

Table 1. Chosen parameters of external partitions

Type of space	Heat transfer coefficient U [$\text{W}/(\text{m}^2 \cdot \text{K})$]		Total solar energy transmittance g [-]
	Full part	Window joinery	Glazing
Living space	0.24	1.20 – 1.23	0.63
Sunspace	0.50	1.66 – 1.69	0.62

All the balcony walls are glazed (Fig. 1). Two types of glazing were analysed:

- on the entire height of the balcony – variant 1,
- above the height of 1.1 m, with a full casing below – variant 2.

Absorptivity of the interior surfaces of the sunspace was assumed to be equal to 0.2, 0.5, or 0.8. In dynamic simulations, radiation losses caused by the retransmission to the outside were taken into account, which is consistent with the physical characteristics of these phenomena.

In the full method of the ISO 13790, it is assumed that the solar gains in a conditioned space are derived from the radiation absorbed on the surface of full partitions of the sunspace or let through the glazing in the partition wall, making them dependent on the optical properties of the surface. This means that only the radiation dose reaching the given surface before the first reflection is used and the remaining part of the radiation is lost. Phenomena related to multiple reflections in the sunspace are omitted, which causes the underestimation of air temperature in the sunspace.

In the calculations following the simplified method, the retransmission of the radiation on the outside of the sunspace was omitted. Such hypothesis is assumed in the literature of the subject [6] as consistent with the general methodology of the standard and compensating for the fact that the simplified method diminishes the effects of the exposure to solar radiation caused by omitting solar gains transmitted through the glazing of the partition wall of the living space.

In reality, the radiation on individual surfaces of the sunspace is not identical. Because of the sun's movement in the sky, it can be expected that the intensity of the direct radiation will be the highest on the partition wall and the floor. Accurate analytical methods determine these values by tracing the path of the sun's rays ("ray tracing"), as in [14], [19].

The distribution of diffuse solar radiation incident on the given surface can be determined in several ways:

- by assuming that radiation division is proportional to surface absorptivity and size; it is the simplest method described in the literature [6, 14, 15],
- using view factors, determining which part of radiation derived from one surface reaches the other surface, depending on their location and geometry; these factors are available in [20], for example.

In the example, the first method was used by deriving factors f_p and f_j from the general formula (Eq. 21)

$$f = \frac{\alpha \cdot A}{\sum_n (1 - \rho_n) \cdot A_n} \quad (21)$$

where: n – the number of the opaque internal surfaces of the sunspace, α – absorptivity of a surface [–], ρ – reflectivity of a surface [–], A – surface area [m²].

These factors were used in total radiation division, which is the sum of direct and diffuse radiation. It is not quite physically correct, however, such simplification was accepted because ISO 13790 methodology does not assume the division of the radiation into individual components. This assumption understates direct solar gains (through the partition wall) in the living space, and therefore it is on the "safe" side.

When comparing the chosen calculation methods below, basic parameters of the system functioning characteristics were presented: air temperature in the sunspace and energy demand in the living space (Tabs 2 and 3).

Table 2. Air temperature [°C] in the sunspace during the heating season, SD – dynamic simulations, ISO p – full method, ISO u – simplified method

Air temperature in the sunspace [°C]												MAPE		
Month		IX	X	XI	XII	I	II	III	IV	V		[%]		
Variant 1	$\alpha = 0.2$	SD	17.9	12.5	7.2	5.1	4.2	4.8	10.2	12.2	18.0			
		ISO p	14.1	10.4	6.1	4.4	2.7	3.0	7.3	8.8	13.6	24.6		
		ISO u	37.1	24.6	13.3	10.2	12.6	15.0	26.8	34.8	46.7	145.5		
	$\alpha = 0.5$	SD	20.8	14.3	8.1	5.7	5.3	6.0	12.5	14.8	21.5			
		ISO p	14.1	10.4	6.1	4.4	2.7	3.0	7.3	8.8	13.6	36.1		
		ISO u	37.1	24.6	13.3	10.2	12.6	15.0	26.8	34.8	46.7	105.2		
	$\alpha = 0.8$	SD	22.2	15.2	8.5	6.0	6.0	6.7	13.7	16.2	23.4			
		ISO p	14.1	10.4	6.1	4.4	2.7	3.0	7.3	8.8	13.6	40.8		
		ISO u	37.1	24.6	13.3	10.2	12.6	15.0	26.8	34.8	46.7	89.0		
	Variant 2	$\alpha = 0.2$	SD	19.2	13.6	8.4	6.3	5.6	6.2	11.6	13.7	19.3		
			ISO p	14.2	10.4	6.2	4.5	2.8	3.1	7.4	8.9	13.7	34.0	
			ISO u	27.3	18.6	10.3	7.8	8.5	10.0	18.5	23.7	32.6	48.8	
$\alpha = 0.5$		SD	21.1	14.8	9.0	6.7	6.3	7.0	13.2	15.4	21.6			
		ISO p	14.2	10.4	6.2	4.5	2.8	3.1	7.4	8.9	13.7	40.2		
		ISO u	27.3	18.6	10.3	7.8	8.5	10.0	18.5	23.7	32.6	34.2		
$\alpha = 0.8$		SD	22.0	15.3	9.2	6.8	6.6	7.4	13.8	16.1	22.6			
		ISO p	14.2	10.4	6.2	4.5	2.8	3.1	7.4	8.9	13.7	42.0		
		ISO u	27.3	18.6	10.3	7.8	8.5	10.0	18.5	23.7	32.6	29.0		

Table 3. Heating demand in the living space [kWh] during the heating season. SD – dynamic simulations, ISO p – full method, ISO u – simplified method

Heating demand in the living space [kWh]												Sum	Change to SD*	MAPE	
Month		IX	X	XI	XII	I	II	III	IV	V	[kWh]	[%]	[%]		
Variant 1	$\alpha = 0.2$	SD	1.3	62.8	135.4	169.5	177.1	155.5	96.2	66.3	18.2	882.3			
		ISO p	0.4	49.3	139.8	176.3	183.5	154.1	73.4	26.6	0.1	803.4	-8.9	32.2	
		ISO u	0.0	35.1	133.0	170.6	173.9	143.4	54.0	1.6	0.0	711.6	-19.4	44.2	
	$\alpha = 0.5$	SD	0.0	36.0	124.5	161.4	163.7	140.7	66.8	36.0	0.4	729.4			
		ISO p	0.0	23.3	125.0	163.9	162.5	130.9	35.9	4.5	0.0	646.1	-11.4	30.9	
		ISO u	0.0	35.1	133.0	170.6	173.9	143.4	54.0	1.6	0.0	711.6	-2.4	26.4	
	$\alpha = 0.8$	SD	0.0	22.7	117.7	156.4	155.5	131.6	49.1	24.0	0.0	657.1			
		ISO p	0.0	7.9	110.2	151.6	141.5	107.9	12.3	0.6	0.0	531.9	-19.0	30.4	
		ISO u	0.0	35.1	133.0	170.6	173.9	143.4	54.0	1.6	0.0	711.6	8.3	22.3	
	Variant 2	$\alpha = 0.2$	SD	0.4	59.5	130.8	164.6	171.4	150.4	92.3	63.9	17.1	850.4		
			ISO p	8.2	78.0	153.7	187.8	203.4	176.0	113.0	73.1	3.7	996.8	17.2	34.8
			ISO u	0.0	66.8	148.2	183.2	195.6	167.4	97.6	53.2	0.0	912.0	7.2	31.6
$\alpha = 0.5$		SD	0.0	42.1	124.2	159.8	163.3	141.5	74.2	43.6	6.1	754.7			
		ISO p	1.2	60.2	145.0	180.5	190.9	162.4	88.5	42.8	0.3	871.8	15.5	24.6	
		ISO u	0.0	66.8	148.2	183.2	195.6	167.4	97.6	53.2	0.0	912.0	20.8	31.6	
$\alpha = 0.8$		SD	0.0	35.0	121.1	157.5	159.4	137.3	65.7	36.0	1.1	713.0			
		ISO p	0.2	43.0	136.2	173.2	178.5	148.7	64.5	19.1	0.0	763.4	7.1	23.6	
		ISO u	0.0	66.8	148.2	183.2	195.6	167.4	97.6	53.2	0.0	912.0	27.9	41.2	

* The change of heating demand in the entire heating season under the ISO method compared to dynamic simulation results.

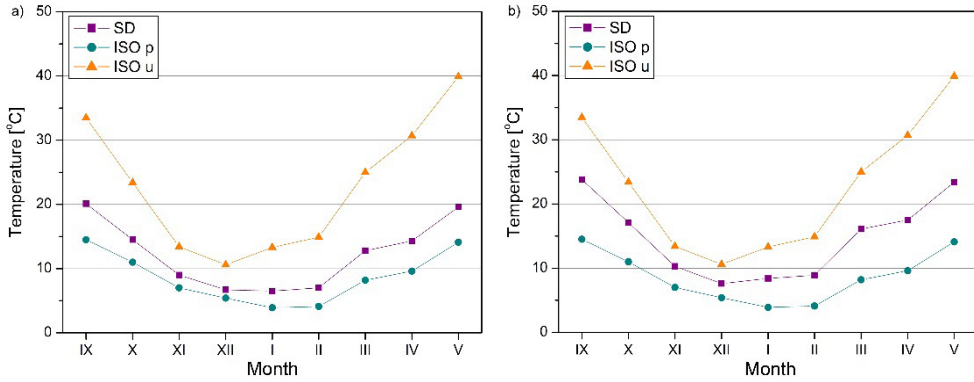


Fig. 2. Air temperature in the sunspace during the heating season: a) variant 1, $\alpha = 0.5$, b) variant 2, $\alpha = 0.5$

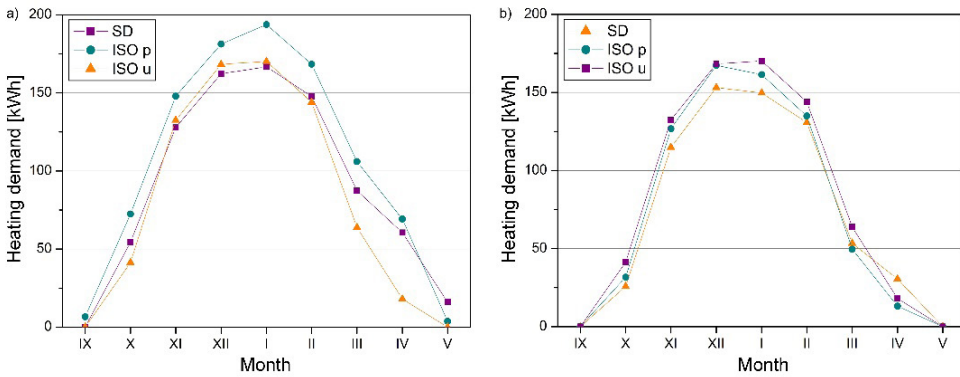


Fig. 3. Heating demand in the living space during the heating season: a) variant 1, $\alpha = 0.5$, b) variant 2, $\alpha = 0.5$

In ISO 13790 methods, both in full and simplified versions, the absorptivity of the interior surfaces of the sunspace does not influence its interior temperature. This temperature is determined as dependent only on inflow and outflow of heat through transmission (full method), or as a derivative of solar gains through glazing and thermal features of the construction (simplified method). As a result of these hypotheses, the full method understates, and the simplified method quite significantly overstates interior temperatures, which is especially noticeable in spring and autumn months (Fig. 2). The results of dynamic simulations indicate the increase of interior temperature along with the increase of surface absorptivity. The temperature takes intermediate values between the results obtained for the full and simplified method, which can be regarded as a kind of upper and lower limit of the actual inside temperature

The course of average monthly temperatures and the heating demand in the subsequent months of the heating season were compared with the results of dynamic simulations, determining the Mean Absolute Percentage Error MAPE (Eq. 22):

$$MAPE = \frac{100}{n} \sum_{i=1}^n \left| \frac{P_i - S_i}{S_i} \right| \quad (22)$$

where: n – number of forecast values, P – forecast value (according to ISO 13790), S – accurate value (according to dynamic simulations).

If $\text{MAPE} > 15\%$ (which was the case in all instances), the forecasts are inaccurate, and they should not be accepted in the analysis of the phenomenon [21]. This does not disqualify the methods presented in the standard, because they are expected to produce a result of the seasonal heating demand that is merely close to the more accurate calculations.

In assumption, quasi-stationary methods ISO 13790 should be “on the safe side”, overstating the seasonal heating demand compared with the calculations with the hourly step, whereas the full method (which is more accurate) should produce a lower heating demand. Such regularity is noticeable only in two calculation cases – variant 2, $\alpha = 0.5$, and 0.8 (Fig. 3, Tab. 3). In these instances, the differences between the full method and simulations, are 15.5% and 7.1%, and between simplified method and simulations – 20.8% and 27.9%. This sort of approximation in engineering calculations can be regarded as satisfactory.

The results obtained for the lowest surface absorptivity (in casing variant 2) can raise some doubts in terms of the correct mapping of the psychical processes by both methods of the standard [1], even though differences between them and dynamic simulations alone are, in the worst case, close to 17%. If the absorptivity of the sunspace casing is low, the full ISO method gives the highest heating demand, which is the result of joining smaller indirect solar gains with the incomplete consideration of the buffer effect of the sunspace as a result of lowered inside temperature and indirect gains. In this variant, the simplified ISO method, which overstates the buffer effect of the sunspace, turned out to be closer to dynamic simulations.

Modelling of solar spaces with a high degree of glazing (variant 1) according to the ISO 13790 standard should be regarded as unsatisfactory. The simplified method overstates energy gains when large, glazed surface areas are involved, which is a result of the omitting of radiation retransmission. The significance of this phenomenon diminishes only in the instances of the highest surface absorptivity. In the full method, in turn, omitting the retransmission causes the overstatement of direct and indirect gains, which causes a drop in the heating demand, which is particularly noticeable when the absorptivity increases.

5. Summary

Summing up, ISO 13790 methods (after proposed modifications were taken into account) allowed to satisfactorily predict the functioning of the exemplary sunspace with a smaller area of glazed partitions and higher radiation absorptivity inside of the casing, that is space similar in terms of solar radiation utilisation to traditional living spaces. The phenomena typical for sunspaces with a high degree of glazing, such as the retransmission of reflected radiation, were not sufficiently taken into account in the calculation method of the standard. This effects in bigger discrepancies in results obtained for the sunspace glazed on all surfaces, and for high reflectivity inside the casing.

It is important to remember that the above analyses were carried out for a specific radiation distribution in the sunspace. A better estimation of surface irradiation could affect the accuracy of calculations. However, a detailed analysis of the radiation path goes beyond the area of engineering calculations, which is to be used by the methods contained in ISO 13790.

Among the presented calculation methods, dynamic simulations are a tool that allows taking into account the largest number of factors determining the functioning of a sunspace, i.e. primarily:

- the spatial nature of solar radiation,
- optical properties of the glazing as a function of the angle of incidence,
- radiation retransmission due to reflections in the sunspace,
- varied surface absorptivity,
- ventilation of the sunspace and airflow between the greenhouse and the conditioned room.

Therefore, it is a method with the greatest research potential, if it is consciously used and, if possible, validated in the conditions of the actual operation of the tested objects.


References


- [1] ISO 13790:2008 “Energy performance of buildings. Calculation of energy consumption for heating and cooling”, International Organization for Standardization, Geneva, 2008.
- [2] Announcement of the Minister of Infrastructure and Development of 17 July 2015 on the announcement of the uniform text of the ordinance of the Minister of Infrastructure on technical conditions to be met by buildings and their location, Journal of Laws of 2015, No. 0, item 1422.
- [3] Regulation of the Minister of Infrastructure and Development of 27 February 2015 on the methodology for determining the energy performance of a building or part of a building and energy performance certificates, Journal of Laws of 2015, item 376.
- [4] Bourdeau L., Buscarlet C.: “PASSYS, Final Report of the Simplified Design Tool Subgroup”, Commission of the European Communities, Directorate-General XII, Brussels 1989.
- [5] ISO 52016-1:2017 “Energy performance of buildings. Energy needs for heating and cooling, internal temperatures and sensible and latent heat loads. Part 1: Calculation procedures”, International Organization for Standardization, Geneva, 2017.
- [6] Leenknecht S., Saelens D.: “Comparison between simplified and dynamic calculation of highly glazed spaces”, in: *Proceedings of the 1st Central European Symposium on Building Physics*, Cracow – Lodz, September 2010, pp. 335-342.
- [7] Passerini F., Albatici R., Frattari A.: “Quasi-steady state calculation method for energy contribution of sunspaces: a proposal for the European standard improvement”, in: *Proceedings of Building Simulation Applications BSA 2013*, 1st IBPSA Italy Conference, Bozen-Bolzano, Italy, pp. 141-150. Available: <http://www.ibpsa.org/proceedings/BSA2013/15.pdf> [Accessed: 18 Feb 2017]
- [8] ISO/FDIS 13790:2006(E) “Energy performance of buildings. Calculation of energy use for space heating and cooling”, Draft for comments by CEN and ISO WG. Available: www.cres.gr/green-building/PDF/prend/set3/WI_14_TC-draft-ISO13790_2006-07-10.pdf [Accessed: 23 Feb 2017]
- [9] Gawin D., Kossecka E. (ed.), *Typowy rok meteorologiczny do symulacji wymiany ciepła i masy w budynkach*. Lodz Univeristy of Technology, Łódź 2002.
- [10] Clarke J.A., *Energy Simulation in Building Design*. Butterworth-Heinemann, Oxford 2001.
- [11] Jokisalo J., Kurnitski J.: “Performance of EN ISO 13790 utilisation factor heat demand calculation method in a cold climate”, *Energy and Buildings*, 39 (2007), pp. 236-247. <https://doi.org/10.1016/j.enbuild.2006.06.007>
- [12] Kokogiannakis G., Strachan P., Clarke J.: “Comparison of the simplified methods of the ISO 13790 Standard and detailed modelling programs in a regulatory context”, *Journal of Building Performance Simulation*, 1 (2008), pp. 209-219. <https://doi.org/10.1080/19401490802509388>
- [13] Wall M.: “Climate and energy use in glazed spaces”, Report TABK-96/1009, Lund University, Department of Building Science, Lund 1996.


-
- [14] Roux J.J., Teodosiu C., Covallet D., Chareille R.: "Validation of a glazed space simulation model using full-scale experimental data", *Energy and Buildings*, 36 (2004), pp. 557-565. <https://doi.org/10.1016/j.enbuild.2004.01.030>
- [15] Oliveti G., De Simone M., Ruffolo S.: "Evaluation of the absorption coefficient for solar radiation in sunspaces and windowed rooms", *Solar energy*, 82 (2008), 212-219. <https://doi.org/10.1016/j.solener.2007.07.009>
- [16] Hilliaho K., Lahdensivu J., Vinha J.: "Glazed space thermal simulation with IDA-ICE 4.61 software – suitability analysis with case study", *Energy and Buildings*, 89 (2015), pp. 132-141. <https://doi.org/10.1016/j.enbuild.2014.12.041>
- [17] Wittchen K.B., Johnsen K., Grau K., *BSim user's guide*. Danish Building Research Institute, Hørsholm 2004.
- [18] Narowski P., „Dane klimatyczne do obliczeń energetycznych w budownictwie”, *Ciepłownictwo, Ogrzewnictwo, Wentylacja*, 11 (2006), pp. 22-27.
- [19] Tiwari G.N., Gupta A., Gupta R.: "Evaluation of solar fraction on north partition wall for various shapes of solarium by Auto-Cad", *Energy and Buildings*, 35 (2003), pp. 507-514. [https://doi.org/10.1016/S0378-7788\(02\)00158-5](https://doi.org/10.1016/S0378-7788(02)00158-5)
- [20] Wiśniewski S., Wiśniewski T.S., *Wymiana ciepła*. Wydawnictwa Naukowo-Techniczne, Warszawa 1994.
- [21] Rogalska M., *Wieloczynnikowe modele w prognozowaniu czasu procesów budowlanych*. Lublin University of Technology, Lublin 2016.

Digitalization of historic buildings using modern technologies and tools

Anna Prokop¹, Piotr Nazarko², Leonard Ziemiański³

¹ *Department of Architectural Design and Engineering Graphics; Faculty of Civil and Environmental Engineering and Architecture; Rzeszow University of Technology;
12 Powstańców Warszawy Av, 35-959 Rzeszów, Poland;
a.prokop@prz.edu.pl  0000-0003-2666-1002*

² *Department of Structural Mechanics; Faculty of Civil and Environmental Engineering and Architecture; Rzeszow University of Technology;
12 Powstańców Warszawy Av, 35-959 Rzeszów, Poland;
pnazarko@prz.edu.pl  0000-0002-6135-2486*

³ *Department of Structural Mechanics; Faculty of Civil and Environmental Engineering and Architecture; Rzeszow University of Technology;
12 Powstańców Warszawy Av, 35-959 Rzeszów, Poland;
ziele@prz.edu.pl  0000-0002-4012-0002*

Abstract: The aim of the paper is to present some experiences of using modern technologies to historical buildings digitalization. The emphasis is placed on the possibilities of spatial data collecting, as well as on subsequent 3D modelling. The paper describes the proposed survey techniques which are based on the Terrestrial Laser Scanning and photogrammetry. The authors obtained the point cloud by using the laser scanner Faro Focus 3D and dedicated software to combine scans (target based and cloud to cloud methods). The paper also provides an introduction to issues related to a method of building structure modelling based on a point cloud. The authors proposed some computer software tools that could improve work with a point cloud and the modelling process. The resulting 3D model could be both a source of information about historical building and a sufficient base to create computational model with spatial finite elements. The subject of the case study is the St. Hubert Chapel located in Rzeszów (Poland) and built in the middle of the 18th century under the patronage of the Lubomirski family. This rococo chapel is one of the most valuable architectural monuments in the region. Historical Building Information Model (HBIM) could be helpful in analysis, visualisations and conservation practice of this precious monument. Diagnosing the current object state and assessing its technical condition could be the purpose of creating a computational FEM model.

Keywords: digitalization of heritage buildings, laser scanning, Historical Building Information Modelling, point cloud, 3D modelling

1. Introduction

Monuments and heritage structures are an important factor for the economic development of many countries. The protection of monuments includes all actions taken to preserve their values and enable the society to use them. This protection can be equated with the concept of historical buildings conservation. Their preservation and maintenance require a balance between architectural values and construction safety [1]-[4].

When rapid changes take place in the world, heritage conservation should be multidisciplinary, as well as tools and methods should reflect scientific progress [5]. Laser scanning technology is emerging as a potential opportunity to be utilised in this area.

The main purpose of the paper is to present the possibility of applying reverse engineering in analysis and monuments conservation practice.

The case study presented in this paper is the St. Hubert Chapel in Rzeszów (Poland), an eighteenth-century sacral building from the rococo period. Digitalization of this object is important to preserve its cultural heritage and promote this monument in the region.

In the paper the authors used reverse engineering to create a solid model of the chapel from the TLS data. The 3D model contains information about geometry of the elements. The implementation of a BIM idea to this model allows to obtain a dataset of information and current documentation, which would be useful during maintenance and restoration of this building. In the future this model could be used for various types of analysis, for example structural stability analysis because of the railway line nearby.

2. Methodology

This paper presents some experiences of 3D structure modelling of a historical heritage building. The combination of contactless, non-invasive measurement techniques together with Building Information Modelling (BIM) and the finite element method can be an excellent tool for digitizing cultural heritage, assessing technical condition and determining ways to strengthen and secure the structure.

In accordance with the regulation, laser scanning is a method of terrain surface imaging, consisting in measuring the distance between the measured object and the device (scanner). The scanner can be installed on an aircraft, car or stationary structure, emitting and receiving laser pulses reflected from the object [6].

The scanner sends a laser beam towards the object (Fig. 1), which reflects it back to the device. Distance, vertical angle and horizontal angle are polar coordinates, which are then converted into the Cartesian system.

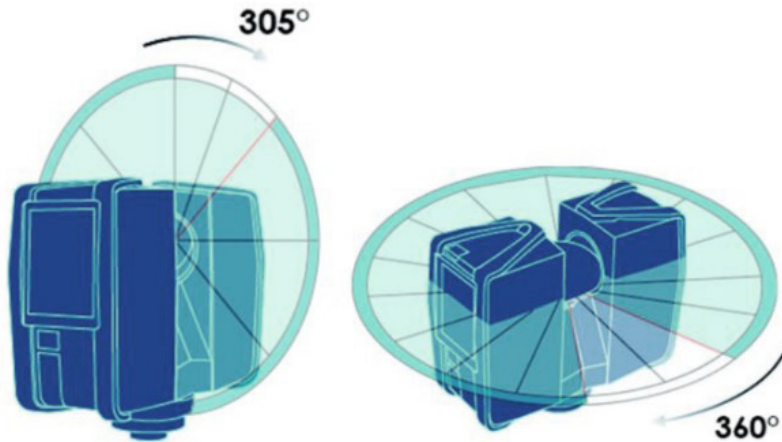


Fig. 1. Vertical and horizontal measuring range of the laser scanner used [7]

The measurement result of laser scanning technology is a point cloud – a set of measured points of space with coordinates (x, y, z). Points can contain information about the RGB colour. Their number depends on the quality settings for scanning and measurement time [7].

In order to create a point cloud for the whole measured object, it is necessary to combine individual scans (or measurements) taken from various positions by using dedicated software. The point cloud is a source of information about the object, its dimensions, geometry and colours.

The process of matching scans can be manual, semi – automatic or automatic. Much research has been carried out in automatic registration scans. Efforts have been made to create algorithms which merge scans without using the reference point as landmarks, targets and with small overlapped area to make registration faster and less data gathering time consuming without reducing accuracy [8].

Photogrammetry is another source of obtaining a point cloud. This is a field of technical sciences dealing with the acquisition, transformation, presentation and collection of information (quantitative and qualitative) related to the site (or object) based on photogrammetric photos (the so-called photograms) or their digital representations [9]. With this method, the accuracy of the resulting image -based point cloud is lower than that generated by the scanners [10].

The source of a point cloud could be also a combination of laser scanning and photogrammetry. These two methods of mapping space allow combining their advantages. Laser scanning ensures the accuracy of measured points, whereas photogrammetry ensures the accuracy of color reproduction [11]. Computer programs allow combining object photos and create a point cloud based on them. One of such programs is ReCap Photo, which processes photographs to create 3D representations of current sites or objects conditions. It allows creating and editing a point cloud based on both photographs and laser scans.

Point clouds can be used as a design background in programs such as AutoCAD, Navisworks or Inventor Professional. In 3D modelling programs, for example Revit or Archicad, the point cloud is a base layout for which it is possible to set views of projections, sections, perspectives or axonometry.

Inventorying by laser scanning technology allows to maintain a high level of detail, therefore using this technology for inventory of historic buildings allows digitalizing their

complex, intricate shapes (often with irregular walls, haunches and curvatures) in 3D. These modern methods can also be used to create technical documentation for existing buildings in a process called reverse engineering [1, 12, 13]. Comparison of the point cloud with 3D CAD model allows for use in as-built modelling [14].

Reverse engineering largely allows to restore knowledge about the building and to adopt its management strategy. This technology, combined with parametric object modelling, is extremely useful for modernization, renovation and conservation of architectural monuments.

Designs of new buildings are increasingly based on the ideas of BIM (Building Information Modelling). It gives the possibility of accurate planning of the entire investment, making cost estimates or work schedules as well as easier coordination of all involved industries. The BIM idea can also be applied to existing buildings. This is especially important for historic buildings with or without the outdated documentation – it is called the HBIM (Historical Building Information Model) [3]. The main requirement to use BIM for the analysis and representation of historical objects (HBIM) is the high model quality and reliability regarding to its geometry.

After receiving the point cloud, a further step is a process of object modelling. Possible methods, for example in Revit, are manual modelling (a time-consuming and labour-intensive process) or the use of program add-ons (accelerating the work in automatic or semi-automatic way). Examples of such solutions are: As-Built for AutoCAD Software, As-Built for Autodesk Revit, VirtuSurv. The As-Built (FARO) software provides a whole range of advanced tools for analysis and modelling based on a point cloud data directly in AutoCAD and Revit. It contains among others features such as: automatic polyline matching, creating 2D projections using automatic line extraction, matching cylinders and planes to point groups or drawing and dimensioning building elements (for instance windows, doors or staircases). Moreover, it allows to generate detailed images by expanding point clouds and photos into the plane (for example towers, arches, frescoes on the vaults and external facades) or to adjust and align walls, pipes and planes inside the generated point cloud. VirtuSurv software enables to process photographic laser scans containing a large amount of graphic data as well as drawing which use coordinates sent directly from the scan view [12, 15]. Academic and industrial research make efforts towards to fully automated recognition scans and extract CAD objects from point cloud to BIM models or 3D as-built models [10, 16].

From the created geometric model in Revit, it is possible to generate projections, cross-sections, elevations, 3D views and statements of data needed to complete the technical documentation of the modelled object.

The geometric model can be used as the basis for generating a computational model. The possibilities of exporting the Revit file format are as follows:

- Files in CAD format (.dwg). Exporting the solid model enables its import into FEM calculations programs. The advantage of this approach is the ability to use solid modelling to recreate the existing state of the object. After importing the file into the FEM program, it is necessary to suitably prepare the solid model for the discretization process.
- Automatic export between Revit and ARSA (Autodesk Robot Structural Analysis)/RFEM. During physical modelling, elements marked as structural (for instance beam, column, wall, slab, foundation) automatically contain the analytical models that are transferred to calculation programs. Such an analytical model is ready for discretiza-

tion. It is greatly useful for modelling newly designed objects due to the ideal state of geometry assumptions. In the case of existing objects, it is necessary to idealize the existing state regarding to the fact that structural elements were used only at the stage of modelling. For historical objects with complicated, irregular geometry, it may be necessary to use solid modelling elements that do not contain analytical models. Regarding structural elements, there is a need to create them in the calculation program using its tools and appropriate finite elements.

The authors used laser scanning (Faro Focus 3D) to survey the chapel outside and inside. Targets such as spheres and checkerboards were used as reference points. Individual scans were combined by using dedicated Faro Scene software. The point cloud was obtained by merging scans with target based and cloud to cloud methods. The model of building was done manually in Revit on the point cloud. Structural elements (walls, slabs) and solid blocks were used to create the model of the chapel. Then the project was exported to ARSA. Better results were obtained when the model was exported to a dwg file and imported into FEM program – ANSYS. A detailed description of the procedure and settings are presented in the “Case study” section.

3. The case study of St. Hubert Chapel

The process of 3D scanning and HBIM discussed in this paper are based on the St. Hubert Chapel located in Rzeszów (Poland) (Fig. 2). The chapel is a rococo building and it was built in the mid-18th century. The monument has a central system on an eight-sided projection. The eastern, western, southern and northern sides are developed into rectangular apsis. The chapel is arched with a dome. The structure is a brick wall with limestone mortar. It is plastered on both sides (Fig. 3).



Fig. 2. Location the St. Hubert Chapel in Rzeszów

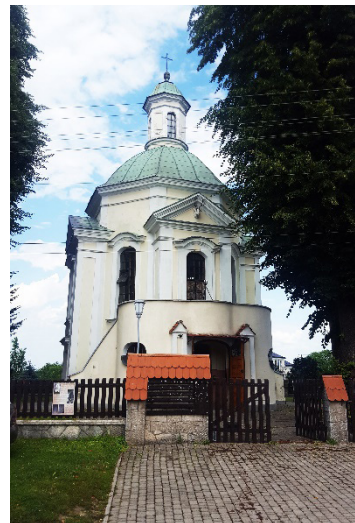
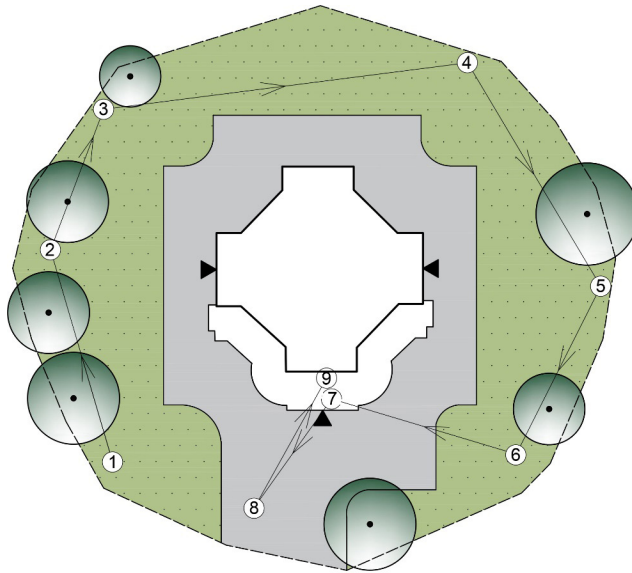


Fig. 3. The St. Hubert Chapel

The St. Hubert Chapel, also known as the Hunting Chapel, is one of the most valuable architectural monuments in the region. It was built during the Lubomirski patronage period. St. Hubert Chapel was built in the forest. It was a favourite hunting place of gentlemen from

Rzeszów. The chapel was forgotten after the fall of the Lubomirski latifundium in the late 18th century. Around mid-19th century it was already heavily devastated. Settlements developed in this area in the next decades. The chapel functioned as a parish church in Miłocin. On all sides the chapel is surrounded by farm buildings and arable fields. The chapel is situated on a circular plot, surrounded by a wreath of trees. The entrance to the church grounds is from the road leading through the village. After the construction of a new parish church (early 21st century), the chapel stands unused. In the years 2010-2011, it was possible to renovate the window and door joinery, lightning protection and facade. In the years 2011-2012 and from 2014, conservation works were carried out on the wall paintings in the dome and on the walls of the nave of the altar with the illusionist painting of St. Hubert. In 2018, conservation works were carried out on the dome [17-19].

The starting point of the research was data collection, carried out with contactless surveying methods – laser scanner (Terrestrial Laser Scanning). Point clouds were obtained with a laser scanner Faro Focus 3D. It was selected scanning profiles „Outdoor 20 m...” and “Indoor 10 m...” and scan registration in colour. In the scanner software the resolution was set to $\frac{1}{4}$ for outdoors measurements and $\frac{1}{5}$ for indoor measurements. In real numbers it means 6.136 mm/10 m (10240 pt/360°) and 7.67 mm/10 m (8192 pt/360°) respectively, where point distance mm/10 m is the distance between the captured scan points in mm with respect to a scan distance of 10 meters. The device had the measuring speed of 122000 points/s. Size of the scan in points (horizontally x vertically) was 10242 x 4339 for outdoor and 8196 x 3471 for indoor. A set of 10 outdoor measuring stations were planned (Fig. 4).



10

Fig. 4. Location of measuring stations (1–10) outside the building

Measurements were made outside and inside the building (Fig. 5a, b). Due to ongoing conservation work, inside measurements were hampered by scaffolding set from floor to dome (Fig. 5c). For this reason, 13 measuring stations were required inside the building. Reference points such as spheres and checkerboards were used.

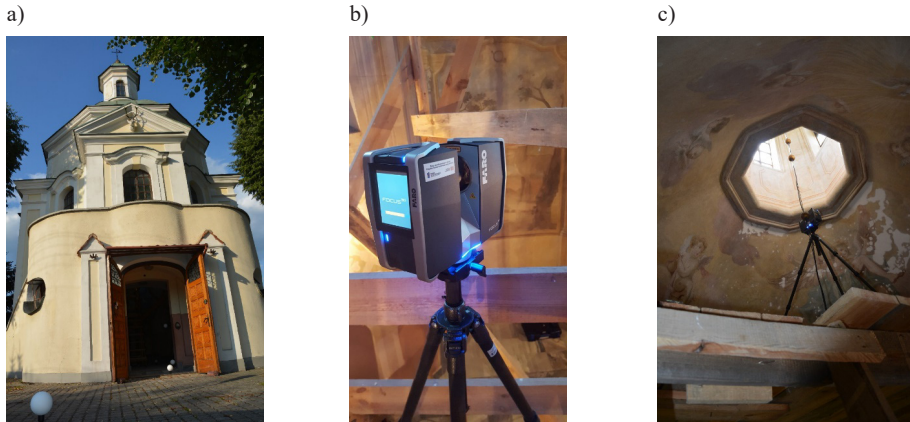


Fig. 5. Measurements with the Faro Focus 3D scanner: a) outside, b-c) inside

In this case 23 terrestrial scans were registered through Faro Scene. The scans were combined using the semi-automatic and manual methods (Fig. 6a, b). Reference points like spheres and checkerboards were detected automatically. Outer scans and scans in the basement have well measured targets so registration was target based. Additionally for inner scans, it was necessary to manually detect the reference planes and the registration method was cloud-to-cloud. To merge outer and inner clusters of scans cloud-to-cloud matching was used. In cloud to cloud subsampling average point distance after uniform subsampling of scans was 10 mm. The maximum number of iterations allowed for the algorithm to find the best solution is 30 iterations. The registered point cloud was composed of 3.273 million points and the obtained mean point error was equal to 2.1 mm.

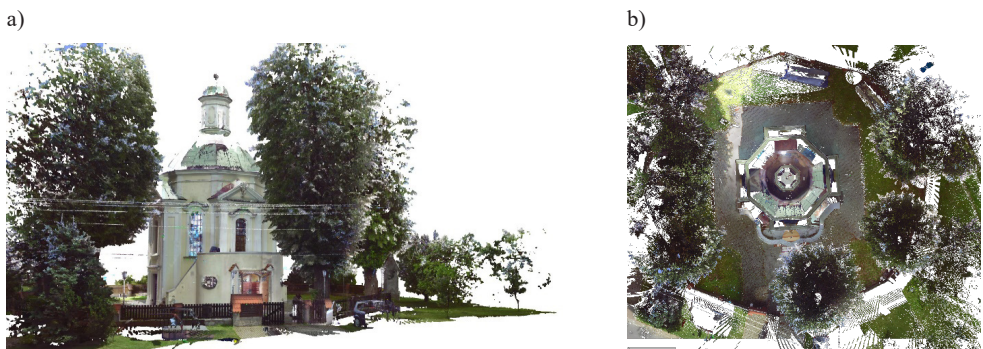
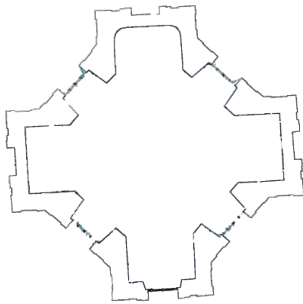


Fig. 6. Point cloud after connection in Faro Scene: a) perspective, b) top view

Geometric model (architectural and structural) was created in Autodesk Revit. Modelling was done manually. Initially, in modelling the use of structural elements (walls, slabs) was attempted in order to transfer their analytical properties after exporting project to ARSA (Autodesk Robot Structural Analysis). Unfortunately, Revit does not contain the family of structural elements related to dome structures. Its remodelling in ARSA (with 8th solid curve panels) allowed to obtain FEM model, but it could not be uploaded to Revit in order to show the dome architecture.

a)



b)

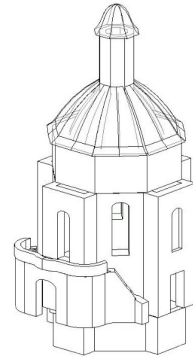
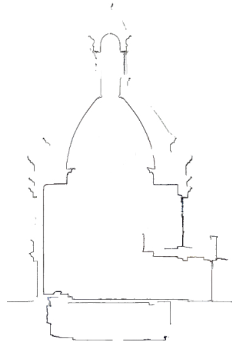


Fig. 7. View from point cloud: a) projection, b) cross section Fig. 8. Geometric solid model in Revit

Finally, it was not possible to fully match the architectural and computational model obtained in Revit and ARSA. In the future work, due to the quite complicated geometry of this historical building (Fig. 7a, b), it would probably be necessary to manually idealize geometry after all.

The next stage was to use solid modelling, which allowed to recreate the object geometry (Fig. 8). Problems and difficulties with modelling were caused by the irregular geometry of the object (for example, a problem associated with joining walls, vertical walls deviation or mapping niches in the walls). Despite the assumptions of the chapel's design as a symmetrical object, the actual state of the object is asymmetrical, which probably results from the execution inaccuracies during the construction of the object. These aspects increased the labour-intensiveness of chapel modelling.

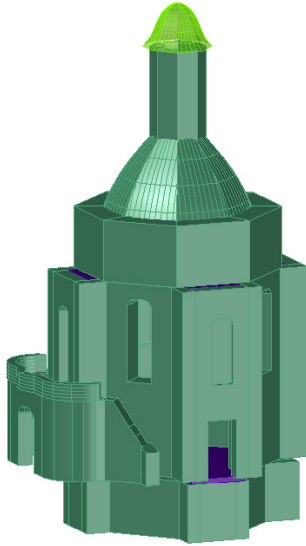


Fig. 9. Export of solid model to .dwg format

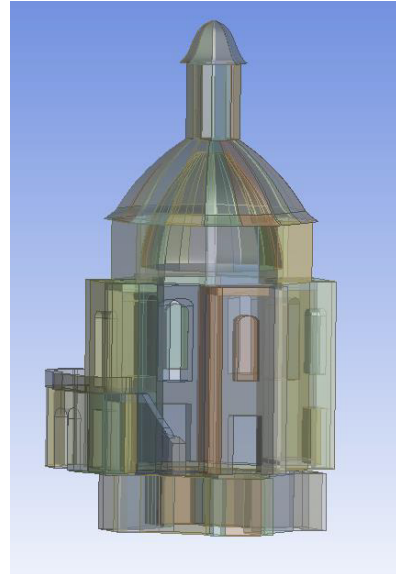


Fig. 10. Import of solid model into Ansys

Finally, the solid blocks were exported to a .dwg file (Fig. 9) which enables their further processing and discretization in FEM programs (Ansys or Inventor). In this case, a geometrical model defined in Revit was exported to ANSYS (Fig. 10). This way, a very precise computational model with spatial finite elements can be obtained and used for static or dynamic analyses.

4. Conclusions

Point clouds are definitely a good source of information about a historical building, especially when there is no existing documentation or it is unavailable. Point clouds can be archived and reused when needed.

The authors encountered some difficulties during the measurements inside the chapel. The reason was the ongoing conservation work. The solution was adding more measuring stations, also on the scaffolding from the floor to the dome.

Problems with modelling of the chapel were caused by the irregular geometry (irregular dome, off-centre lantern, complex staircase geometry). It increased the labour-intensiveness of the modelling process. The use of only construction elements such as walls or slabs has failed to reproduce the existing geometry. Solid modelling was a helpful strategy. The applied manual modelling is time-consuming. Automatic or semi-automatic methods would accelerate this process but their application was not considered in this paper.

The HBIM model contains full engineering drawings (projections, sections, details) for the conservation of historic structures. Moreover, it also includes 3D and orthographic documentation.

Obtaining a computational FEM model consistent with the actual state of the structure elements is a complex task. It requires taking into consideration many factors, which is the goal of the further research. Obtaining a computational FEM model that illustrates the real work of the structure allows diagnosing the current object state and designing necessary

structure reinforcements. Repeating this process periodically may allow monitoring structural health of historic buildings.


References

- [1] Biagini C., Capone P., Donato V., Facchini N., “Towards the BIM implementation for historical building restoration sites”, *Automation in Construction*, vol. 71, 2016, pp. 74 – 86. <https://doi.org/10.1016/j.autcon.2016.03.003>
- [2] Barazzetti L., Banfi F., Brumana R. et al., “Cloud-to-BIM-to-FEM: Structural simulation with accurate historic BIM from laser scans”, *Simulation Modelling Practice and Theory*, vol. 57, 2015, pp. 71 – 87. <https://doi.org/10.1016/j.simpat.2015.06.004>
- [3] Quattrini R., Malinverni E.S., Clini P., Nespeca R., Orlietti E., “From TLS To HBIM. High quality semantically-aware 3D modeling of complex architecture”, *ISPRS – International Archives of the Photogrammetry, Remote Sensing and Spatial Information Sciences*, vol. XL-5/W4, 2015, pp. 367-374. <https://doi.org/10.5194/isprsarchives-XL-5-W4-367-2015>
- [4] Guarnieri A., Fissore F., Masiero A., Vettore A., “From TLS Survey to 3d Solid Modeling for Documentation of Built Heritage: the Case Study of Porta Savonarola in Padua”, *ISPRS – International Archives of the Photogrammetry, Remote Sensing and Spatial Information Sciences*, volume XLII-2/W5, 2017, pp. 303-308. <https://doi.org/10.5194/isprs-archives-XLII-2-W5-303-2017>
- [5] Gosztyła M., Jagieła B., *Metodologia konserwacji zabytków architektury w praktyce*. Rzeszów, 2015.
- [6] Regulation of the Minister of Internal Affairs and Administration of 9 November 2011 on the technical standards for carrying out situational and altimetric surveying and for developing and transferring the results of such measurements to the state geodetic and cartographic resource.
- [7] FARO Technologies Inc., “FARO Laser Scanner Focus 3D Manual”, February 2013. Available: <https://faro.app.box.com/s/kfpwjofogeegocr7mf2s866s2qalnaqw> [Accessed: 18 Dec 2020]
- [8] Kim P., Chen J., Cho Y., “Automated Point Clouds Registration using Visual and Planar Features for Construction Environments”, *ASCE Journal of Computing in Civil Engineering*, volume 32, 2017. <https://doi.org/10.1061/%28ASCE%29CP.1943-5487.0000720>
- [9] “Fotogrametria”, in: *Encyclopaedia PWN*. Available: <https://encyklopedia.pwn.pl/haslo/fotogrametria;3902234.html> [Accessed: 01 May 2021]
- [10] Golparvar-Fard M., Bohn J., Teizer J., Savarese S., Peña-Mora F., “Evaluation of image-based modeling and laser scanning accuracy for emerging automated performance monitoring techniques”, *Automation in Construction*, volume 20, issue 8, 2011, pp. 1143-1155. <https://doi.org/10.1016/j.autcon.2011.04.016>
- [11] Bęcek K., Gawronek P., Kłapa P. et al., *Modelowanie i wizualizacja danych 3D na podstawie pomiarów fotogrametrycznych i skaningu laserowego*. Rzeszów, 2015.
- [12] Chiabrando F., Lo Turco M., Rinaudo F., “Modeling the decay in an HBIM starting from 3D point clouds. A followed approach for cultural heritage knowledge”, *ISPRS – International Archives of the Photogrammetry, Remote Sensing and Spatial Information Sciences*, volume XLII-2/W5, 2017, pp. 605-612. <https://doi.org/10.5194/isprs-archives-XLII-2-W5-605-2017>
- [13] Campi M., Di Luggo A., Scandurra S., “3d modeling for the knowledge of architectural heritage and virtual reconstruction of its historical memory”, *ISPRS – International Archives of the Photogrammetry, Remote Sensing and Spatial Information Sciences*, volume XLII-2/W3, 2017, pp. 133-139. <https://doi.org/10.5194/isprs-archives-XLII-2-W3-133-2017>
- [14] Kim Ch., Son H., Kim Ch., „Fully automated registration of 3D data to a 3D CAD model for project progress monitoring”, *Automation in Construction*, volume 35, 2013, pp. 587-594. <https://doi.org/10.1016/j.autcon.2013.01.005>

-
- [15] FARO Knowledge Base, “As-Built”. Available: <https://knowledge.faro.com/Software/As-Built> [Accessed: 18 Dec 2020]
- [16] Son H., Bosché F., Kim Ch., “As-built data acquisition and its use in production monitoring and automated layout of civil infrastructure: A survey”, *Advanced Engineering Informatics*, Volume 29, Issue 2, 2015, pp. 172-183. <https://doi.org/10.1016/J.AEI.2015.01.009>
- [17] Kotula F., „Kaplica myśliwska pod wezwaniem św. Huberta w Miłocinie k. Rzeszowa”, *Ochrona Zabytków*, 4/1-2 (12-13), 1951, pp. 95-98
- [18] Karta ewidencyjna, Kaplica p.w. św. Huberta, oprac.: Malczewski J., 1993, Archiwum Wojewódzkiego Urzędu Ochrony Zabytków Delegatury w Rzeszowie.
- [19] Karta ewidencyjna, Kaplica p.w. św. Huberta, oprac.: Żurawska T., 1959, Archiwum Wojewódzkiego Urzędu Ochrony Zabytków Delegatury w Rzeszowie.

Hybrid methodology of multi-sensory research of public space in urban planning

Ewa Jarecka-Bidzińska

*Faculty of Geodesy and Cartography; Warsaw University of Technology;
1 Politechniki Sq., 00-661 Warsaw, Poland;
ewa.bidzinska@pw.edu.pl  0000-0002-1289-9784*

Financing: The research was co-financed by the Dean's Grant at the Faculty of Geodesy and Cartography of the Warsaw University of Technology obtained in 2018, No. 504/04093/1060 / 42.000100, entitled "The importance of identity in shaping selected new urban spaces in Warsaw's Praga – Północ district".

Abstract: The concept of multi-sensory perception of cities is one of the elements shaping the complete image of the city. It is an aspect as important to the recipient as the urban structure. The study of the multisensory record of public spaces gives a better chance to understand: the identity of the place, the changing dimensions of cultural heritage, local social problems, and even conditions influencing spatial decisions. Multisensory research has an implementation value and can be an important, previously unaccounted for factor, influencing the revitalization program and planning decisions. Therefore, it is so important to analyze the available literature on the subject, conduct scientific observation of the research area, create a proposal for a hybrid research methodology on multi-sensory recording of space and determine their relationship with activities in the field of urban planning. The trial area – selected public spaces of the Praga – Północ district in Warsaw was adopted according to predetermined criteria, the most important of which were: authentic urban tissue, downtown area, architectural and functional diversity of buildings.

Keywords: multisensory research, multisensory space, public space, Praga – Północ

1. Introduction

1.1. Justification and purpose of the undertaken research

The city is a multi-spatial work, the perception of which is based on multi-sensory perception. The study of multisensory recording of space allows to obtain information on multisensory perception, valorization and their relation to space also as part of in situ assessment. This is important for holistic assessment of the quality of public spaces, their potential

and cultural heritage. This knowledge allows for fully conscious organization and transformation of public spaces. It has an implementation value and may constitute an important factor, previously not taken into account in urban planning, influencing the revitalization program and planning decisions. This is the basis for constructing an assessment and conclusions regarding the transformation of public spaces, taking into account its invisible dimensions. The essence of multi-sensory research is defined sociologically by B. Jałowicki – *contemporary interest in research on the perception of space has become important due to the degradation of the natural environment [of the city – ed. author] and the living conditions of inhabitants of large cities deteriorating despite the development of civilization* [1]. Problems such as, for example: destruction of historical buildings, poor technical condition of residential buildings, developer pressure, lack of green areas, recreation and rest, long journeys to work, uniform architecture, spatial disorder or lack of basic services affect the multi-sensory perception of public spaces. These problems worsen the health of the inhabitants and, consequently, lead to pathologies, acts of vandalism, affect social migrations, suburbanization and urban sprawl.

The aim of the work was, after analyzing the existing data and conducting scientific observations and reviewing the literature on the subject, to create a proposal for a hybrid methodology of multisensory research in public spaces and verify it on a trial group of respondents, and to present urban design suggestions based on the conducted hybrid multisensory research. The proposed research methodology may turn out to be useful in urban planning activities, serve to construct a multi-sensory record of space and urban design suggestions. An attempt was made to describe the reasons for the obtained initial multi-sensory assessment of public spaces. A trial study of the proposed methodology confirmed the possibility of its wider application in other areas and revealed the differences between the recording and sensory valorization of space in the context of various senses. Some spaces, assessed positively in terms of visuals, received a low score in terms of the sense of hearing or smell, which affects the overall multi-sensory image and constitutes the legitimacy of taking up the title methodology. The article ends with considerations on finding design solutions that take into account the multi-sensory record of space and favor the improvement of the current situation. The legitimacy of research is also based on the activity to support innovative development strategies related to the cooperation agreement between the Capital City of Warsaw, the Praga-Północ District Office, and the Department Geodesy and Cartography of the Warsaw University of Technology.

2. Analysis and review of literature

The senses were first described by the Greek philosopher Aristotle around 350 BCE, distinguishing five senses: sight, hearing, smell, taste and touch [2]. According to the *Mały Słownik Psychologiczny* [3], the concept of sense is “sensitivity, the ability to perceive a specific category of stimuli in the form of impressions”. The number of senses includes sense of sight, hearing, smell, taste, touch, temperature, kinesthetic, balance, joint and muscular, cenesthetic, pain. It definitely exceeds the colloquial five mentioned as the number of human senses. According to *Słownik Psychologii* [4] sense is “each of the faculties by which one can experience the outside world or the internal states of one’s own organism.”

The sensual record of public space was initiated with the publication of “The Image of the City” in the 1950s, where the American urban planner and writer Kevin Lynch created the memory-related visual sense method of mental maps in city studies. The theory of research on the multisensory perception of public spaces was later developed in many disciplines: environmental psychology, sociology, geography, cartography, ethnography, urban anthropology, cultural studies, geographic information systems and psychocartography. The K. Lynch

collective map is the most common and cited – the quantitative signature method involving the counting of objects. He created a method that was effective in research on the urban landscape and urban composition, in which sketchy cognitive maps were used. The elements presented in them were counted and assigned in 5 categories: paths, borders, nodes, landmarks and regions, and compared with the frequency of indications. According to Lynch, the title “image of the city” is based on social relations and staying in given spaces, and depends on the sensitivity of the senses. However, this method applies mainly to the sense of sight, and freehand sketches made by the respondents are drawn outside the area covered by the study and contain distortions of distance or direction. As part of this method, the respondent does not specify the assessment, but only a distorted drawing of the projection of a part of the city with the marking of points that are the material in the quantitative method. The answer to the search for a method of sensual study of space with the character of valorization is the research of another architect and urban planner – K. Wejchert. He created a qualitative method covering the meanings and assessments of sensations, a graphic representation of the record of these sensations and the perception of urban spaces [6], [7]. He also developed a methodology of research and valorization, useful in urban planning, showing the aesthetic value of urban spaces using a graph known as the “Wejchert impression curve”. This study, covering only the sense of sight, inspired the development of the title methodology to include other senses as well.

Previous research in the disciplines of sociology and environmental psychology was aimed at examining the mechanism of perception, mapping real space and determining the impact of perception on society. The problems of the city in the experiences of individuals and communities as well as human behavior in the urban environment were studied. In Poland, the precursors of research on the perception of the environment and cognitive maps of the environment were, under the supervision of T. Tomaszewski [8], [9] – M. Susłowska and M. Sawicka in Kraków, and A. Eliaz, K. Skarżyńska and T. Szustrow in Warsaw. The development of the theory of cognitive maps was investigated by A. Hauziński in the publication “Evolution of the concept of a cognitive map in psychology. Review of research on the hierarchy of plans and action goals” [10]. It distinguishes several types of cognitive maps, including: image of oneself, the closest surroundings, a diagram of the environment, a map of the world, a map of the universe and a worldview – representation of the real world. In his opinion, cognitive maps are used to acquire, use and formulate assumptions based on knowledge about oneself, the spatial and social environment and one’s orientation in it. However, in the publication “The evolution of the concept of a cognitive map in psychology and its use in urban planning, architecture and geography” [11] he describes disciplines outside of psychology in which cognitive maps are used, inter alia, urban planning, architecture and geography. Environmental psychology issues have also been included in numerous publications by R.G. Golledge “Methods and methodological issues in environmental cognition research” [12], GW Evans “Cognitive mapping: Knowledge of real-world distance and location information” [13], “Environmental cognition” [14], “Environmental learning and cognitive mapping. Environment and Behavior” [15], “The effects of pathway configuration, landmarks and stress on environmental cognition. Journal of Environmental Psychology” [16] or J. E. Foley “Working mental representations of the environment. Environment and Behavior” [17]. J. O’Keefe, J., Nadel, L. in “The hippocampus as a cognitive map” [18] proposed two types of thematic and topographic cognitive maps, and in the structure of the image of spatial knowledge they proposed two basic categories of road and maps. The research on the relationship between environmental psychology and architecture is described by: A. Bańka, among others, in the publications “Architecture of the psychological space of life. Behavioral foundations of design.” [19] and

“Social environmental psychology” [20]. It determines that everything that is covered by human senses or images must exist in real or mental space. It presents architectural and urban spatial problems, their causes and recommendations for design based on psychological knowledge. Numerous observations turned out to be also important in the title article due to the reference to many senses in space and the explanation of problems and proposals for spatial solutions related to it. However, it does not address the question of the methodology of researching these senses in space, and the conclusions are a set of general knowledge about implementation values. The publication “Environmental Psychology” [21] P.A. Bell, T.C. Greene, J.D. Fisher and A. Baum defines that the term cognitive maps has a different meaning and that the term “cognitive collage” is appropriate.

The issues of using the senses in the perception of the surrounding space in the sociological aspect were described, among others, by B. Jałowiecki in “Perception of the space of Warsaw” [22] and B. Jałowiecki and M.S. Szczepański in the publication “City and space in a sociological perspective” [1]. The chapter devoted to the sociological concept of space is descriptive and emphasizes the importance of perception and valorization of urban spaces. However, it does not contain a proposal of a research methodology on the multisensory study of space. The cultural and psychological aspects of urban anthropology in the perception of space have been described in the publications of E. Szkuřat “Psychological and cultural determinants of the perception of the environment” [23] and “Beyond writing / reading the city” by E. Rybicka [24]. Another researcher, Ewa Rewers, stated: *“I wrote about cities that I not only saw and met, but also experienced in the practical effort of my mind and the kinetic experience of the body. It is rather a record of multidirectional, but not chaotic movement, than forcing urbanity into a ready-made network of concepts and terms”* [25]. Nevertheless, in the field of social sciences, the research of B. Kietlińska in the article entitled “Research on the sensual perception of the city using qualitative methods” is the closest to the subject of the title [26]. Georg Simmel devoted his text “Sociology of the Senses” to the subject of the senses in society [27]. Sarah Pink described sensory ethnography in the publication “Doing sensory ethnography” [28]. These are sociological, ethnographic and descriptive research. These studies do not contain a deformation-free graphic record of multisensory research or reference to functional, spatial and compositional aspects. They are used to analyze the phenomenon of perception and it is not important to place them in a specific space.

The issues of social geography in terms of the perception of space, urban planning and planning based on the ideas contained in mental maps were included in the publication by M. Bartnicka “Wyobrażenia Miejskiej Warszawy” [29]. This is shaped by the trend of the geography of perception developed by other researchers, H. Libura [30] and S. Mordwa [31], who undertake the problem of comparing spatial images of different cities. Standardized Esthetic Landscape Estimation – SBE – Scenic Beauty Estimation was created and published by Daniel T.C., Boster R.S. in “Measuring Landscape Esthetics: The Scenic Beauty Estimation Method” [32]. Further research in this area was performed by M.A. Okořowicz and J.M. Kowalska in the publication “What kind of nature do we want in cities? Measurement of the aesthetics of the landscape on the Vistula River in Warsaw using the Scenic Beauty Estimation method” [33]. The riverside areas located in the central part of the city were examined in terms of spatial order by analyzing the visual assessment of the inhabitants. The study area was divided into elements of spatial composition: forest, path, shore, beaches, bridges, playgrounds and boulevard. The respondents assessed individual places on the basis of photos solely. Thus, they may not even have had experiences with them. Nonetheless, the aim of the title article is to create

a methodology of research carried out in situ – in place, by people who know a given space, e.g. residents, employees or students.

Research on the border of psychology and cartography can be divided into two trends: structural and evaluative mapping. Structural mapping derived from the research of K. Lynch was developed by R. Kitchin in numerous publications, including: “Cognitive maps: what are they and why study them?” [34], “Methodological convergence in cognitive mapping research: Investigating configurational knowledge” [35], or “The cognition of geographic space” [36]. He introduced two-dimensional regressions and pointers to reduce the sum of position errors. Sonia Maria Vanzella Castellar and Paula Cristiane Strina Juliasz in the publication “Mental map and spatial thinking” [37] describe the issues of relations of mental maps and their reference to the real space of cartography. The publication of S. Waterman and D. Gordon “A quantitative-comparative approach to analysis of distortion in mental maps” [38] presents a quantitative procedure for the analysis and comparison of distortions in mental maps. In studies of cognitive maps in the structural trend, the interpretation of the results of sketch maps is hindered by differences in style, scale and detail. However, information is provided on the significance of selected spatial objects in the study area for the social community. Another trend of research on cognitive maps is evaluative mapping, the precursor of which was P. Gould, which he described in the publication “On mental maps” [39]. He examined the valuation of fragments of space by a certain community. These studies were further developed – H. Libura in “Some Cartographic Aspects of Imaginary Maps” [30]. Information is obtained using the choropleth method by ranking areas or marking areas by the respondent on the prepared maps. Evaluative mapping, although associated with the mechanisms of stereotyping, is important in planning and spatial decisions.

Research in the field of psychocartography by A. Gendźwiłł [40], A. Foland in “Psychocartography – a method of studying urban space” [41], or M. Lewicka [42] usually present a broader, more general and developed in larger areas cartographic image of the valorization of areas. Unlike Gould maps, they are not limited to the administrative boundaries of areas. However, imaging the “psychological properties of space” on a city scale does not allow for a detailed assessment of, for example, a single street or building, which is obtained by combining various methods carried out on the spot: interview, valorization and questionnaire. This problem is described by B. Iwańczak in “Research methods for the overall perception of city space on the example of Warsaw” [43], who at the outset proposes functionally and spatially coherent research areas of the city using GIS tools. The issues of using the geodetic and cartographic information system as well as the presentation of mental maps are also described by K. Nieścioruk in the publications “Cartographic image of mental maps of urban space and its presentation and analysis with the use of geographic information systems” [44], “The use of mental and sketch maps as a tool to evaluate cartography teaching effectiveness” [45]. These studies became an inspiration to include in the title methodology of research multi-sensory functional and spatial analyzes of the area performed in a traditional way and preceding the next stages of the research process. So far, research in the field of psychocartography has not covered multi-sensory studies of spaces, but only, for example, the assessment of attractiveness or a sense of security performed outside the place subject to assessment. The location of the valorization not in real time and in isolation from the studied area allows only the memory of the senses to be used. Therefore, it would not be applicable in this case.

Interactive tools are used more and more often in the study of public spaces: geo-questionnaires, computer programs, mobile applications, virtual reality [46]-[48]. However, these methods were not taken into account when constructing the title research methodology due

to the target lack of possibility to include digitally excluded people (the poor, the elderly, the uneducated) and the negative impact of electronic devices, such as smartphones or tablets, on the actual perception of space, or even its limitation. Development of the title methodology in the future would make it possible to introduce, depending on the preparation of the respondent, traditional questionnaires and geo-questionnaires and to compare the results.

However, the concept and definition of “public space” have been precisely defined in the Charter of Public Spaces [49], “as a common good, deliberately shaped by man, in accordance with social principles and values – serving to meet the needs of local and supra-local communities”. On the other hand, The Act on Spatial Planning and Development [50] contains the following entry: “An area of particular importance for meeting the needs of residents, improving their quality of life and conducive to establishing social contacts due to its location and functional and spatial features, specified in the study of the conditions and directions of spatial development of the borough.”

The current state of research does not include literature that focuses on linking the content of multi-sensory field research and the functional and spatial characteristics of places. So far, in Poland, no publication has appeared devoted solely to multi-sensory research in public space and its relationship with urban design.

3. Research procedure in hybrid research methodology – basic theoretical assumptions

So far, the research methodologies used and described in the literature are limited to one or two research techniques. Some of them are descriptive and concern only purely psychological issues related to the phenomenon and mechanism of perception. Some analyze representations of reality deformed by the respondents, but made outside the research site. Others relate only to the sense of sight or the assessment of attractiveness. Currently, no methodology has been developed that would lead to direct use in urban planning activities, the process of shaping and transforming public spaces. Therefore, an innovative solution was proposed that combines various research methods and presents a hybrid methodology covering at various stages: literature and data analysis, photo documentation of the areas covered by the study, in situ observation, functional and spatial analysis, discussions with experts and interviews, a scientific walk, a questionnaire and valorization of space. This allows, among others, to study multi-sensory perception while actually being in space.

The conducted research procedure (Fig. 1) consists essentially of several stages remaining in a hierarchical or more complex relationship, as presented in the diagram. The empirical part of the hybrid test method was conducted in the field. In large cities, the number of potential research points – public spaces, and the distances between them and their size are significant. The researcher’s financial and time constraints do not allow for a detailed examination of everyone. Therefore, it is necessary to delimit the area and the number of points on the basis of the previously adopted criteria. The site selection process followed is complex and has several steps. It was necessary to carry out such a classification based on the analysis of aerial and satellite photos, archival plans and maps, publications and planning documents concerning the studied area. Some of the components of this procedure do not concern the subject of the article, and therefore have not been discussed in more detail. Arbitrary selection of the site influences the efficient conduct of research in the field and limits the impact of the respondent’s abilities and context on the results. The research is limited by the physical condition and time disposition of the respondents (route length). Imposing on the respondents both the area and points selected for sample surveys also allowed for focusing the assessment of all respondents in pre-adopted places and the subsequent aggregation of the obtained data.

RESEARCH PROCEDURE IN HYBRID RESEARCH METHODOLOGY

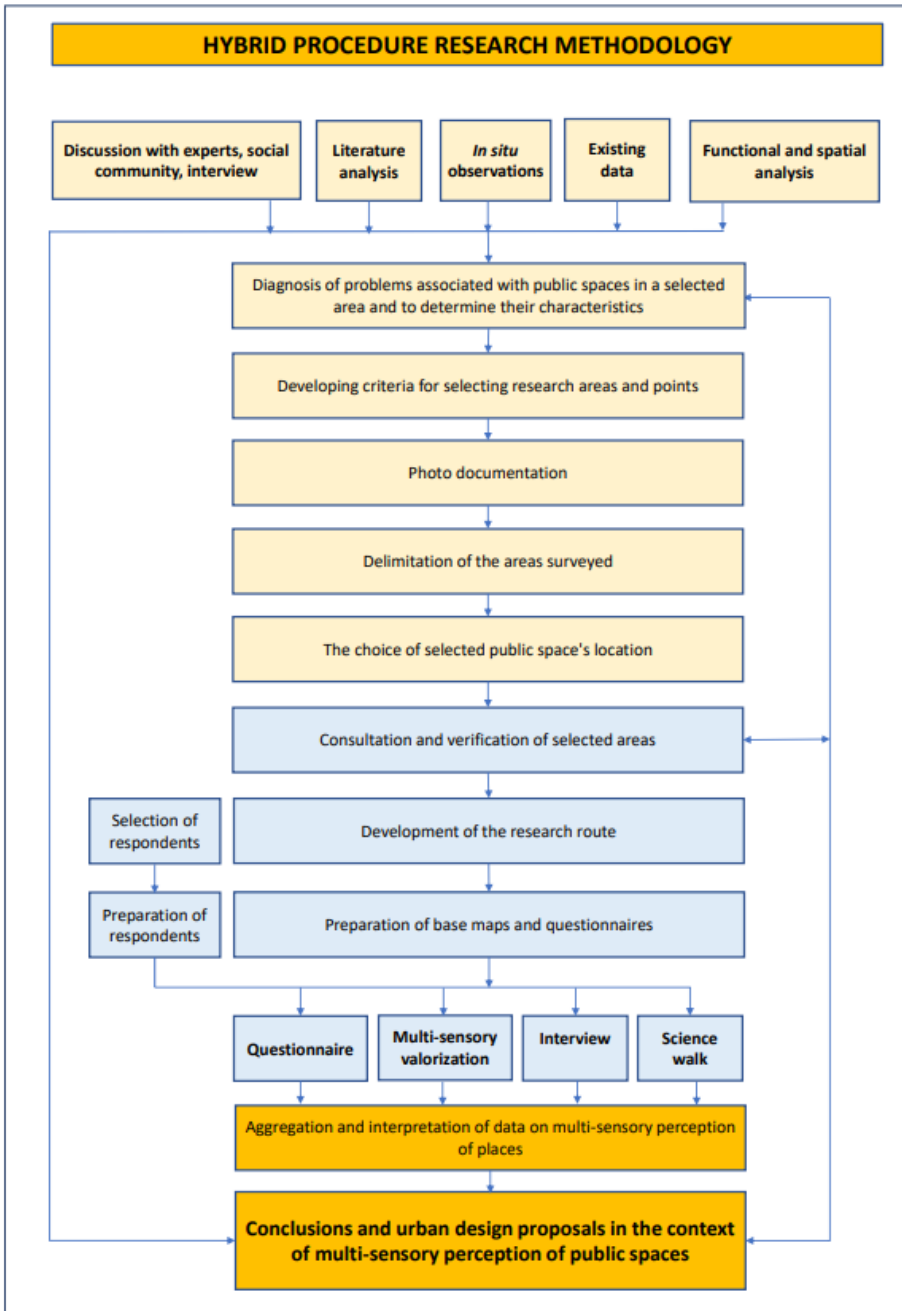


Fig. 1. Diagram of the test procedure. Source: own study

4. Basic criteria for selecting the area and research points

The area and test points should be the same for all groups participating in the study. They are proposed by the person who conducts the study on the basis of the results of the previously conducted delimitation based on the established selection criteria. However, you can define the initial criteria for selecting the area and research points:

- authentic urban fabric (historic building structure and street network, preserved squares and other elements of the urban structure)
- downtown area with multi-family housing and inhabited by the local community
- presence of public utility buildings of local and supra-local importance
- partially degraded area,
- area covered by the revitalization program or planned for revitalization
- architectural and functional diversity
- the location of subsequent public spaces at a distance of no more than 500 m from each other (maintains the level of attention of the recipient, and at the same time allows for a smooth interpenetration of multi-sensory experiences)
- a minimum of 10, but not more than 15, public spaces within the route, including those of different nature and functions (streets, squares, marketplaces), too little space does not give a representative research area, and too much space requires more than 2 hours for carrying out research and is at risk of obtaining superficial and random multisensory assessment, and the obtained results would be unreliable
- attractiveness in terms of tourism, the presence of unique elements in the city scale described in the theory of K. Lynch (outstanding architecture, historical urban layout, landscape and natural values, but also social significance – e.g. memorial sites, important for the local community)
- linking the paths with the pedestrian function – a common trail

When using this methodology in another area, it is allowed to slightly modify the criteria, e.g. in small areas or on the outskirts of large cities. The route, the image of which on the map allows you to create a circumference of a closed figure, allowing for a cyclical scientific walk, and at the same time delimiting an area which, together with a buffer zone of at least 1 km, may constitute an intermediate zone of influence on the senses (heard sounds, visible architectural dominants). Such a route allows for re-examining and reading the senses in the public space after the expiry of the time allocated for one cycle. The study covered a trial area of the Warsaw district of Warsaw – Praga – Północ, as it met the set criteria.

5. The area of trial hybrid multi-sensory research of public space in urban planning

The scope of the research procedure included the most important public spaces of Praga – Północ on a continuous route, including: Różycki Bazaar, Ząbkowska Street, Targowa Street, Wileński Square, Weteranów Squarr 1863, Floriańska Street, but also commercial places such as Koneser Square. The reasons for choosing these particular parts of the district were: the historical significance of the area, the concentration of services and trade, and the associated greatest social, as well as cultural and tourist popularity. The dynamics of functional and spatial changes, but also social and economic changes, were important. The area of Praga – Północ selected for research is the only area in Warsaw where the process of spatial transformations of

the city in the 19th – 20th centuries is visible in the urban tissue, mainly industry. The left-bank development of Warsaw was demolished in 85% during World War II, Praga – Północ only in 25%, therein mainly industry. This area also presents Christian, Jewish and Orthodox cultural and religious heritage. It is an area containing, among others, fragment of the UNESCO buffer zone, areas included in the register of monuments and in the municipal register.

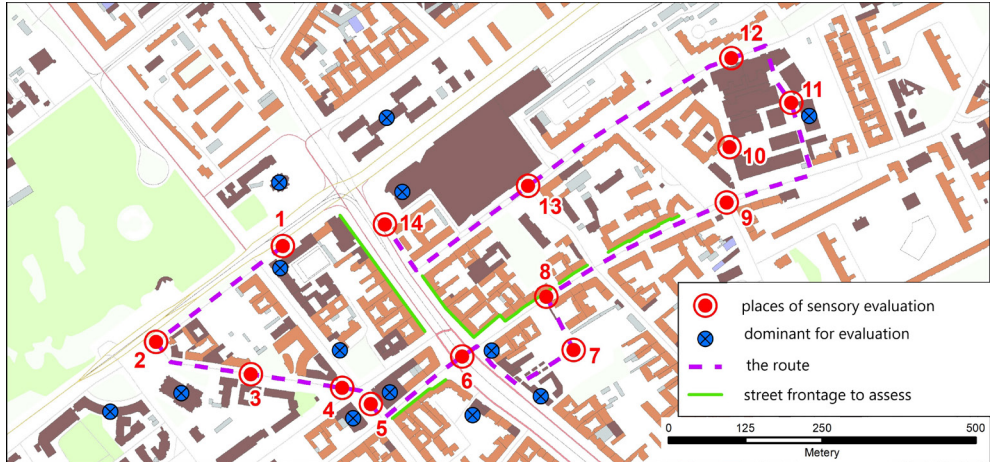


Fig. 2. The route of the field study on the creation of mental maps of public spaces, October 2019, source: author of the graphic presentation of the map, M.Sc.Eng. M. Delnicki on the basis of research by the author. Public spaces: 1 – near Władysława IV High School, 2 – Veterans Square in 1863, 3 – 4 Floriańska St, 4 – square at Praska Kapela, 5 – square at the Tax Office, 6 – intersection of Targowa St. and Jagiellońska St., 7 – Różycki Bazaar, 8 – Ząbkowska St., 9 – intersection of Ząbkowska St. and Markowska St., 10 – entrance to the Koneser Praga Center, 11 – Koneser Square, 12 – Białostocka St., 13 – corner of Brzeska and Białostocka streets, entrance to the shopping center, 14 – Dworzec Wileński entrance zone

The route starts near Wileński Square (Fig. 2, no. 1), which is currently the largest communication junction (15 thousand 176 to 31 thousand 628 passengers a day) [52] and the most recognizable place in the district. This intersection of multi-lane roads is located next to the Vilnius Railway Station (Fig. 2, no. 14), and at the location of the metro station. Together with the development and domination of the communication function, this square no longer meets other social needs. It is rarely chosen by individual users for recreational or interpersonal integration purposes, and these functions are performed by users in the shopping center located above the Vilnius Railway Station. Then, the route leads through Veterans Square of 1863. (Fig. 2, no. 2), an important element of the local spatial order and a historical fragment of the urban layout associated with the Royal Castle from the times of Tsar Alexander II. according to a design by J. Kubicki. It is definitely one of the most recognizable places in the district, mainly due to the Praga Hospital operating in the historic buildings and the landscape dominant visible from the left bank of Warsaw, which is the Cathedral of St. Florian the Martyr and Michael the Archangel. The route continues along one of the most charming streets of Praga – Północ – along Floriańska Street (Fig. 2, no. 3; Fig. 5), where the modern architecture blends harmoniously with the historic buildings, and the spatial order is complemented by rows of trees, creepers growing on the walls and urban details such as lanterns type of the Warsaw crosier, authentic pavement, or the famous Monument to the Praga Backyard Band.

The route continues through the space between the Tax Office, the Warsaw-Praga Curia, and the Marshal's Office (Fig. 2, no. 4-5; Fig. 5), which, despite its potential, currently serves as a car park. Subsequently, the research was carried out along the frontage of historical buildings at Okrzei St., which together with Ząbkowska Street, commonly known as the "Praga New World", is a part of the Praga Princely Route. Next, the route of the research leads through Targowa Street (Fig. 2, no. 6; Fig. 4), which in the urban structure also includes the preserved elements of the medieval street layout related to the original physiographic conditions of the area and a spindle-shaped commercial settlement. The former large market, which was a city-forming element, was transformed into the settlement of Targowe Wielkie in the 14th century, which gave its name to the most important street in Praga. Then, the route leads to the adjacent Różycki Bazaar, built in 1901, which used to be the "functional heart of Praga". Currently, less popular, although it still has a commercial function and due to its importance for local heritage, it is revitalized (Fig. 2, no. 7; Fig. 6). The course of the route returns to Ząbkowska Street (Fig. 2, no. 8-9; Fig. 4) and then into Praga's Koneser Center Square (Fig. 2, no. 10-11; Fig. 3) – a commercial multi-functional public space constituting a juxtaposition of contemporary facilities and adapted to new historical functions of the former Koneser Vodka Factory. Due to the supra-local functional and spatial attractiveness, historic, unique buildings, aesthetics, and cultural aspects, the space is focused on tourism and social life. Next, the route runs through the opposite exit from Koneser Square along Białostocka St. (Fig. 2, no. 12–13; Fig. 3) passes the 1980s multi-family housing development by the railway line and ends at the square in front of the Vilnius Railway Station (Fig. 2, no. 14)



Fig. 3. Koneser Square, October 2019, Source: author's own archive

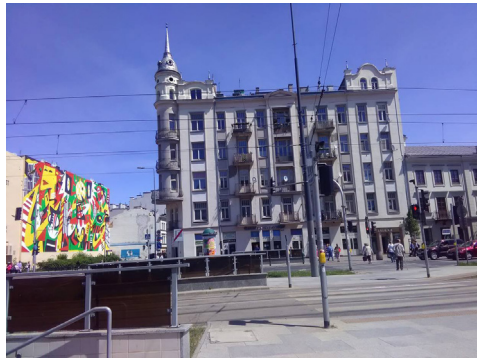


Fig. 4. The intersection of Ząbkowska and Targowa Streets, 2016, Source: author's own archive

6. Hybrid multi-sensory research of public space in a trial area – case study

The area of trial research was selected on the basis of the criteria adopted previously and discussed in the preceding chapter, the most important of which are: authentic urban tissue and architectural and functional diversity of buildings. 14 unique research areas were distinguished, and each of them was assigned 1 point. They are located in close proximity and allow you to create a pedestrian route – a closed-circuit route. In order to minimize subjective classification, the methodology uses in the initial stages of the research: functional and spatial

analysis, observation of the terrain in situ and discussion with experts. Photographs were taken at the designated research points and observation protocols were prepared.



Fig. 5. Square at the intersection of Floriańska and Kłopotowskiego Streets, visible sculpture and children interested in it, May 2016, Source: author's own archive



Fig. 6. Różycki Bazaar, 12:00 p.m, visible variety of colors at the stalls, October 2018, Source: author's own archive

The preparatory stage consisted in setting out, according to the established criteria and after delimiting the areas by the author, the research route, places for reading multi-sensory experiences, as well as dominants and frontages to be assessed. The route and test points (dashed purple line, Fig. 2) were selected in such a way as to objectively present the complex nature of Praga – Północ. The route covered the most important public spaces of the functional center of Praga – Północ. It started at the school building Władysława IV VIII High School at the intersection of Jagiellońska Street and Solidarności Avenue, and then historical areas dominated by monuments (Floriańska St., Fig. 5; Ząbkowska St., Fig. 4), very degraded areas of great social importance (Bazar Różyckiego, Fig. 6), large communication arteries (Targowa St., Fig. 4), areas of a commercial character and high aesthetic value (Centrum Praskie Koneser, Fig. 3). The examination lasted approximately 2 hours and proceeded at a pace adjusted to the needs of the group, so that the multi-sensory assessment of the site could be carried out on an individual basis. The study area (Fig. 2) was divided into sections, the most important point of which was the selected public space with an assigned number and name in the table. For many years, the author conducted research in the area of Praga – Północ and was based on the results of the doctoral dissertation entitled “Praga – Północ in Warsaw as an” art district “against the background of selected examples from the metropolises of Europe and North America” [51]. During the site visits carried out many times from 2016 to 2019, a total of over 150 photos were taken, 10 for each public space. The photos were taken from the observer's level and from viewpoints. The acquired knowledge and conclusions from previous consultations with the local government, including the Head of the European Funds Department in the Praga-Północ District Office, became the basis for choosing the route on which the assessment was made as representative of the district.

As part of the study, in the last phase, questionnaires, multi-sensory valorization on base maps, an interview and a scientific walk were performed. The following senses were selected for the study: sight, touch, taste, smell, hearing, time perception and proprioception. The technique allowed for scoring according to individual senses in the questionnaire in the form of a table on the assessment of the place in terms of the specified senses and on the map in the form of graphic symbols, as an evaluation. In addition, it made it possible to place

other information that was also the equivalent of free interview, including those related to the assessment of spatial order or subjective experiences in precise definition. The assessment in the questionnaire was three-level and presented in a table in the window corresponding to specific senses. Table – the questionnaire related to specific places on the map. The spaces were scored with points from -1 to 1. The rating scale was (-1,0,1), where -1 means negative, 0 – neutral, and 1 – positive. The sum of points obtained in the assessment for a given place is presented in the figure below in the charts. The participants of the study made an assessments of all the places previously selected by the author without any exception.

In addition to the scoring of public spaces in the questionnaire, graphic studies were also prepared – multi-sensory valorizations with detailed information and handwritten on the printed map with the use of sticky circle markers (of different colors depending on the assessment) of arrows, colored lines symbolizing various information, markers, felt-tip pens and post-it notes (Fig. 7). The individual graphic elements applied by the participants of the study had the meaning assigned in the legend, e.g. attractive and unattractive space, negative and positive dominants, socially important place, directions of population movement, valuable greenery and tree stand, etc. It was also a rich study in terms of presenting subtle feelings. This method also uses, among others, the assessment of areas by the respondents. Attractiveness or social significance, and a dichotomous scale (attractive/unattractive space, dominant) was adopted for the respondents' points as well. The aggregation and processing of these data was based on the research by A. Foland [41] and B. Iwańczak [43] in a simplified version – allowing for the formulation of project conclusions and confirmation of the effectiveness of the developed methodology. The respondents, using appropriate markings, assessed the following described and categorized by K. Lynch: [5] knots, regions, landmarks – waypoints and selected edges and bands with an assessment. This allows you to determine the importance of individual elements in space. Table 1 presents the definition, identification and recording of descriptive data formulated by the respondents.

Table 1. Example of a coding fragment for multi-sensory perception interviews. Source: own study

Text	Descriptive code
<i>„there are many services here and everyone will find something for themselves “, “ a beautiful place, I’ll be happy to come back in here “, “ how good that there are no cars here “, “ this environment is inspiring “, “ you can spend time here”</i>	Freedom of action in space
<i>„it stinks, you can’t breathe “, “ you can’t hear anything, you have to go away from here “, “ those old and dirty yards are terrible, damp and musty everywhere “, “ it smells like construction site and dust is everywhere”</i>	Irritation, excess stimuli, stressors
<i>„you can see the church tower from afar “, “ this school is right at the crossroads “, “ you can see the church from here “, “ the entrance gate to the courtyard can be seen from a distance “, “ everyone goes one way in the morning and the other in the evening ”</i>	Proper orientation in space
<i>„nice place and a lot of people “, “ you can hear nice music in the cafe garden “, “ there are always a lot of people here “, “ smells beautifully with donuts “, “ wonderful smell of dinner”</i>	Living space
<i>„empty, no people “, “ smells of old age “, “ It’s boring in here, nothing is happening ”</i>	A socially dead space
<i>„this street is nice with trees and greenery, you can stay here longer “, “ this is my favorite street because it’s so quiet, green and pretty”</i>	Positive value of urban greenery
<i>„this is a special place, because I like these people and this building “, “ it is a very fashionable place now, even tourists come here “, “ this is the most popular street “, “ epic place”</i>	The identity of the place
<i>„this is the largest intersection, I drive this way every day, there is always a lot of people “, “ here, it is close to everything, close to services, to the center”</i>	Understandable space

As part of the accepted research, the penultimate phase of research, was carried out on various groups of respondents. The first research procedure in October 2019 involved 5 teams of subjects of the same age but of different sex, included 35 people. Each group consisted of 5-7 people who were students of a secondary school located in the center of the study area.¹ Most of the respondents were residents or everyday users of the studied areas of right-hand Warsaw, i.e. the studied area or its vicinity. The group of respondents was selected on purpose – as a trial group. They were the students of Władysław IV, VIII High School in Warsaw, which is located in the studied area. It can therefore be assumed that these are people who meet the requirements described by environmental psychology in the previously discussed sections, including A. Bańka [19] The respondents knew the studied spaces through the prism of personal experiences and everyday social interactions. They efficiently and consciously moved around the studied area and were able to work as a team on the development of the valuation and the questionnaire. Children are also the social group which, quoting S. Mordwa [31] most willingly makes graphic studies or a graphic presentation of ideas of space. This group of respondents favored the achievement of the goal – efficient conduct of the survey, and thus checking the entire innovative methodology. It is possible to perform the title methodology on another community as well. In such research, it is also important to properly prepare the respondents (A. Hauziński) [10] [11]. Therefore, the field research was preceded by classroom activities presenting the theory of the research and explaining the goals and method of execution.

¹ The second study took place in November 2019. with the participation of a small group of municipal authorities and residents. It has not been described in greater detail due to the slight influence on the results of the research.

Later, after the field research, another 2nd meeting at the school allowed for the presentation of the survey results to the respondents and a group discussion. The schematic appendix was an instruction and a map with marked route, dominants and frontages requiring assessment.

The respondents received instructions on exemplary assessments and symbols, and then entered information on the sensory assessment of public spaces in the table, which was attached to the main graphic study – valorization on the prepared map.

Through field research, observations and graphical assessment, it was determined how a given public space affects the senses, whether it is assessed positively or negatively, and how the visual assessment differs from that made by other senses. As part of the visual assessment in terms of the sense of sight, spatial order, aesthetics, dominants, architectural details, greenery, etc. were assessed. Here, the assessment was similar to the “Wejchert impression curve” [6] [7] however, the aspect of landscape elements on the left and right side of the evaluator was taken into account, but also those located in a different spatial relationship, e.g. above, below or behind it. The following elements of space have become important: balconies, tree crowns, authentic pavement, closings and perspective openings seen in a given place, visible church towers, or a panorama of the left bank of Warsaw.

Assessment by touch included a wide range of sensations, including: temperature, sun, shade, humidity, dry air, the type of wind on the face (open and closed areas), and even materials or textures, sculptures, walls, paving, pavement or greenery. While examining by touch, the participants gently or strongly pressed the surfaces, knocked, stroked, stomped, scratched, nudged, squeezed, leaned against the walls of tenement houses, and even hugged, for example, trees. The research revealed that sometimes people traverse a space and come into contact with other people or buildings. Sometimes, while waiting for someone, they lean against the walls of buildings. The following ratings appeared in the description: “grainy, rough, soft, smooth, muddy, fluffy, spiky, dirty, dry, wet, cold, warm, hard, slippery, moss-covered, wooden, steel, stone, brick, concrete, plastic, sticky, lumpy. “

By examining the sense of hearing, for example, the following sensations were determined: music from a restaurant, rustling leaves, pigeons, rattling of wheels on pavement, noise of construction sites, noise of streets, sound of a tram, train, church bells, chimes on the school tower, conversations of passers-by, their language, nationality, vocabulary, dialect, tone of voice, restaurant buzz, sounds of a performance event. The following sensations were defined in the sense of smell: the smell of chocolate, donuts, stew, dumplings, tripe, dried mushrooms, lord’s crust, cookies, construction, dust, concrete, autumn leaves, earth, cobblestones, concrete, brick walls, decayed wood, pizza, stench gate and underground passages, exhaust gases, etc.

In addition, the perception of time was examined and here were defined: spaces in which the passage of time or the circadian cycle is clearly visible, or where time stops or ceases to matter. Clock towers, chimes, clocks on parking meters, open shop windows and restaurants, neon signs, street lamps, lighting, visible increased traffic or traffic jams, other characteristic events in public space that inform us about the passage of time, orientation towards the sides of the world turned out to be important, people’s relationships in the space, rush or quiet conversations in restaurants, birds singing in the morning, dogs barking in the evening and more. In the study of the sense of proprioception – the feeling of balance, the sense of stability, information about high curbs (e.g. Floriańska Street), stairs (e.g. in front of the Warsaw-Praga Diocese Curia), unevenness, e.g. authentic pavement, barriers or thresholds were determined.

The taste test was the most difficult to describe. According to the theory, we also taste using the senses of smell and sight, we remember the flavors of food eaten in restaurants

(goulash, pork chops) or on the street (dumplings, tripe, candyfloss). Where and how are the dishes served (street, restaurant, milk bar, oriental cuisine, Polish cuisine, exotic dishes, cafe, bar with alcohol only, etc.). Do people eat while standing up? Do they eat their meals comfortably at the tables? Is it elegant? What's the atmosphere like? Is it fast food? Do people enjoy the taste? Is it a to-go dish? Do we eat on a busy street, in the aisle? They can also be childhood memories or dishes prepared by residents and eaten in apartments along the route. As part of the study, there was no separate time for tasting, but the participants could consume their own tastes that fit into the multi-sensory landscape of the district. These include, for example, the famous and almost regional product "dumplings from the Różycki Bazaar" made in a traditional way and sold at the market stall.

In the next stage of hybrid research, the aggregation and interpretation of data on multi-sensory perception of places obtained as part of: questionnaires, multisensory valorization, interview and scientific walk were prepared. The results from the questionnaire were presented in the form of a graph (Fig. 8) presenting the indications in the examined points in the field for the three most important senses in a trial assessment: sight, hearing and smell. Whereas, graphic studies – multi-sensory valorization (Fig. 7) with detailed information constituted the background illustrating the decisions visible in the assessment. Information on the issues accompanying the multi-sensory perception of public spaces was provided by the coding of interviews (Table 1) and a science walk.

7. Findings

The graph (Fig. 8) with the assessment was prepared on the basis of questionnaires concerning the multisensory assessment of research points. It presents a clear discrepancy in the perception of some public spaces in terms of different senses. Places that were highly rated visually (no. 1- at Solidarności Avenue, Targowa St. – no. 5, Ząbkowska St. – no. 9) received an extremely low score in terms of the sense of hearing. You can also see that the visual assessment of space is much higher than that made in terms of other senses. In terms of smell, places where gastronomy is located and the aroma of meals is noticeable (square in front of the church and the Rusalka bar located there – no. 2, Ząbkowska Street no. 8 and 9 and Konesera Square – no. 9 and 10) were highly rated. This illustrates the validity of the above research and illustrates how much other senses affect the perception of space and the importance of non-visual stimuli for the attractiveness of the place. Although the following senses were examined: sight, touch, taste, smell, hearing, time perception and proprioception, in the case of Praga-Północ, the senses of sight, hearing and smell played a key role in the multi-sensory assessment.

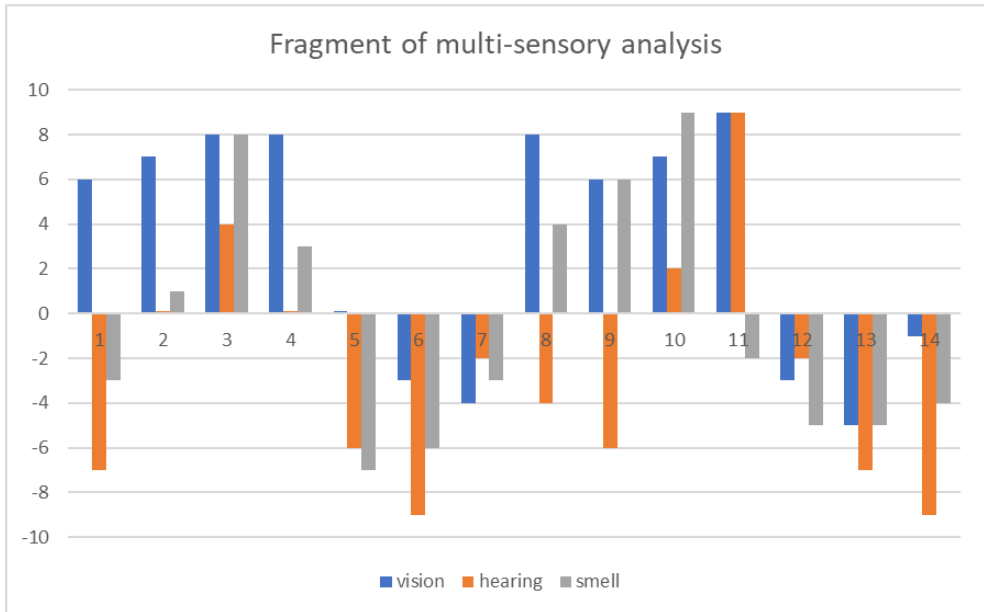


Fig. 8. Summary of evaluation graphs in terms of the three senses in relation to selected spaces. 1-14 – public spaces – assessment points. The graph shows the sum of the points received by each of the individual places from all groups participating in the study

In the multi-sensory evaluation as well as the transcribed and interpreted interview, the respondents noted primarily: “unusual historical architecture”, landscape elements: “nice view”, “ivy on the wall”, “nice greenery”, “sunny street” details “ugly signboard”, “a red brick that creates a mood, but also the “dying away” of public spaces: “decaying buildings” or “no people”. In the landscape of Praga’s – Północ scents, incl. the smells of the restaurant were noticed: “smells like hot-dog”, “smells like black pudding”, “smells like ketchup”, “it stinks”, but also “smells like rosebuds”, “smells like vodka”, “feels like there is construction sight nearby”. Among the noises, the following were distinguished: heavy traffic, “renovation of a historic tenement house”, “noise of cafe gardens”, “rattling of wheels on pavement”, “rustling of leaves”, “nice music”. Terms referring to all the senses appeared: “nice atmosphere”, “cool place”. The multi-sensory perception was fuller and richer in places where road traffic was excluded or limited (eg Koneser Square, Floriańska Street)

The multi-sensory valorizations of Praga-Północ, the questionnaires and interviews with the research groups are consistent on the basic issues concerning the core elements of the urban composition and the reactions caused by the strongest stimuli. The multitude of received stimuli and observations clearly depended on the sex of the respondents and their individual sensitivity. All those public spaces characterized by high spatial order, good technical condition of buildings, greenery and a diverse offer of social infrastructure, mainly trade and services, were positively assessed. (Floriańska Street, Koneser Square, Ząbkowska Street)

The following spaces were assessed negatively: with a lot of noise and traffic, urban tissue degradation, “socially dead”, with visible phenomena of social pathology in the public space (intersection of Targowa and Ząbkowska streets with an underground passage, Bazar Różyckiego). The multi-sensory valorization of public spaces in Praga-Północ was similar

in the assessment of all groups of respondents. However, in such a dynamically changing socio-economic area, the valorization should be repeated in subsequent groups of respondents, as this was only a sample group.

8. Summary

The multi-stage hybrid research procedure allows for a comprehensive multi-sensory evaluation of public spaces, covering many complex stages, including consultations with experts, functional and spatial analyzes, in situ research and other hierarchically related, although sometimes in a complex relationship. One of the final stages is work with previously selected respondents, taking various and parallel forms: questionnaire, multi-sensory valorization, interview and scientific walk. This is an important element related to social participation and the involvement of residents associated with the area in determining its potential, which in turn may translate into the stage of formulating design guidelines. The final stages of the hybrid research methodology concern the aggregation and interpretation of data on multisensory perception of places. The research procedure culminates conclusions and proposals in terms of the multi-sensory perception of public spaces in urban planning. Depending on the case, however, they influence the re-verification of their characteristics in terms of the diagnosis of problems related to public spaces, as demonstrated by trial studies.

New investments affect the “dying away” of other public spaces, and this in turn affects their perception by the observer in terms of many senses. The investment of Centrum Praskie Koneser, highly rated by the respondents, attracts visitors and residents. On the other hand, the neglect of many other public spaces, both technically and socio-economically, visible in the research results, contributes to low attractiveness and evaluation. The research in the trial area reflects the desolation of Żąbkowska St. much more negative among the surveyed observers was the impression of “dead spaces” than unsightly architecture. The attractive commercial offer of the CPK, neat, well-equipped and aesthetic spaces, and unique monuments made this place a clear success. During the year, this drastically affected the number of users and the structure of services and trade on Żąbkowska St. Activities of the local government to revive Żąbkowska St, among others the “Otwarta Żąbkowska” event, did not bring the expected results. The multi-sensory valorization of these spaces confirms above mentioned observations. The respondents referred to it as “nothing is happening”, “lack of people” or “emptiness”.

What could be competitive or otherwise supplementary to the space of the Praga Koneser Center, highly rated by the respondents, is authenticity related to multi-sensory perception. Building a community of residents through events such as former backyard meetings under the slogan “Neighbors to neighbors” and social participation with involvement in deciding about changes in the public space. Individual public spaces should be adapted so that both young and old residents of the immediate vicinity can comfortably spend their time there. Only such action in space will allow for its permanent revival, also outside organized events or the tourist season. Referring to A. Bańka [19] [20], in order to enliven places, one should not study history, but refer to the memory of events in places where life was vibrant. The influence on increasing the attractiveness of the space is the creation of sequences of connections between them – this is “kinostatic” memory – passages, promenades, piers or numerous pedestrian precincts illustrate the remembering of urban spaces through movement. However, due to the change in the social structure, cultural patterns, emotional attitudes and the concept of socially important places are also changing. The historical significance of places such as the Różycki Bazaar does not function in the minds of young people and immigrant communities. They

have not experienced social interactions in this public space and evaluate it through the prism of the present. Thus, the value of the memory of the senses is also diminishing.

Quoting after A. Bańka “The acoustic space is compulsory – you cannot close your ears. Acoustic space control is important for the quality of life.” The trial study showed how important it is to limit car traffic, create a system of connections between individual public spaces and introduce greenery and ecological solutions in various forms: green walls and terraces, plant and architectural hybrids, pocket parks, community gardens, green tracks, flower meadows, street retention canals, or renewable energy sources. Sensual spatial diversity far from “bedroom districts” stimulates social behavior. In terms of multi-sensory aspects, the attractiveness of space can be increased, among others, by: smells and calm, moderately quiet music coming from the restaurant, introducing splash and noise of water, playing benches, sculptures, playground equipment and reducing heat islands through greenery. Then, you can obtain a sonic valorization of the space in which the rustling of leaves, children’s laughter, barking dogs and singing birds in the morning reappear. Small architecture, and especially sculptural forms, have a different temperature and texture, which triggers different spheres of sensory perception. Additionally, it is important to keep the elements on a good “human” scale, avoid glaring contrasts, and introduce soft lighting and related colors. All this determines the harmony in multi-sensory perception.

In the light of these research processes, the concept of establishing a statutory form of protection of the area by creating a Cultural Park [46] in Warsaw’s Praga – Północ district, aimed at preserving the heritage and increasing its attractiveness, seems to be correct. It will also be significant to use research on multi-sensory valorization in order to preserve these important stimuli that are part of the landscape of the district, which constitute the multi-sensory heritage: “rattle of wheels on authentic stone pavement”, “church bells”, “chimes on the tower”, “market buzzing”, “Praga band”, “Wedel chocolate fragrance” and others. As part of the activities in the field of the Cultural Park, action on all senses should also be considered. Hence, to revive the degraded Różycki Bazaar. Introduce the Open Workshops of Craftsmen available on one tourist route and open workshops (ceramics, seamstress, umbrella maker, shoemaker, purse maker, furrier and others). This procedure, emphasizing the heritage of Praga related to craftsmanship, would at the same time have a positive impact on all senses to revive selected public spaces.

According to A. Hauziński [10] [11] “An optimal environment should provide stimuli of varying intensity, combine movement with activity, express the attitudes and values of the inhabitants. Such an environment is conducive to shaping local identity among groups of residents. “The optimal space perceived in many senses allows for efficient orientation in the environment, especially in a difficult situation related to the threat, when there is no support of navigation devices, signs or other people. This reduces the feeling of aesthetic chaos, stress and danger. The optimal sensory urban environment allows freedom of behavior and interpersonal interactions, as well as the regulation of the supply of stimulation. On the daily journey from home to school or work, an individual is exposed to an overload of information, of which only some of it reaches them. Others, unaware, act as stressors on the psyche (A. Bańka) [19] [20]. People also naturally strive to define their territory, which is difficult in an urban environment. Then, the solution is space therapy – access to places with moderate environmental stimulation, especially important for the elderly.

Comprehensive – hybrid research methodology allows for conducting research on multi-sensory perception of space and its recording based on, inter alia, qualitative research – multi-sensory valorization, but most of all it is preceded by an empirical method: literature

on the subject was searched, collected and analyzed. Archival and present documents, plans, cartographic sources and satellite photos were studied. A rich photographic documentation was made, presenting the valorization of the space of places in the course of time, at different seasons, different times and circumstances. Research stages include, among others work with the social community, which means the proper selection of respondents (people who know the given spaces from their own experiences and interactions) and preparation of the group of respondents so that it is possible to later efficiently interpret the data and aggregate it A. Gendźwił [40]. This led to the description and interpretation of research in the area and sample group. Finally, conclusions related to the multi-sensory perception of space were formulated regarding the proposed improvement actions in the functional and spatial aspect. This illustrates the essence of the hybrid methodology of research into multi-sensory public spaces in urban planning.

Knowledge about multi-sensory experiences can help urban designers in shaping space in a way that reduces negative feelings, e.g. fear, and strengthens the positive ones – freedom and liberty. The hybrid methodology of research on the multi-sensory perception of public spaces allows for a full, more conscious and reliable assessment of the surrounding reality. The use of multi-sensory valorization of public spaces, questionnaires, interviews and walks, preceded by other studies, including analysis of literature and data, observation, discussion with representatives of the local community and experts, functional and spatial analysis as well as photographic inventory, allow for the creation of a multi-sensory image of selected places. The development of these activities will lead to the determination of: connecting the city's form with the structure of the needs and goals of its inhabitants, establishing the elements important for the multi-sensory character of the district and their significance in the local identity.

Literature

- [1] Jałowicki B. and Szczepański M.S., *Miasto i przestrzeń w perspektywie socjologicznej*. Warszawa: Wydawnictwo Naukowe Scholar, 2010.
- [2] Aristotle, "O Duszy", in *Dzieła wszystkie*, Warszawa: Wyd. Naukowe PWN, tome 3, 1992.
- [3] J. Ekel, J. Jaroszyński, J. Ostaszewska. *Mały Słownik Psychologiczny*. Warszawa: Wiedza Powszechna, 1965, p. 180.
- [4] Colman A.M., *Słownik psychologii*. Warszawa: Wydawnictwo Naukowe PWN, 2009.
- [5] Lynch K. *The image of the city*. Cambridge: MIT press, vol. 11, 1960.
- [6] Wejchert K., *Elementy kompozycji urbanistycznej*. Warszawa: Wydawnictwa Arkady, 1984.
- [7] Wejchert K., *Przestrzeń wokół nas*, Katowice: Fibak Norma Press, 1993.
- [8] Tomaszewski T., „Człowiek i otoczenie”, in *Psychologia*, Warszawa: PWN, 1975.
- [9] Tomaszewski T., „Orientacja w otoczeniu”, in *Psychologia*, Warszawa: PWN, 1976.
- [10] Hauziński A., "The evolution of the cognitive map in psychology. Discussion regarding the research of hierarchy plans and goals of activity", *Czasopismo Psychologiczne*, vol. 16., no.2, 2010, pp. 275-288.
- [11] Hauziński A., "Ewolucja pojęcia mapy poznawczej w psychologii i jej wykorzystanie w urbanistyce, architekturze oraz geografii", *Zachowanie, Środowisko, Architektura*, vol. 5, 2011, pp. 15-38,
- [12] Golledge Reginald G. "Methods and methodological issues in environment recognition research", in *Environment Knowing: Theories, Research and Methods*, Stroudsburg: Dowden, Hutchinson & Ross, 1976, pp. 300-313,

- [13] Evans G.W., Pezdek K., "Cognitive mapping: Knowledge of real-world distance and location information", *Journal of Experimental Psychology: Human Learning and Memory*, vol. 6, 1980, pp. 13–24.
- [14] Evans G.W., "Environmental cognition", *Psychological Bulletin*, vol. 88, 1980, pp. 259–287.
- [15] Evans G.W., Marrero D.G., Butler P.A., "Environmental learning and cognitive mapping". *Environment and Behavior*, vol. 13., no.1., 1981, pp. 83–104.
- [16] Evans G.W., Skorpanich M. A. Garling T., Bryant K.J., Bresolin, B., "The effects of pathway configuration, landmarks and stress on environmental cognition", *Journal of Environmental Psychology*, vol. 4, 1984, pp.323–335.
- [17] Foley J.E., Cohen A.J., "Working mental representations of the environment", *Environment and Behavior*, vol. 16, 1984, pp. 713–729.
- [18] O'Keefe J., Nadel L., *The Hippocampus as a Cognitive Map*. New York: Clarendon, 1978.
- [19] Bańka A., *Architektura psychologicznej przestrzeni życia. Behawioralne podstawy projektowania*. Poznań: Gemini S.C., 1997.
- [20] Bańka A., *Spoleczna psychologia środowiskowa*. Warszawa: Wydawnictwo Naukowe "Scholar", 2002.
- [21] Bell P. A. et al., *Psychologia środowiskowa*. Gdańsk: GWP, 2004.
- [22] Jałowiecki B., "Percepcja przestrzeni Warszawy", *Studia Regionalne i Lokalne*, vol. 2(2), 2000, pp. 79-100.
- [23] Szkuřat E., "Psychologiczne i kulturowe uwarunkowania percepcji środowiska", in *Percepcja współczesnej przestrzeni miejskiej*, Warszawa: Wydział Geografii i Studiów Regionalnych Uniwersytetu Warszawskiego, 2007, pp. 63–72.
- [24] Rybicka, E., "Poza pisanie/czytanie miasta", *Teksty Drugie*, vol. 3, 2007, pp. 107-112.
- [25] Rewers E., "Post-polis: wstęp do filozofii ponowoczesnego miasta", Kraków: Universitas, vol. 41, 2005.
- [26] Kietlińska B., "Jak za pomocą metod jakościowych zbadać zmysłowy odbiór miasta?", *Nauka i Szkolnictwo Wyższe*, vol.1(41), 2013, pp.131-142.
- [27] Simmel G., "Socjologia zmysłów", in: *Most i drzwi. Wybór esejów*. 2006, pp.184-203.
- [28] Pink S., "Doing visual ethnography". London: SAGE Publications, Ltd., 2007.
- [29] Bartnicka M., "Wyobrażenia przestrzeni miejskiej Warszawy (Studium geografii percepcji)", *Dokumentacja Geograficzna*, vol. 2, 1989.
- [30] Libura H., "Aspekty kartograficzne map wyobrażeniowych", *Polski Przegląd Kartograficzny*, vol. 15(3), 1983, pp. 126-131.
- [31] Mordwa S., *Wyobrażenia przestrzeni miast Polski Środkowej. Na podstawie badań grupy młodzieży licealnej*. Łódź: Wydawnictwo Uniwersytetu Łódzkiego, 2003.
- [32] Daniel T.C., Boster R.S., "Measuring Landscape Esthetics: The Scenic Beauty Estimation Method", in: *Proc. Our National Landscape: A Conference on Applied Techniques for Analysis and Management of the Visual Resource – 1976*, USDA Forest Service Research Paper, Department of Agriculture, Forest Service, Rocky Mountain Forest and Range Experiment Station, vol. 167, pp. 514-523.
- [33] Okołowicz M.A., Kowalska J.M., "Jakiej przyrody chcemy w miastach? Pomiar estetyki krajobrazu nad Wisłą w Warszawie metodą Scenic Beauty Estimation", *Przestrzeń i Forma*, vol.26, 2016, pp. 243-256. <https://doi.org/10.21005/pif.2016.26.D-07>
- [34] Kitchin R., "Cognitive maps: what are they and why study them?", *Journal of Environmental Psychology*, vol. 14, 1994, pp. 1-19.
- [35] Kitchin R., "Methodological convergence in cognitive mapping research: Investigating configurational knowledge", *Journal of Environmental Psychology*, vol. 16, 1996, pp. 163-185.

- [36] Kitchin R., Blades M., *The cognition of geographic space*. London, New York: L. B. Tauris Publishers, 2002.
- [37] Castellar S.M.V., Juliasz P.C.S., “Mental map and spatial thinking”, in *Proceedings of the ICA 1*, vol. 1, 2018. <https://doi.org/10.5194/ica-proc-1-18-2018>
- [38] Waterman S., Gordon D., “A quantitative-comparative approach to analysis of distortion in mental maps”, *Professional Geographer*, vol. 36(3), 1984, pp. 326–337.
- [39] Gould P., *On mental maps*. University of Michigan: Ann Arbor, 1966.
- [40] Gendźwił A., “O prezentacji kartograficznej wyników badań map poznawczych”, *Polski Przegląd Kartograficzny*, vol. 41(2), 2009, pp.115-127.
- [41] Foland, A., “Psychokartografia–metoda badania przestrzeni miejskiej”, in: *Dynamika przestrzeni miejskiej*, Poznań: Wydawnictwo Poznańskie, pp. 107-119, 2006.
- [42] Lewicka M., “Ewaluatywna mapa Warszawy: Warszawa na tle innych miast”, in: *Spoleczna mapa Warszawy. Interdyscyplinarne studium metropolii warszawskiej*, Warszawa: Scholar, 2004, pp. 316–336.
- [43] Iwańczak B., “Metody badawcze całościowej percepcji przestrzeni miasta na przykładzie Warszawy”, *Kwartalnik Architektury i Urbanistyki*, vol. 62, 2017, pp. 69-85.
- [44] Nieścioruk K., “Kartograficzny obraz map mentalnych przestrzeni miejskiej i jego prezentacja oraz analiza z zastosowaniem narzędzi systemów informacji geograficznej”, *Acta Scientiarum Polonorum. Geodesia et Descriptio Terrarum*, vol. 12(4), 2013, pp. 27-40.
- [45] Nieścioruk K., “The use of mental and sketch maps as a tool to evaluate cartography teaching effectiveness”, *The Cartographic Journal*, vol. 53(2), (2016), pp. 186-196. <https://doi.org/10.1080/00087041.2015.1108064>
- [46] Czepkiewicz M., Jankowski P., Zwoliński Z., “Geo-questionnaire: a spatially explicit method for eliciting public preferences, behavioural patterns, and local knowledge—an overview”. *Quaestiones Geographicae*, vol. 37(3), 2018, pp. 177-190. <http://doi.org/10.2478/quageo-2018-0033>
- [47] Haklay M., Jankowski P., Zwoliński Z., “Selected modern methods and tools for public participation in urban planning—a review”, *Quaestiones Geographicae*, 37(3), 2018, pp. 127-149. <https://doi.org/10.2478/quageo-2018-0030>
- [48] Czepkiewicz, M. et al., “Public Participation GIS for sustainable urban mobility planning: methods, applications and challenges”, *Rozwój Regionalny i Polityka Regionalna*, vol. 35, 2016, pp. 9-35.
- [49] Biegański L., Buczek G., Gzell S., Kowalewski A., Markowski T., Cichy-Pazder E., “Karta Przestrzeni Publicznej”, in *III Kongres Urbanistyki Polskiej ZMP i TUP*, Poznań 2009.
- [50] Ustawa z dnia 27 marca 2003 r. o planowaniu i zagospodarowaniu przestrzennym, Warszawa: Rada Ministrów, DzU 2003, Nr 80, poz. 717 z późn. zm.
- [51] Jarecka – Bidzińska E., “Praga – Północ w Warszawie jako „dzielnica sztuki” na tle wybranych przykładów z metropolii Europy i Ameryki Północnej”. Ph.D. desideration, Warsaw University of Technology, Warsaw 2018.
- [52] Osowski J., “Ile osób jeździ drugą linią metra? Mamy szczegółowe dane. Stacja Wileński oblegana, a Powiśle... “, *Gazeta Wyborcza*, 20 March 2015. Available: <https://warszawa.wyborcza.pl/warszawa/7,34862,17627910,ile-osob-jezdzi-druga-linia-metra-mamy-szczegolowe-dane-stacja.html> [Access: 01 Jun 2021]

ISSN 1899-0665